Rev.Adv.Mater.Sci. 1 (2000) 61-107

INTERFACES AND MISFIT DEFECTS IN NANOSTRUCTURED AND POLYCRYSTALLINE FILMS

Ilya A. Ovid'ko

Institute for Problems of Mechanical Engineering, Russian Academy of Sciences,
Bolshoj 61, Vas. Ostrov, St. Petersburg 199178, Russia

Received: July 23, 2000; received in revised form: December 7, 2000.

Abstract. Theoretical models are reviewed which describe misfit defect structures at interfaces (intergrain and interphase boundaries) in nanostructured and polycrystalline films. The specific structural and behavioral features of interfaces in nanostructured and polycrystalline films are discussed which influence the macroscopic properties of such films. The special attention is paid to theoretical models describing partial misfit dislocation structures, misfit disclinations, misfit dislocation walls, grain boundary dislocations as misfit defects, and partly incoherent interphase boundaries in nanostructured and polycrystalline films. Also, the effects of misfit strains on phase transformations in multilayer composites as well as the behavior of nano-islands on composite substrates are considered. Theoretical models are reviewed which describe the structure and transport properties of grain boundaries in high-T_c superconducting polycrystalline films.

CONTENTS

Corresponding author: Ilya A. Ovid'ko, e-mail: ovidko@def.ipme.ru

1. INTRODUCTION

Nanostructured and polycrystalline films exhibit outstanding physical, mechanical and chemical properties which are widely exploited in contemporary high technologies; see, e.g., [1-9]. The outstanding properties of nanostructured and polycrystalline films essentially depend on both the structure and the properties of internal interfaces, that is, intergrain and interphase boundaries. In particular, interfaces play the crucial role in processes occuring in nanocrystalline films where the volume fraction of the interfacial phase ranges from 10 to 50 %.

The structure and the properties of interfaces in nanostructured and polycrystalline films are strongly influenced by technological parameters of synthesis of such films. At the same time, interfaces serve as carriers of many physical and chemical processes occuring in nanostructured and polycrystalline films, in which case the macroscopic properties of films, in many respects, are caused by the behavior of interfaces. In these circumstances, in order to technologically control and improve the functional characteristics of nanostructured and polycrystalline films, it is important to understand the behavior of interfaces in films.

In description and controlling of the contribution of interfaces to the properties of nanostructured and polycrystalline films, of special interest are theoretical models of the interfacial structures. Modelling of the interfacial structures, in fact, serves as a very important constituent in description of the relationship between synthesis technologies, structure and properties of films. Models of interfaces include, in particular, computer, geometric and continuum models. So, computer models concentrate on simulations of the atomic structure of interfaces. Geometric models of solid/solid interfaces are concerned with their translational and rotational symmetries, in which case interfacial defects are treated as local violations of these symmetries. Continuum models use results of geometric and/or computer models in description of interfaces and interfacial defects as sources of internal stress fields, contributing to structural stability, mechanical, transport and other properties of films. Continuum models, in fact, provide a link between descriptions of the structure of interfaces and their properties. This review deals with geometric and continuum models describing the specific structural and behavioral peculiarities of interfaces in nanostructured and polycrystalline films. In doing so, the special attention is paid to a theoretical description of misfit defects (generated at interfaces) as defects causing partial relaxation of misfit stresses in films.

2. SPECIFIC FEATURES OF INTERFACES IN NANOSTRUCTURED AND POLYCRYSTALLINE FILMS

In general, nanostructured films deposited on substrates can be divided into the following basic categories, depending on both their structure and the shape of the crystallites: nanocrystalline films composed of equaxed nm-sized crystallites (nano-grains) (Fig. 1a), films composed of rod-shaped crystallites with rod diameters in the order of a few nm (Fig. 1b), layer-shaped films with thickness in the order of a few nm (Fig. 1c), island films composed of equaxed nm-sized islands (Fig. 1d), island films composed of rod-shaped islands with rod diameters in the order of a few nm (Fig. 1e), equaxed nm-sized particles embedded into a thick layer-shaped matrix (Fig. 1f), nm-sized rods embedded into a thick layer-shaped matrix (Fig. 1g), and nano-sized layers embedded into a thick layer-shaped matrix (Fig. 1h). In this paper we will focus our consideration on the three classes of nanostructured films, that are most widespread in both fundamental researches and technological applications. These are nanocrystalline films composed of nano-grains (Fig. 1a), layer-shaped films of nano-scaled thickness (Fig. 1c) and island films composed of equaxed nano-sized islands (Fig. 1d), which, hereinafter, will be denoted as nanocrystalline films, nano-layers and nano-islands, respectively, for ease of reference.

Nanocrystalline films. Nanocrystalline films (Fig. 1a) can be treated as polycrystalline films in the limiting case, where the grain size is in the order of a few nm. With this taken into consideration, nanocrystalline films have the «conventional» structural and behavioral features that are inherent to both nanocrystalline and polycrystalline films as well as the "specific" structural and behavioral features associated with their nano-scaled spatial organization.

The existence of both grain boundaries and film/substrate boundaries causes the "conventional" features of nanocrystalline and polycrystalline films, that are as follows: (A) There is a strong elastic interaction between grain boundaries in a nanocrystalline (or polycrystalline) film and the film/substrate interface which is a source of misfit stresses. (B) Film/substrate interfaces are complicately arranged; each interface consists of fragments with various structures and properties, bounded by junctions of grain boundaries and the film/substrate interface. Due to the features (A) and (B), grain boundaries and film/substrate interfaces affect both the structure and the properties of each other in nanocrystalline and polycrystalline films.

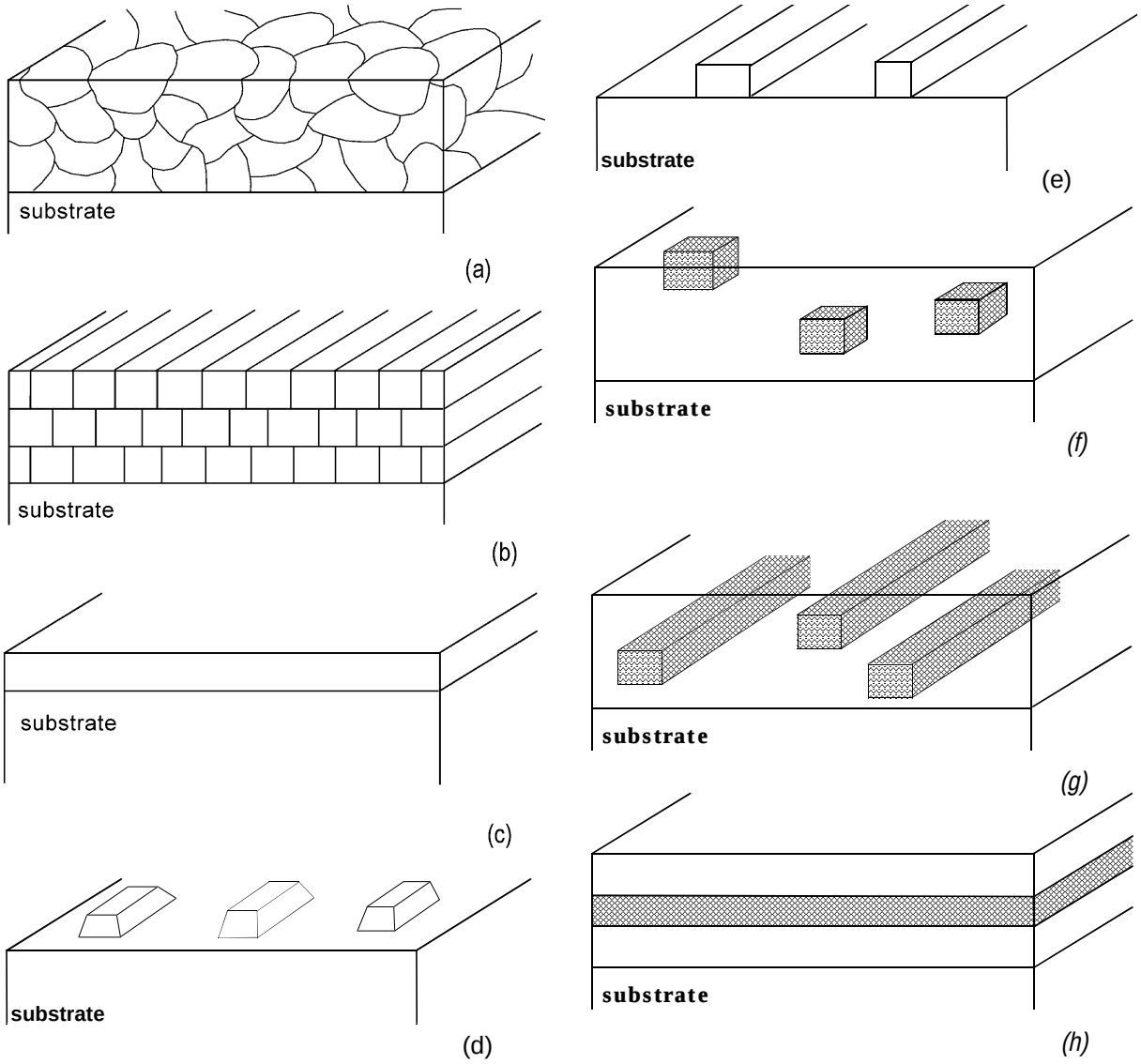

Fig. 1. Classes of nanostructured films. (a) Nanocrystalline films composed of equaxed nano-grains. (b) Films composed of nano-rods. (c) Nano-layers. (d) Equaxed nano-islands. (e) Nano-rod-shaped islands. (f) Nano-particles, (g) nano-rods and (h) nano-layers embedded into a thick layer-shaped matrix.

In addition, interfaces in nanocrystalline films have the following "specific" features related to their nano-scaled structure:

(1) The volume fraction of the interfacial phase is extremely high in nanocrystalline films.

(2) Grain boundaries as structural elements mostly have extremely short dimensions in nanocrystalline films.

(3) There is a strong elastic interaction between neighbouring interfaces, because (extremely short) distances between them are close to the characteristic scales of their stress fields.

(4) In nanocrystalline films there is a strong effect of triple junctions and nanograins on interfaces and vice versa, because the volume fraction of triple junctions is extremely high in nanocrystalline solids and because nanograins commonly are more distorted than conventional grains in polycrystalline films.

(5) Formation of nanostructured films frequently occurs at highly non-equilibrium conditions that essentially influence the interfacial structures.*

* The same features are inherent also to bulk nanocrystalline materials

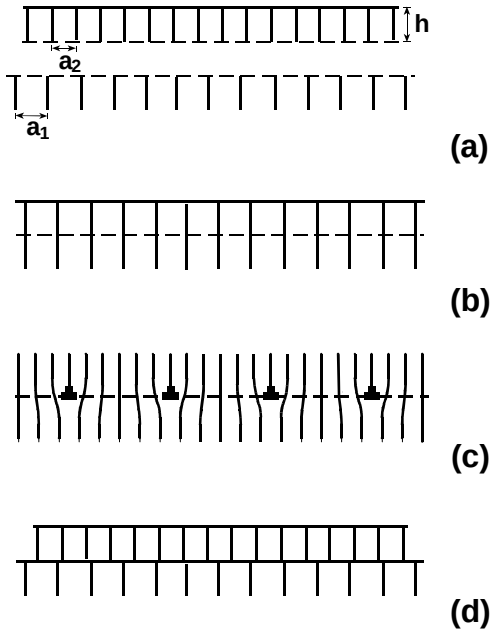

Fig. 2. Interphase boundaries between single crystalline films and substrates. (a) Origin of misfit stresses is the geometric mismatch between crystal lattice parameters, a_1 and a_2, of substrate and film, respectively. (b) Coherent boundary. (c) Semi-coherent boundary. (d) Incoherent interphase boundary.

The points under discussion should be definitely taken into account in theoretical models of the interfacial structures in nanocrystalline and polycrystalline films, which, in most cases, can not be unambigiously identified with the help of contemporary experimental methods. In next sections we will consider several models of interfaces in nanocrystalline and polycrystalline films with focusing to the specific structural and behavioral features of interfacial misfit defects (see sections 3-9).

Nano-layers. In fact, there is just one specific structural feature of nano-layers which is responsible for their behavioral peculiarities. It is nano-scaled thickness that causes, in particular, the strong effects of the film/substrate interface and the film free surface on the behavior of a film (nano-layer). In this review we will discuss models describing the formation of partial misfit dislocations associated with stacking faults in nano-layers (see section 10) and misfit stresses and their effects on phase transformations in nano-layered composites (see sections 11, 12, 13 and 14).

Nano-islands. The basic specific features of nano-islands (e.g., quantum dots), in particlular, are as follows: (i) Tentatively equaxed nano-sized shape of nano-islands causes the strong effects of the island/substrate interface and the island free surfaces on their behavior. In particular, spatial positions, shape and characteristic sizes of nano-islands depend on the geometric mismatch at the island/substrate interface. (ii) Mobility of nano-islands; they can move on a substrate. These features cause the effects of misfit defects (serving as sources of stresses) at internal interphase boundary in a composite substrate on spatial organization of ensembles of nano-islands deposited on the substrate [10]. We will discuss this effect in section 15. Section 16 deals with interfaces in high-T_c superconducting films.

3. CLASSIFICATION OF INTERPHASE BOUNDARIES BETWEEN (CRYSTALLINE, POLYCRYSTALLINE, NANOCRYSTALLINE) FILMS AND SINGLE CRYSTALLINE SUBSTRATES

First, let us consider interphase boundaries between single crystalline films and single crystalline substrates. In general, such interphase boundaries can be coherent, incoherent or semi-coherent, depending on the structural and chemical features of the matched phases as well as on external factors such as temperature and the geometric sizes (e.g., thickness) of the matched crystalline samples. According to a qualitative description of the coherent, incoherent and semi-coherent states of interfaces, given by Mobus et al [11], one can briefly determine these states as follows. The key classifying factor is supposed to be the way in which the mismatch (geometric misfit) between the adjacent crystalline lattices (Fig. 2a) is accommodated. (i) For a coherent interface between a thin film and thick substrate, the mismatch is accommodated completely by straining the lattice of the adjacent film (Fig. 2b). In this event, misfit stresses (stresses occuring due to the mismatch at interface) are characterized by the spatial scale being the film thickness. (ii) For a semi-coherent interface, localized misfit dislocations (MDs) provide, at least, partial compensation of long-range misfit stresses(Fig. 2c) (for more details, see book [12] and reviews [13-16]). (iii) A completely incoherent interface can be treated as resulted from a rigid contact of two crystalline lattices distorted only at the contact regions (Fig. 2d). Incoherent interfaces do not induce long-range strains; there are only short-range distortions occuring due to faults in chemical binding at the interface. Such distortions are characterized by a spatial scale close to interatomic distances in the adjacent phases.

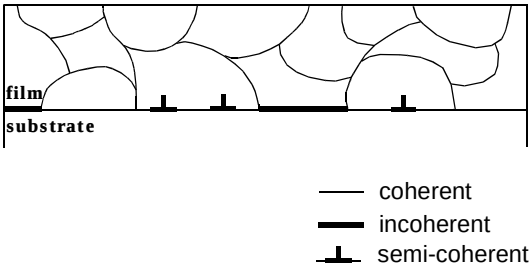

Fig. 3. Partly coherent, semi-coherent and incoherent interphase boundary between polycrystalline (or nanocrystalline) film and single crystalline substrate.

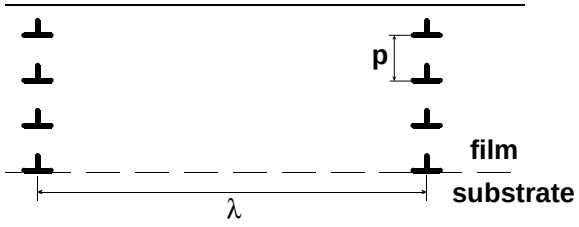

Fig. 4. Relaxation of misfit stresses via formation of misfit dislocation walls. λ and *p* are the interspacings between walls and dislocations in a wall, respectively.

Now let us turn to a classification of interphase boundaries between nanocrystalline (or polycrystalline) films and single crystalline substrates. As noted in section 2, any nanocrystalline (or polycrystalline) film/substrate interface consists of many fragments bounded by junctions of grain boundaries and the interface. Grains of the film, that are adjacent to the film/substrate interface, are misoriented relative to each other and, generally speaking, relative to the substrate. As a corollary, fragments of the film/substrate boundary are characterized by the misorientation and the misfit between the crystalline lattices of the film grains and the substrate. Each fragment of the film/substrate interface is either coherent, incoherent or semi-coherent, depending on its misfit and misorientation parameters, the structural and chemical features of the matched grain and the substrate as well as on external factors such as temperature and the film thickness. Thus, in general, the film/substrate interface is partly coherent, semi-coherent and incoherent; it consists of coherent, semi-coherent and incoherent fragments (Fig. 3). In this situation, the film/substrate interface contains defects of the two types: misfit defects (responsible for partial compensation of misfit stresses generated due to mismatch between the lattice parameters of the film and the substrate) and misorientation defects (that provide misorientation between the adjacent grains of the film and the single crystalline substrate). More than that, misfit defects can be generated not only at film/substrate interfaces, but also at grain boundaries of the film. In next sections 4-8 we will consider geometric and continuum models of interphase boundaries between nanocrystalline (or polycrystalline) films and single crystalline substrates with focusing on misfit defects at film/substrate interfaces and grain boundaries in the film interiors.

4. MISFIT DISLOCATION WALLS (LOW-ANGLE BOUNDARIES) IN SOLID FILMS

Misfit stresses occur in crystalline films due to the geometric mismatch at interphase boundaries between crystalline lattices of films and substrates. In most cases a partial relaxation of misfit stresses in single crystalline films is realized via generation of MDs that form dislocation rows in interphase boundary plane (Fig. 2c); see, e.g., experimental and theoretical works [11-40]. Generally speaking, the formation of MD rows at interphase boundaries is either desirable or disappointing, from an applications viewpoint, depending on the roles of films and interphase boundaries in applications of heteroepitaxial systems. So, if the properties of a film are exploited, the formation of MD rows commonly is desirable as it results in a (partial) compensation of misfit stresses in the film. If the properties of an interphase boundary are exploited, the formation of MD rows commonly is undesirable, since the formed MD cores violate the pre-existent ideal (coherent) structure of the interphase boundary. In this section we, following [41], will consider an alternative physical micromechanism for relaxation of misfit stresses which results in a more “weak” violation of the ideal (coherent) interphase boundary structure than the “standard” formation of MD rows. This new micromechanism is the formation of MD walls in crystalline films. Such MD walls, in fact, are low-angle boundaries whose formation in a film is caused by an influence of the interphase boundary. That is, low-angle boundaries – MD walls – are formed in response to the action of misfit stresses generated at the interphase boundary. On the other hand, the formation of low-angle boundaries strongly influences the structure (and, therefore, the properties) of the interphase boundary; the

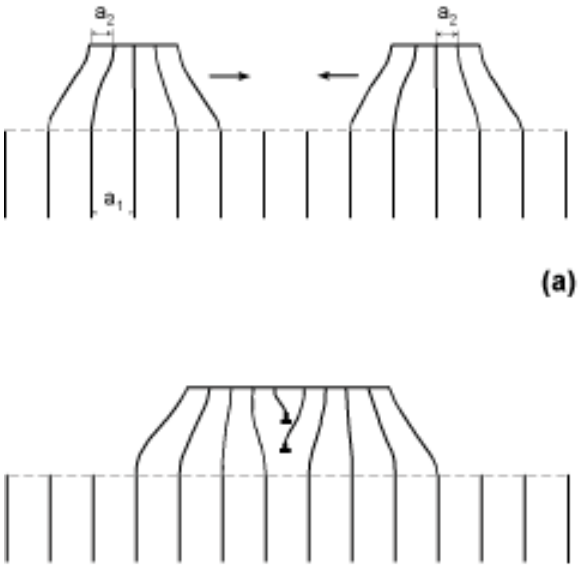

Fig. 5. Convergence of island films (schematically). (a) Island films migrate towards each other. (b) Island films converge, in which case a misfit dislocation wall (a low-angle boundary) is formed.

density of MD cores that violate the ideal (coherent) structure of the interphase boundary is low when MD walls are formed in the film. Dislocation walls in crystals represent low-angle grain boundaries [42], in which case the formation of MD walls in a film is attributed with the polycrystalline structure of the film.

Let us consider a model heteroepitaxial system consisting of an elastically isotropic semi-infinite crystalline substrate and an elastically isotropic thin crystalline film with thickness h. For simplicity, hereinafter we confine our examination to the situation with one-dimensional misfit characterized by misfit parameter $f = (a_2 - a_1)/a_1 < 0$, where a_1 and a_2 are the crystal lattice parameters of the substrate and the film, respectively. The shear stress G and the Poisson ratio ν are assumed to be identical for the substrate and the film.

Let us consider the model heteroepitaxial system in the situation with a coherent interphase boundary. Owing to the geometric mismatch between crystalline lattices of the film and the substrate, the film is elastically uniformly distorted. It is characterized by elastic strain $\varepsilon = - f$. Since $f<0$, the corresponding misfit stresses are tensile in the film.

The standard physical micromechanism for relaxation of misfit stresses is the formation of a row of MDs in the interphase boundary plane (Fig. 2c) that induce compressive stress fields partly compensating the tensile misfit stresses (or, in other words, partly accommodating the misfit f) [12-16]. We think that an effective alternative to the standard micromechanism is the formation of walls of MDs in the film (Fig. 4) that induce compressive stress fields. Realization of either standard or alternative micromechanism for relaxation of misfit stresses depends on kinetic factors (related to technologies of the film deposition on the substrate) and the degree of misfit stress relaxation caused by such micromechanisms.

Let us briefly discuss a situation where formation of MD walls is kinetically favourable. Regardless of values of the "equilibrium" parameters (critical thickness of a film, elastic energy density, etc.) which characterize MD walls, their formation can occur at non-equilibrium conditions in films resulted from convergence of island films. Actually, misfit stresses in an island film partly relax via slope of edge surfaces of the island film (Fig. 5a). In these circumstances, when two island films converge, their contact edge surfaces are crystallographically misoriented. As a corollary, the convergence process results in formation of a boundary with a low-angle crystallographic misorientation in the contact area of the films (Fig. 5). That is, the convergence of two island films leads to transformation of their contact edge surfaces (being crystallographically misoriented) into an interface, a low-angle grain boundary (Fig. 5). At the same time, any low-angle boundary in a crystal is represented as a wall of dislocations [42]. In the discussed situation, a low-angle boundary in the film resulted from convergence of two island films (Fig. 5) is naturally interpreted as a wall of MDs.

Now let us turn to analysis of the "equilibrium" characteristics of MD walls, specifying their contribution to misfit stress relaxation. In order to evaluate the degree of misfit stress relaxation in the situation with MD walls (Fig. 4), let us estimate the elastic energy density W of a film with MD walls. In doing so, for simplicity, we assume the following: MD walls are periodically arranged with period λ along the interphase boundary; MDs are edge dislocations of the 90° type, that is, edge dislocations with a glide plane being perpendicular to the normal to the interphase boundary plane; Burgers vectors of MDs are identical and equal to $b = a_2$; and distances between neighbouring MDs in dislocation walls are identical and equal to p. Also, it should be noted that MD walls are of finite extent, in which case (in the spirit of the theory of disclinations, e.g.

[43]) a stress field source of the disclination type exists at the "internal" termination point of every MD wall. In other words, disclinations exist at junctions of the MD walls and the interphase boundary (Fig. 4). In these circumstances, in the first approximation (which corresponds to the Matthews approximation [44] for MD rows), the elastic energy density W has the three basic constituents:

$$= W^{f} + W^{d} + W^{w}, \qquad (1)$$

where W^{f} is the proper elastic energy density of the residual misfit (uncompensated by MDs), W^{w} and W^{d} are respectively the energy densities of MD walls and the disclinations associated with MD walls.

Generally speaking, misfit disclinations provide only a partial relaxation of misfit stresses, in which case there is some residual elastic strain ε which corresponds to the residual misfit stresses in the film. The corresponding elastic energy density W^{f} is determined in the standard way [12-16] as follows:

$$^{f} = \frac{2G\varepsilon^{2}h(1+\nu)}{1-\nu}. \qquad (2)$$

In calculations of W^{d}, we use results of calculations [43] that deal with the proper elastic energy of a wedge disclination located near a free surface in a semi-infinite solid. In doing so, for simplicity, we restrict our consideration to the situation with the film thickness h being lower than the distance λ between neighboring MD walls and, as a corollary, between neighbouring disclinations located at termination points of MD walls at the interphase boundary. Such a situation ($h<\lambda$) can often come into play in real heteroepitaxial systems. Actually, MDs, in general, provide only a partial accommodation of the misfit f, in which case the residual strain is $\varepsilon = |f| - \boldsymbol{B}/\lambda$, where $\boldsymbol{B}$ denotes the Burgers vector sum of MDs in one wall, and $\boldsymbol{B}/\lambda$ the part of the preexistent misfit f, which is accommodated by MDs. The parameters of MD wall in our model (Fig. 4) force the relationship $\boldsymbol{B}=hb/p$, where h/p is the number of MDs in one wall. As a result, we have the following relationship between h and λ:

$$\lambda = \frac{hb}{p(|f|-\varepsilon)}. \qquad (3)$$

Since $|f| - \varepsilon \le |f|$ and $|f|$ ranges from 10^{-3} or 10^{-2} in real heteroepitaxial systems, the situation with $h<\lambda$ (or, as it results from formula (3), the situation with the distance between neighbouring MDs in a MD wall $p \le 10^{2}\,b$ to $10^{3}\,b$) can often occur in such systems. With this taken into account, in terms of our model we find with the help of calculations [43] the proper elastic energy density of misfit disclinations, whose periodic distribution along the interphase boundary is characterized by linear density λ^{-1}, as follows:

$$^{d} = \frac{G\omega^{2}h^{2}}{4\pi(1-\nu)\lambda}, \qquad (4)$$

where the thickness h of the film plays the role as distance between misfit disclinations and the free surface of the film, and ω is the disclination power (in our model, $\omega \approx b/p << 1$). It should be noted that the elastic interaction between the disclinations is negligibly small in the discussed situation (Fig. 4), since the screening length h (distance between a disclination and the free surface) for disclination stress fields is lower than the interspacing λ between the disclinations ($h < \lambda$).

Let us estimate the energy density W^{w} which specifies MD walls (without taking into account the contribution related to the disclinations, see above). W^{w} can be calculated with the help of (known in the theory of dislocations, e.g. [42]) formula for the energy density of an infinite dislocation wall as follows:

$$^{w} = \frac{Gb^{2}h}{4\pi(1-\nu)p\lambda}\left(\ln\frac{R}{r_{0}} + Z\right). \qquad (5)$$

Here R denotes the screening length for stress fields of MDs composing a wall ($R \approx p$), r_{0} the radius of a MD core ($r_{0} \approx a_{2}$), Z the factor taking into account the contribution of a MD core to the elastic energy density ($Z \approx 1$).

From (1), (2), (4) and (5) for characteristic values of $R \approx p$, $Z \approx 1$, $\omega \approx b/p$ and $r_{0} \approx a_{2}$, we obtain the following formula for the elastic energy density of the film with MD walls:

$$\approx 2G\frac{1+\nu}{1-\nu}\varepsilon^{2}h + \frac{Gb^{2}h}{4\pi(1-\nu)p\lambda}\left(\ln\frac{p}{a_{2}} + 1\right) + \frac{Gh^{2}b^{2}}{4\pi(1-\nu)\lambda p^{2}}. \qquad (6)$$

From (3) and (6) one can find dependence $W(\varepsilon)$ whose minimum corresponds to the so-called equilibrium value $\tilde{\varepsilon}$ of the residual strain in the film. This value characterizes the elastically deformed film with MD walls at equilibrium conditions. From (3) and (6) it follows:

$$\tilde{\varepsilon} = -\frac{b}{16\pi(1+\nu)h}\left(\ln\frac{p}{a_2}+\frac{h}{p}+1\right). \qquad (7)$$

Another important parameter of the film is its critical thickness h_c which, as with the situation with MD rows (e.g., [12-16]), is defined as follows. For the film with thickness h being higher (lower, respectively) than h_c, the existence of misfit disclinations is energetically preferable (unpreferable, respectively) as compared to the coherent state of the interphase boundary. h_c is derived from Eqn. 7 with $\tilde{\varepsilon}$ substituted by $-f$, in which case we find

$$h_c = \frac{bp\left[\ln\frac{p}{a_2}+1\right]}{16\pi f(1+\nu)p-b}. \qquad (8)$$

Let us consider the two situations: the situation with a film containing walls of MDs (Fig. 4) and the situation with a film containing a row of MDs (Fig. 2c), both are characterized by the same averaged MD density. For characteristic values of $h/p > 1$, the elastic energy W of the film with MD walls, given by formula (6) (with (3) taken into account) is larger than the energy density W^* of the film with a row of MDs, given by Matthews formula (e.g., [12,44]):

$$W^* = 2G\frac{1+\nu}{1-\nu}\varepsilon^2 h + \frac{Gb(|f|-\varepsilon)}{4\pi(1-\nu)}\left(\ln\frac{h}{a_2}+1\right). \qquad (9)$$

For a quantitative characterization of the difference between elastic energy densities of MD rows (Fig. 2c) and MD walls (Fig. 4), let us estimate the characteristic ratio $r=(W-W^*)/W^*$ defined by the following formula which entails from formulae (5), (6) and (9):

$$r = \frac{b(|f|-\varepsilon)\left[\frac{h}{p}-\ln\frac{h}{p}\right]}{8\pi(1+\nu)\varepsilon^2 h + b(|f|-\varepsilon)\left[\ln\frac{h}{a_2}+1\right]}. \qquad (10)$$

At the initial stage of formation of MD structures (Figs. 2c and 4), values of $|f|-\varepsilon$ are small, in which case r is small. So, for characteristic values of $|f|-\varepsilon \approx 10^{-3}|f|$, $\varepsilon \approx |f| \approx 10^{-3}$ to 10^{-2}, $h/p \approx 3$ to 10, $h \approx (10^2$ to $10^3)a_2$, $b \approx a_2$, $\nu \approx 1/3$, from formula (10) we find that the characteristic ratio r ranges from $7\cdot10^{-6}$ to $2.5\cdot10^{-3}$. At the late stages of evolution of MD structures (Fig. 1a and b), values of $|f|-\varepsilon$ are of the same order as $|f|$, in which case r is comparatively large. So, for characteristic values of $|f|-\varepsilon \approx |f|$ and $\varepsilon \approx 10^{-3}|f|$, and the above values of other parameters ($|f|$, h/p, h, b and ν), from formula (10) we obtain that r ranges from 0.25 to 1.5.

Our estimations of r indicate that MD rows (Fig. 2b) in films, from an energetic viewpoint, are more equilibrium (more stable) misfit defect configurations than MD walls (Fig. 4). This conclusion is supported by numerous experimental observations of MD rows at interphase boundaries in heteroepitaxial systems, e.g. [12-16]. At the same time, the difference between energy densities of MD rows (Fig. 1a) and MD walls (Fig. 4) at the initial stage of their formation in a film is small ($r << 1$), in which case MD wall can be formed due to some kinetic factors.

If MD walls are formed, they exist as metastable misfit defect configurations in films. Actually, the movement of a dislocation (in our case, a MD) from a dislocation wall (in our case, a MD wall) into an adjacent crystalline region needs to overcome an energetic barrier [42]. In other words, in order to remove MD from a MD wall and to place this MD on the interphase boundary far from the wall or, in the general situation, in order to transform a MD wall (Fig. 4) into a MD row (Fig. 2c), energetic barriers have to be overcome.

In these circumstances, MD walls in films (Fig. 4) are metastable configurations, since $W > W^*$. The formation of such metastable MD walls can occur at non-equilibrium conditions, for example, in films resulting from convergence of island films (Fig. 5). This serves as a natural explanation of experimental data [45] indicative of the fact that special interfaces (different from high-angle grain boundaries) are formed in films resulting from convergence of island films.

Also, in general, MD walls are capable of being formed, for kinetic reasons, in films with threading dislocations which (by definition [12,13]) are extended from "parent" dislocations entering from the substrate to the interphase boundary. For instance, a MD wall can be formed due to kinetically favourable re-arrangement of several dislocations being extensions of neighbouring threading dislocations (with the same Burgers vectors) that enter to the interphase boundary in some local region (Fig. 6). In other words, for kinetic reasons related to high local density of the parent dislocations, a "beam" of threading dislocations can be extended into a MD wall ("instead of equilibrium" planar row of MDs in the interphase boundary) in the film (Fig. 6).

In general, MD walls can be formed also at equilibrium conditions, for instance, in multilayer films consisting of alternate layers. In this situation, the misfit stress distribution, and energetic character-

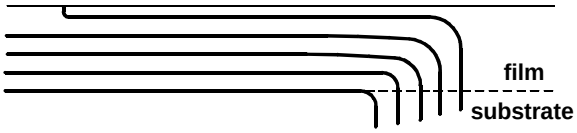

Fig. 6. Arrangement of threading dislocations into misfit dislocation wall.

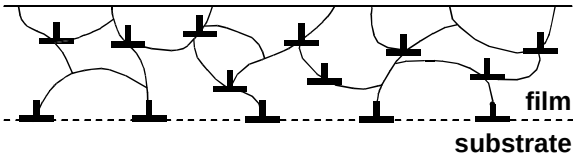

Fig. 7. Grain boundary dislocations as misfit defects in nanocrystalline (or polycrystalline) film.

istics of MD walls are different from those in the situation with single-layer films, and, therefore, MD walls can be stable – energetically favourable – in multilayer films at some values of their parameters (for details, see section 14).

Thus the discussed physical micromechanism for relaxation of misfit stresses – generation of MD walls (Fig. 4) – is an effective alternative to the standard micromechanism – generation of MD rows (Fig. 2c) – in films resulting from convergence of island films. MD walls provide a more "weak" violation of the ideal (coherent) interphase boundary structure, in which case the formation of MD walls is more preferable, from an application viewpoint, than that of MD rows in heteroepitaxial systems with interphase boundaries used as functional elements in applications.

5. GRAIN BOUNDARY DISLOCATIONS AS MISFIT DEFECTS IN NANOCRYSTALLINE AND POLYCRYSTALLINE FILMS

The structure and the properties of nanocrystalline films are different from those of single crystalline films. Therefore, relaxation of misfit stresses in nanocrystalline films, in general, can occur via micromechanisms that are different from the standard micromechanism - the formation of rows of perfect misfit dislocations (Fig. 2c) – that commonly is realized in conventional single crystalline films. In particular, we think that, due to the existence of grain boundaries in nanocrystalline films, an effective alternative to the standard physical micromechanism for relaxation of misfit stresses in such films is the formation of grain boundary dislocations as misfit defects. These grain boundary dislocations (with Burgers vectors being displacement-shift-complete lattice vectors which characterize grain boundary translation symmetries) induce stress fields that compensate for, in part, misfit stresses and are located at grain boundaries and triple junctions of interphase and grain boundaries (Fig. 7). The formation of grain boundary dislocations as misfit defects does not induce any extra violations of coherent fragments of interphase boundaries and, therefore, does not lead to degradation of their functional properties used in applications. In this section we, following [46], will discuss the behavioral peculiarities of nanocrystalline and polycrystalline films with grain boundary dislocations as misfit defects.

First, let us discuss a scenario for the formation of grain boundary dislocations as misfit defects in nanocrystalline films. Nanocrystalline films are often synthesized at highly non-equilibrium conditions, in which case grain boundaries in these films are highly distorted and are characterized by misorientation parameters which, in general, vary along grain boundary planes. Each distorted boundary contains both the so-called "equilibrium" grain boundary dislocations (which provide the mean misorientation characterizing the boundary) and "non-equilibrium" grain boundary dislocations (which provide local deviations of the distorted boundary misorientation from its mean value) (Fig. 8) [47, 48]. "Non-equilibrium" dislocations in a grain boundary, after some relaxation period, disappear via entering to a free surface of a sample and/or via annihilation of dislocations with opposite Burgers vectors (Fig. 8a). As a result of the relaxation processes discussed, a distorted grain boundary commonly transforms into its equilibrium state with the misorientation being (tentatively) constant along the boundary plane.

However, the relaxation processes result in complete disappearance of "non-equilibrium" grain boundary dislocations in materials with initially distorted grain boundaries, only if there are not sources of long-range stresses affecting the grain boundary phase evolution (Fig. 8a). In nanocrystalline films with initially distorted grain boundaries the misfit stresses (generated at film/substrate interfaces) influence evolution of "non-equilibrium" dislocations. More precisely, we expect that the low-energy (equilibrium) state of a nanocrystalline film corresponds to the existence of not only "equilibrium" grain boundary dislocations, but also some residual "non-equilibrium" grain boundary dislocations that play the role as misfit defects (Figs. 7 and 8b) compensating for misfit stresses in the film. In other words, in

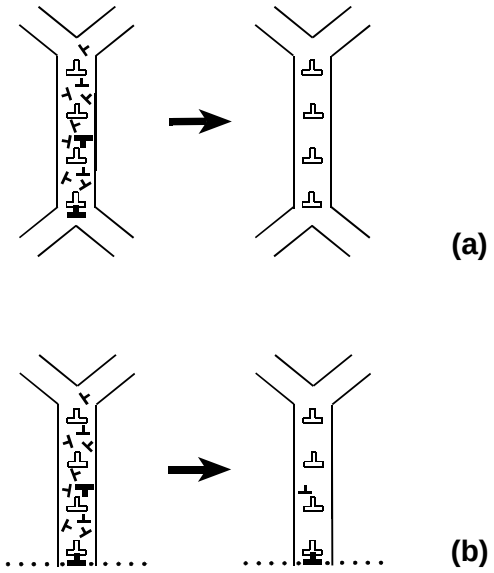

Fig. 8. "Equilibrium" and "non-equilibrium" dislocations (shown as open and solid dislocation signs, respectively) in distorted and low-energy grain boundaries. (a) "Non-equilibrium" dislocations completely disappear after relaxation. (b) Some "non-equilibrium" dislocations keep existing as misfit defects (compensating for misfit stresses generated at interphase boundary shown as dotted line) after relaxation.

the framework of the scenario discussed, synthesis of nanocrystalline films at non-equilibrium conditions produces high-density ensembles of "non-equilibrium" grain boundary dislocations, while misfit stresses generated at interphase (film/substrate) boundaries cause some "non-equilibrium" grain boundary dislocations to keep existing, even after relaxation, as misfit defects compensating for these misfit stresses (Fig. 8b).

In general, the most spatially homogeneous distribution of misfit dislocations is characterized by the minimal elastic energy density and, therefore, is most stable. Grain boundary dislocations commonly are characterized by Burgers vectors being essentially lower than those of perfect misfit dislocations being crystal lattice dislocations. This specific feature allows grain boundary dislocations to be more homogeneously distributed along an interphase boundary as compared with perfect misfit dislocations, if the sum Burgers vectors of ensembles of misfit, grain boundary and perfect, dislocations are the same per unit of the boundary plane area. As a corollary, we expect that the existence of grain boundary dislocations as misfit dislocations often is more energetically favourable than that of perfect misfit dislocations. For more details, below we will analyze energetic characteristics of misfit grain boundary dislocations and compare them with those of perfect misfit dislocations.

To investigate the quantitative difference in the energetics of the formation of perfect and grain boundary misfit dislocations, we shall examine a simple model – a thin, elastically isotropic, nanocrystalline film of thickness h on a semifinite, elastically isotropic substrate. We shall assume the elastic constants, the shear modulus G and the Poisson ratio ν, to be the same for the film and the substrate. Crystalline lattices of the substrate and the film are supposed to be cubic ones with the lattice parameters, a_1 and a_2, respectively. Grains of the film are assumed to be identical cubes with the grain size l.

Any real interface between a nanocrystalline or polycrystalline film and a single crystalline substrate consists of many fragments each dividing the substrate and a grain of the film (Fig. 3). Different fragments of the interface are characterized by different misorientation parameters, in which case the interface serves as a source of spatially inhomogeneous stress fields associated with a spatially inhomogeneous distribution of its misorientation along the interface plane. In general, some fragments of the interface can be incoherent due to their "unfavourable" misorientation destroying the coherency of the interface [46]. The main subject of this section – relaxation of misfit stresses via generation of grain boundary dislocations – is related to the role of interfaces as spatially homogeneous sources of misfit stresses generated due to the geometric mismatch between lattice parameters of the adjacent crystalline phases. With this taken into account, in order to distinguish the effects associated with misfit stresses, here we will not consider any aspects related to spatially inhomogeneous distributions of misorientation that characterize interfaces between nanocrystalline or polycrystalline films and single crystalline substrates. In doing so, in this section we will focus our consideration on a model of interface as a semi-coherent interface which induces misfit stresses and contains periodic (with period l) orthogonal rows of misfit dislocations with small Burgers vectors $\boldsymbol{b}$, that is, vectors belonging to displacement-shift-complete lattices of grain boundaries (Fig. 9).

The pre-existent coherent (misfit-dislocation-free) state of the system is characterized by elastic strain $\varepsilon_0 = -f$, where $f = (a_2 - a_1)/a_1 > 0$ is the two-dimensional misfit between the crystalline lattices of the substrate and the film. The density of the elastic

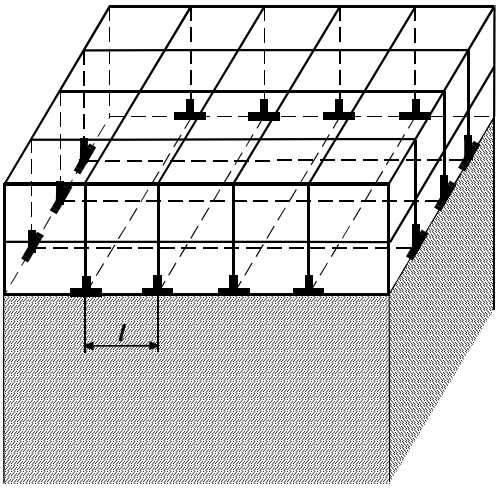

Fig. 9. Network of grain boundary misfit dislocations at interphase boundary. *l* is the grain size of nanocrystalline film.

misfit self-energy (per unit area of the interface) is given by the expression (e.g., [12-16]):

$$\tilde{}_{f} = 2G\frac{1+\nu}{1-\nu}f^{2}h. \qquad (11)$$

As *h* increases to some critical value h_c, relaxation of the misfit *f* starts in the film by formation of an orthogonal network of grain boundary misfit dislocations located at triple junctions of grain boundaries and the interphase boundary (Fig. 9). The system transforms into a semi-coherent state.

In the framework of our model, MDs are boundary dislocations which are located at interphase boundary and form the regular dislocation network (Fig. 9), that is, a regular square lattice characterized by period *l*, the distance between the neighbouring parallel dislocations. In this situation, the new, semi-coherent state is characterized by residual uniform elastic strain $\varepsilon = -(f - \varepsilon_d) < 0$, where $\varepsilon_d = b/l$ is part of the misfit accommodated by the formation of grain boundary misfit dislocations each being characterized by Burgers vector ***b*** (supposed to be the same for all the dislocations). The total energy density of the system in the semi-coherent state can be written in the form (by analogy with the calculation [49] of the energy desit of partial misfit dislocations):

$$= W^{f} + W_{el}^{d} + W_{c}^{d} + W_{int}^{fd}, \qquad (12)$$

where $_{el}^{d}$ is the elastic energy density of grain boundary misfit dislocations, which is obtained by taking account of their interaction with the free surface of the film and with one another; $_{c}^{d} = Gb^2/[2\pi(1-\nu)l]$ is the energy density of the cores of grain boundary misfit dislocations; $_{int}^{fd} = -4Gfb(h-b)(1+\nu)/[(1-\nu)l]$ is the energy density of interaction of grain boundary misfit dislocations with the elastic field of the misfit.

With results [49] of calculations of the energy density $_{el}^{d}$ taken into consideration, we find the following formula for *W*:

$$= 2G\frac{1+\nu}{1-\nu}hf^{2} + \frac{Gb^{2}}{2\pi(1-\nu)l} -$$
$$4Gf\frac{1+\nu}{1-\nu}(h-b)\frac{b}{l} + \frac{Gb^{3}}{2(1-\nu)l^{2}} \times$$
$$\left\{(2(1+2\nu)\frac{h}{b} - 1)\frac{C_1+1}{S_1} - \frac{C_2+1}{S_2} - 4\nu\frac{h}{b}\frac{C_3+1}{S_3}\right. \qquad (13)$$
$$\left. -4\pi\frac{h}{l}(\frac{h}{b} - 1)\frac{1}{C_1 - 1} - \frac{(1+2\nu)l}{2\pi b}\ln\frac{C_2 - 1}{C_1 - 1}\right\}.$$

Here $C_1 = \cosh[2\pi b(2h/b-1)/l]$, $C_2 = \cosh[2\pi b/l]$, $C_3 = \cosh[2\pi h/l]$, $S_1 = \sinh[2\pi b(2h/b-1)/l]$, $S_2 = \sinh[2\pi b/l]$, $S_3 = \sinh[2\pi h/l]$.

Now let us consider two situations: the situation with a nanocrystalline film/substrate system containing a regular network of grain boundary misfit dislocations (Fig. 9) and the situation with a single crystalline film/substrate system containing a regular network of perfect misfit dislocations (each being characterized by Burgers vector ***B***) with the distance between neighbouring parallel dislocations being *L*; they are specified by the same averaged density of misfit dislocations, that is, $b/l = B/L$. The total elastic energy density *W** of the system with perfect misfit dislocations is given by formula (13) with *b* and *l* being replaced by *B* and *L*, respectively. In these circumstances, the difference between the elastic energy densities of the systems with grain boundary misfit dislocations (Fig. 9) and perfect misfit dislocations is quantitatively characterized by ratio

$$r = \frac{W^{*} - W}{W}, \qquad (14)$$

where *W* and *W** are given by formula (13) with corresponding values of the Burgers vector magnitude (*b* and *B*, respectively) and the distance between neighbouring parallel dislocations (*l* and *L*, respectively). The dependencies of *r* on the misfit parameter *f* are shown in Fig. 10 which are nu-

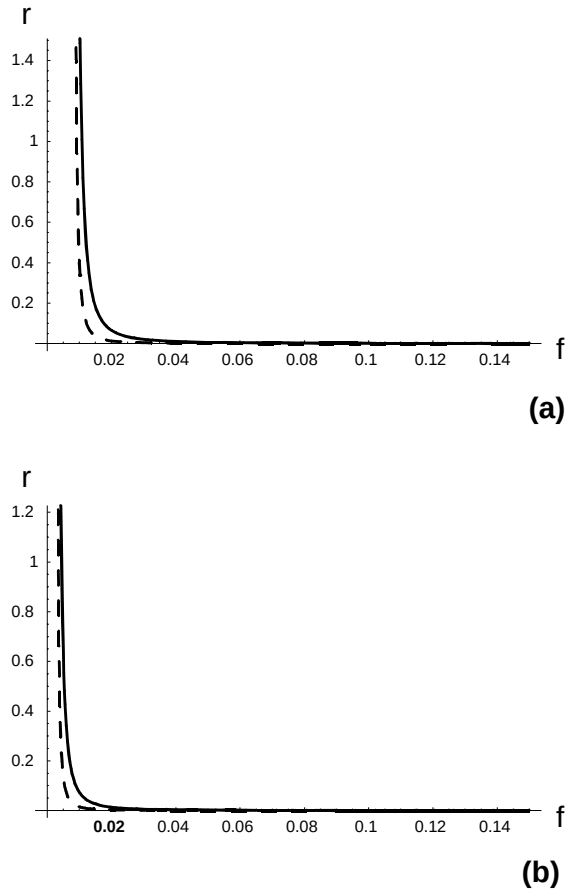

Fig. 10. Dependences of r on misfit parameter f, for (a) h=100 nm and (b) h=500 nm. Solid curves correspond to l = 5 nm, and dashed curves to l = 15 nm.

merically calculated with the help of formulae (13) and (14), for the following values of parameters: ν = 0.3; h = 100 nm and 500 nm; B = 0.4 nm; b = 0.04 nm; l = 5 nm and 15 nm and L = 50 nm and 150 nm, respectively.

The dependences $r(f)$ shown in Fig. 10 allow us to conclude that the generation of grain boundary misfit dislocations at interphase boundaries between nanocrystalline films and single crystalline substrates (Fig. 9) is more energetically favourable and, therefore, more effective in relaxation of misfit stresses than the generation of perfect misfit dislocations in wide ranges of the parameters of film/substrate systems. This conclusion which entails from our theoretical analysis is supported by data of experiments dealing with measurements of residual stresses in nanocrystalline films and coatings. So, as noted in paper [50], residual stresses are low in nanocrystalline cermet coatings (synthesized by thermal spray methods at highly non-equilibrium conditions), resulting in a capability for producing very thick coatings. So, nanocrystalline coatings were fabricated up to 0.65 cm thick and could probably be made with arbitrary thickness [50]. At the same time, in a conventional polycrystalline cermet coating, stress buildup limits coating thickness to typically 500-800 μm. This is naturally explained as the fact caused by a misfit stress relaxation micromechanism (in our model, the formation of grain boundary misfit dislocations) which comes into play in namely nanocrystalline films and coatings, and is different from and more effective than the standard micromechanism, the formation of perfect misfit dislocations.

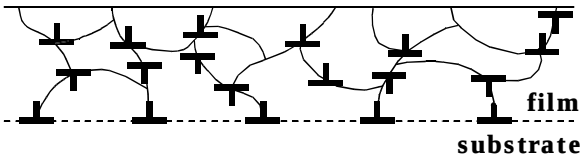

Fig. 11. Grain boundary dislocations and their dipoles as misfit defect configurations in nanocrystalline film.

We have considered the role of grain boundary dislocations with identical Burgers vectors as misfit defects in nanocrystalline films. However, in general, grain boundary dislocations with various Burgers vectors are generated in real nanocrystalline films fabricated at highly non-equilibrium conditions. As with ensembles of dislocations with identical Burgers vectors (Fig. 7), configurations of dislocations with various Burgers vectors are capable of effectively contributing to accommodation of misfit stresses in nanocrystalline films. In particular, dislocation dipoles (Fig. 11) can play the role of misfit defect configurations in nanocrystalline films [51]. This statement is indirectly supported by the experimentally detected fact that misfit dislocation dipoles exist in a single crystalline GaInP film deposited onto a GaAs substrate [52]. Also, dislocation dipoles are recognized as typical misfit defect configurations in capped single crystalline films [53].

The scenario for the formation of dipoles of grain boundary dislocations as misfit defects in nanocrystalline films fabricated at highly non-equilibrium is the same as for the formation of isolated grain boundary dislocations as misfit defects. That is, the dislocation dipoles are typical elements of ensemble of non-equilibrium grain boundary dislocations in as-synthesized nanocrystalline films. The evolution of dislocation dipoles in nanocrystalline films is strongly influenced by misfit stresses. For instance, let us consider the dipoles consisting of

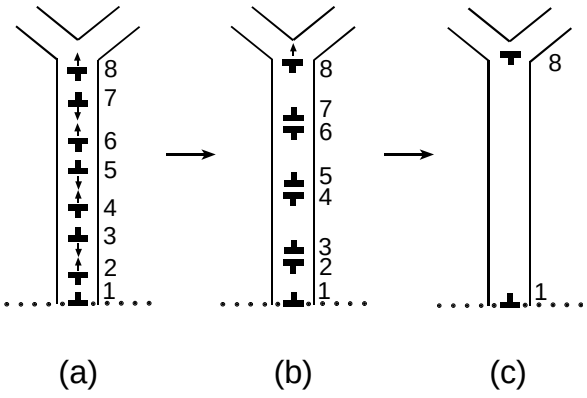

Fig. 12. Evolution and annihilation of dislocation dipoles in nanocrystalline film.

non-equilibrium dislocations which are most sensitive to the action of misfit stresses. Such dislocations are characterized by Burgers vectors parallel with the film/substrate boundary plane (Fig. 12). With misfit stresses in the film assumed to be tensile, the dislocations with positive (negative, respectively) Burgers vectors accommodate (intensify, respectively) the misfit stresses and tend to move towards the interphase boundary (the film free surface, respectively). This occurs due to the elastic interaction between the misfit stresses and the dislocations; for details, see [51].

The moving dislocations which belong to various dipole configurations interact and annihilate, causing transformations of dislocation dipoles. For illustration, let us consider evolution of the four dipoles, 1-2, 3-4, 5-6 and 7-8, in a grain boundary of a nanocrystalline film (Fig. 12). The evolution occurs through the motion of the upper dislocations of the dipoles towards the film free surface. In doing so, the upper dislocations meet the lower dislocations (with opposite Burgers vectors) belonging to their neighbouring dipole configurations, that climb towards the film/substrate boundary. The dislocations with opposite Burgers vectors annihilate, in which case the four dislocation dipoles, 1-2, 3-4, 5-6 and 7-8, transform into one dipole consisting of dislocations 1 and 8 (Fig. 12). Thus, evolution of dislocation dipoles in nanocrystalline films is naturally realized as their expansion accompanied by absorption of neighbouring dislocation dipoles (Fig. 12). In general, the upper dislocation 8 of the dipole (Fig. 12c) can reach the film free surface where it diappears. This process results in transformation of a dislocation dipole configuration into a single dislocation. The energetic conditions of expansion of dislocation dipoles and their transformations into single dislocations have been considered in paper [51].

Thus, generation of dislocation dipoles at grain boundaries is an effective micromechanism for relaxation of misfit stresses in nanocrystalline films. Both formation and evolution of dislocation dipoles are capable of occuring via re-arrangement and annihilation of “non-equilibrium” grain boundary dislocations in nanocrystalline films fabricated at highly non-equilibrium conditions. The dislocation dipoles often are unstable relative to their transformations into single dislocations and, therefore, exist in only as-synthsized nanocrystalline films.

6. MISFIT DISCLINATIONS IN NANOCRYSTALLINE AND POLYCRYSTALLINE FILMS

Parallel with “non-equilibrium” dislocations, the so-called grain boundary disclinations (rotational defects) are generated in nanocrystalline and polycrystalline materials synthesized at highly non-equilibrium conditions [43,54-56]. Such disclinations, after some relaxation period, annihilate in the absence of sources of long-range stresses affecting the grain boundary phase evolution. In nanocrystalline and polycrystalline films containing grain boundary disclinations the misfit stresses (generated at film/substrate interfaces) influence evolution of disclinations. More precisely, in the general situation, the low-energy (equilibrium) state of a nanocrystalline film is expected to correspond to the existence of not only some residual “non-equilibrium” dislocations, but also some residual grain boundary disclinations that play the role as misfit defects (Fig. 13). In this section we, following [46, 57, 58], will briefly discuss the behavioral peculiarities of nanocrystalline and polycrystalline films with grain boundary disclinations as misfit defects.

So, a new micromechanism for relaxation of misfit stresses, namely the formation of misfit disclinations (Fig. 13) [46, 57-61] is an alternative to the formation of misfit dislocation rows (Fig. 2c). The disclination micromechanism is theoretically revealed as that capable of effectively contributing to relaxation of misfit stresses in crystalline films with twin boundaries (see models and experimental data [59, 60]), crystalline films deposited on amorphous substrates [46, 57, 61] as well as nanocrystalline and polycrystalline films (Fig. 13) [46, 57, 58]. The disclination (rotational) mechanisms of misfit strain accommodation realized through the formation of disclinations or disloca-

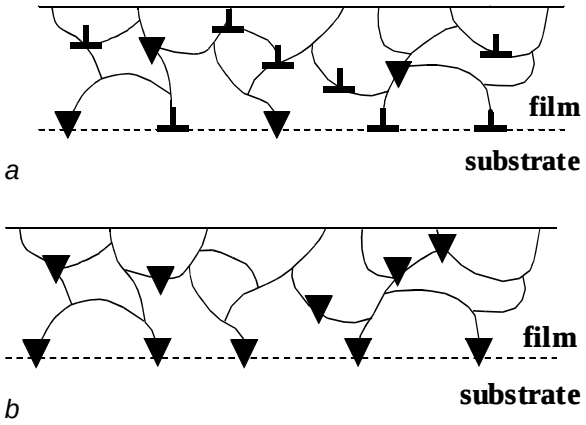

Fig. 13. Grain boundary dislocations and disclinations as misfit defects in nanocrystalline film. (a) Mixed ensemble of grain boundary dislocations and disclinations playing the role of misfit defects. (b) Grain boundary disclinations as misfit defects in nanocrystalline film.

tion walls have been observed experimentally [62-66].

Owing to the presence of the grain boundary phase in nanocrystalline and polycrystalline films, namely grain boundary disclinations play the role as misfit disclinations in such films (Fig. 13). The specific feature of the disclination micromechanism for relaxation of misfit stresses in nanocrystalline and polycrystalline films is that cores of grain boundary disclinations playing the role as misfit defects are located at existent grain boundaries (either at boundaries in film interior or at junctions of interphase and grain boundaries) and, therefore, do not induce any extra violations of the interphase boundary structure. The disclination micromechanism for relaxation of misfit stresses is of particular importance in nanocrystalline films, because grain boundary disclinations are intensively generated in nanocrystalline materials synthesized at highly non-equilibrium conditions (see, e.g., [54]) and because the volume fraction of the grain boundary phase is extremely high in nanocrystalline films.

Any real interface between a nanocrystalline or polycrystalline film and a single crystalline substrate consists of many fragments each dividing the substrate and a grain of the film (Fig. 3). Different fragments of the interface are characterized by different misorientation parameters, in which case the interface serves as a source of spatially inhomogeneous stress fields associated with a spatially inhomogeneous distribution of its misorientation along the interface plane. In general, some fragments of

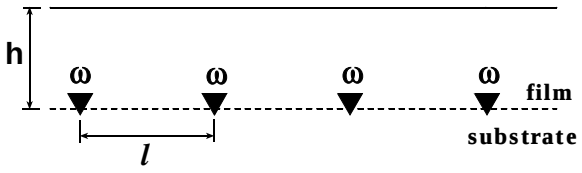

Fig. 14. Model of interphase boundary with misfit disclinations.

the interface can be incoherent due to their "unfavourable" misorientation destroying the coherency of the interface [46]. The main subject of this section – the disclination micromechanism for relaxation of misfit stresses – is related to the role of interfaces as spatially homogeneous sources of misfit stresses generated due to the geometric mismatch between lattice parameters of the adjacent crystalline phases. With this taken into account, in order to distinguish the effects associated with misfit stresses, here we will not consider any aspects related to spatially inhomogeneous distributions of misorientation that characterize interfaces between nanocrystalline or polycrystalline films and single crystalline substrates. In doing so, in this section we, following [57, 58], will focus our consideration on a model of interface as a semi-coherent interface which induces misfit stresses and contains misfit disclinations at junctions of grain boundaries and the interface (Fig. 14). For simplicity, misfit disclinations are assumed to be arranged periodically (Fig. 14) and to be characterized by identical value, ω, of the disclination strength.

In the framework of the model discussed, Kolesnikova *et al* [58] have calculated the basic characteristics (stored elastic energy density, equilibrium residual strain, critical values of film thickness) of a film with misfit disclinations. According to these calculations, the difference, $\Delta E = E_{discl} - E_{coher}$, between the energy densities of the interphase boundary with misfit disclinations and the coherent interphase boundary is as follows:

$$\Delta E = \frac{G}{2\pi(1-\nu)}\omega^2 l\Phi\left(\frac{h}{l}\right) - \frac{G}{2\pi(1-\nu)}\omega f\pi\frac{h^2}{l}, \quad (15)$$

where h denotes the film thickness, l the distance between neighbouring disclinations (or, in other words, period of the misfit disclination array), G the shear modulus, ν the Poisson ratio, f the misfit parameter (defined as $f = |a_2 - a_1|/a_2$, with a_1 and a_2 being the crystal lattice parameters of the substrate and the film, respectively), and

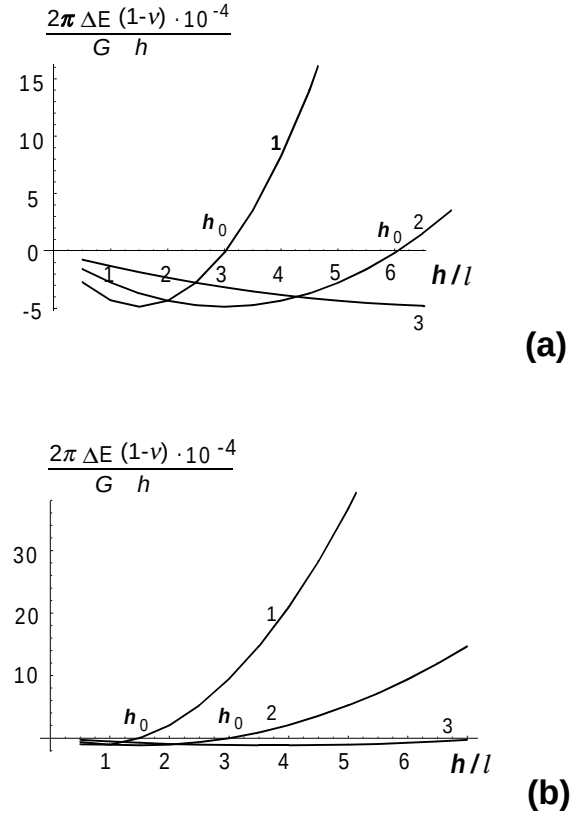

Fig. 15. Dependences of energy difference ΔE (in units of $2\pi(1-\nu)/Gh$) on film thickness h (in units of l), for misfit parameter (a) f = 0.01, and (b) f = 0.005. Curves 1, 2 and 3 correspond to values of disclination strength ω = 0.01, 0.005 and 0.002, respectively.

$$\phi = \int_{-\tilde{h}}^{0}\left[\frac{1}{2}\ln\frac{\cosh 2\pi(\tilde{x}+\tilde{h})-1}{\cosh 2\pi(\tilde{x}-\tilde{h})-1}+\right.$$
$$\pi(\tilde{x}+\tilde{h})\frac{\sinh 2\pi(\tilde{x}+\tilde{h})}{\cosh 2\pi(\tilde{x}-\tilde{h})-1}-$$
$$\pi(\tilde{x}+3\tilde{h})\frac{\sinh 2\pi(\tilde{x}-\tilde{h})}{\cosh 2\pi(\tilde{x}-\tilde{h})-1}- \qquad (16)$$
$$\left.4\pi^2\tilde{x}\tilde{h}\frac{1}{\cosh 2\pi(\tilde{x}-\tilde{h})-1}\right](\tilde{x}-\tilde{h})d\tilde{x},$$

with $\tilde{h} = h/l$. If $\Delta E < 0$ (>0, respectively), the formation of misfit disclinations at the interphase boundary (Fig. 14) is energetically favourable (unfavourable, respectively).

From (15) it follows that the characteristic energy of difference ΔE depends on four parameters of the film with misfit disclinations at the interphase boundary: disclination strength ω, the misfit parameter f, the film thickness h and the distance l between neighbouring disclinations. Analysis [58] of the relationships (given by formula (15)) between ΔE, ω, f, h and l shows the following. The critical thickness for generation of misfit disclinations in nanocrystalline and polycrystalline films is 0, if disclination strength ranges from 0 to some value ω_0 denoted as the optimum disclination strength. More precisely, the formation of misfit disclinations is more energetically favourable (ΔE <0) than the coherent state of the interphase boundary at any value of the film thickness, below some value h_0 denoted as the optimum thickness (Fig. 15). (It is contrasted to the situation with "conventional" misfit dislocations (see, e.g., [12-16]) whose formation in a thin film is energetically favourable compared to the coherent state, only if the film thickness exceeds some critical value.) As a corollary, the new micromechanism for relaxation of misfit stresses - generation of misfit disclinations – serves as an effective alternative to the standard micromechanism – generation of misfit dislocations – in polycrystalline and nanocrystalline films characterized by low values of film thickness, in particular, in films with nano-scaled thickness. The effective action of the disclination micromecheanism for relaxation of misfit stresses in nanocrystalline films can be responsible for experimentally observed fact that residual stresses are low in nanocrystalline cermet coatings synthesized by thermal spray methods (see discussion in paper [50] and previous section).

In the framework of the model discussed here, efficiency of misfit disclinations as defects causing relaxation of misfit stresses decreases with film thickness. Either the coherent state of interphase boundary or the formation of (conventional or grain boundary) misfit dislocations is more energetically favourable than the formation of misfit disclinations in films with thickness exceeding the optimum thickness discussed.

The micromechanism for relaxation of misfit stresses, examined in this section, is based on the concept of disclinations, which has been effectively used also in theoretical description of glassy structures (e.g., [67, 68]), grain boundary structures [69-72], solid state amorphizing transformations [73, 74], and plastic deformation processes in solids (e.g., [43, 55, 56, 75-78]). In this context, the model considered here, from a methodological viewpoint, serves as one more example of the effective application of the disclination theory in materials science and solid state physics.

7. MISFIT DISLOCATIONS AT INTERFACES IN FILM/SUBSTRATE COMPOSITES OF WIRE FORM

Intensive experimental and theoretical studies commonly deal with plate-like composite solids, e.g. [12-16]. However, in parallel with plate-like composites, film/substrate composites of wire form are conventional functional elements used in contemporary high technologies. In most cases films in such composites are polycrystalline. The cylindrical geometry of wire composites causes MDs in such composites to exhibit behavior which is, in general, different from commonly studied behavior of interfaces in platelike composites. In this section we, following [79], will consider a first approximation model of MDs in film/substrate composites of wire form and theoretically analyze (by methods of elasticity theory of defects in solids) the effect of geometric parameters of such composites on generation of MDs.

According to [79], a wire composite (consisting of a wire substrate covered by either a thin or thick film) is modeled as a composite cylinder with radius R_2 and infinite length. The model cylinder is composed of an internal cylinder (substrate) of radius $R_1<R_2$ and a film of thickness $H=R_2-R_1$, which envelops the internal cylinder as shown in Fig. 16. In the framework of the first approximation model, we will not take into account the crystallography of the adjacent film and substrate, in which case the interphase (film/substrate) boundary is treated as a surface of the internal cylinder (Fig. 16). (That is, there are no facets at the interphase boundary). Also the polycrystalline (or nanocrystalline) structure of films in wire composites is not directly taken into account in the model discussed. However, since films in wire composite solids often are polycrystalline, we include this model into the list of models dealing with polycrystalline films.

The film and substrate are assumed to be isotropic solids having the same values of the shear modulus G and the same values of Poisson ratio ν. The film/substrate boundary is characterized by the misfit parameter

$$f = \frac{2(a_2 - a_1)}{a_2 + a_1}, \qquad (16)$$

where a_1 and a_2 are the crystall lattice parameters of the substrate and the film, respectively.

Misfit stresses occur in film/substrate composite solids due to the geometric mismatch characterized by f at interphase boundaries between crystalline lattices of films and substrates. In most cases, a partial relaxation of the misfit stresses is realized via generation of MDs; see, e.g, reviews [13-16]. Let us consider MDs in the situation discussed (Fig. 16). Since the crystallography of the adjacent film and substrate is not taken into account, MDs, if they are formed, are supposed to be regularly distributed along the interphase boundary at thermodynamic equilibrium (Fig. 16) and to have Burgers vectors as shown in Fig. 16. In the framework of our model, MDs are of the edge type; their lines are parallel with the axis of the composite cylinder (Fig. 16).

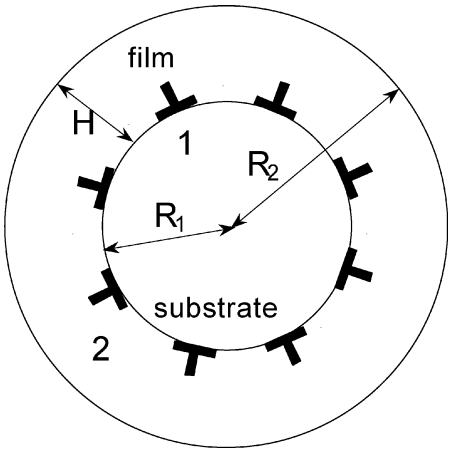

Fig. 16. Misfit dislocations at the interphase boundary in a model wire composite.

Let us analyze the conditions at which the generation of MDs at the interphase boundary is energetically favourable in a wire composite solid. The same problem in the situation with two- and multilayer plate-like composites is commonly solved via both a calculation of the elastic energy density of MDs and its minimization with respect to the MD ensemble density; see, e.g. [12-16]. Here we will use the other calculation scheme suggested by Gutkin and Romanov [32] for an analysis of MD generation in a thin two-layer plate. This scheme is based on a comparison of energetic characteristics of two physical states realized in a composite solid, namely the coherent state with MD-free interphase boundary and the semi-coherent state with the interphase boundary containing one ("first") MD, which accommodates, in part, the misfit stresses. Thus, the wire composite in the coherent (MD-free) state is characterized by the total elastic energy (per unit length of the composite) being equal to the misfit strain energy W^f related to misfitting at the interphase boundary only. When one (first) MD is generated at the interphase boundary in the wire composite, its total energy W consists of the four terms:

$$= W^{f} + W^{d} + W^{c} + W^{int}, \quad (17)$$

where W^{d} denotes the elastic energy of the MD, W^{c} the energy of the MD core, and W^{int} the elastic energy associated with the elastic interaction between the MD and the misfit stresses. The generation of the first MD is energetically favourable, if it leads to a decrease of the total energy, that is, if W-W^{f}<0. With formula (17) taken into account, we come to the following criterion for the generation of the first MD to be energetically favourable:

$$^{d} + W^{c} + W^{int} < 0. \quad (18)$$

In the framework of the model discussed, Gutkin *et al* [79] have calculated the ranges of values of wire composite parameters (wire substrate radius R_1, film thickness H, and misfit parameter f) at which inequality (18) is valid. According to these calculations, there is the following criterion for the generation of MDs in a wire composite to be energetically favourable:

$$f > f_c(R_1, H), \quad (19)$$

where

$$f_c(R_1,H) = \left(1+\frac{h(h-2)(h-r_0)(h-2-r_0)[2h(h-2-r_0)-1+2r_0]}{2[h^2-(2+r_0)h+r_0]^2} + \ln\frac{h(2-h+r_0)}{r_0}\right)\frac{b}{4\pi(1+\nu)R_1h(2-h)}. \quad (20)$$

In equation (20), $h=H/R_2$ and $f_c(R_1, H)$ is the critical misfit above which an MD is favoured to nucleate.

In general, the following three situations can occur depending on the relationship between the substrate radius R_1 and film thickness H:

(*I*) Thin film ($H << R_1$). In this situation, the energetic criterion for the generation of MDs entails from both equation (19) and the relationship $R_1/H >> 1$. The generation of MDs is energetically favourable at interphase boundaries, if the film thickness is higher than the critical thickness H_c derived from the equation

$$1-\frac{2H_c(H_c-r_c)}{(2H_c-r_c)^2}+\ln\frac{2H_c-b}{r_c} = 8\pi(1+\nu)f\frac{H_c}{b}. \quad (21)$$

This equation for the critical thickness of a thin wire film coincides with that for the critical thickness of a thin plate-like film.

(*II*) Small cylindrical substrate ($H >> R_1$). In this situation, the energetic criterion for the generation of MDs is caused by both equation (19) and the relationship $R_1/H << 1$. So, the generation of MDs is energetically favourable, if

$$H < b\exp\left(4\pi(1+\nu)f\frac{R_1}{b}+\frac{1}{2}\right), \quad (22)$$

that is, if the film thickness is lower than some critical thickness. Inequality (22) can be rewritten as follows:

$$R_1 > \frac{\left(\ln\frac{H}{b}-\frac{1}{2}\right)b}{4\pi(1+\nu)f}. \quad (23)$$

Formula (23) is indicative of the fact that the generation of MDs is energetically favourable, if the substrate radius R_1 is higher than some critical radius.

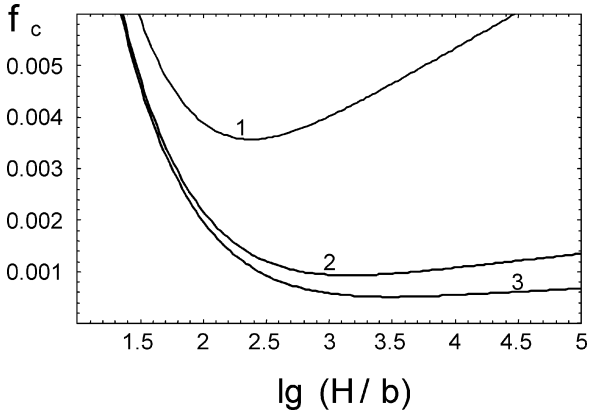

Fig. 17. The dependences of critical misfit parameter f_c on lg (H/b). Curves 1, 2 and 3 correspond to substrate radius R_1=100 b, 500 b, and 1000 b, respectively.

(*III*) Substrate radius and film thickness are of the same order ($R_1 \approx H$). In this situation, the following cases can be realized depending on the parameters of a wire composite: (*III a*) Generation of MDs is energetically unfavourable at any value of the film thickness. (*III b*) Generation of MDs is energetically favourable, if the film thickness H is in some range, that is, if $H_{c1} < H < H_{c2}$. Also, it should be noted that the formation of MDs is energetically unfavourable in wire composites with misfit parameter f lower than some misfit parameter f_0 depending on the substrate radius R_1 ($f < f_0(R_1)$). In order to reveal the character of dependences of H_{c1}, H_{c2} and f_0 on R_1, the functions f_c (R_1,H) are calculated and shown in Fig. 17. From Fig. 17 it follows that f_0 in-

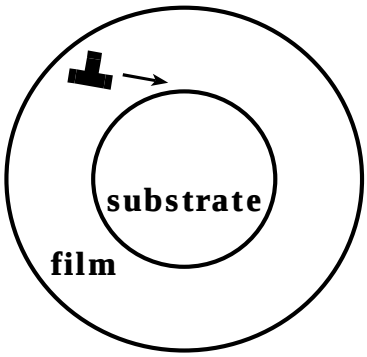

Fig. 18. Nucleation of a dislocation at a free surface and its consequent motion to the interphase boundary.

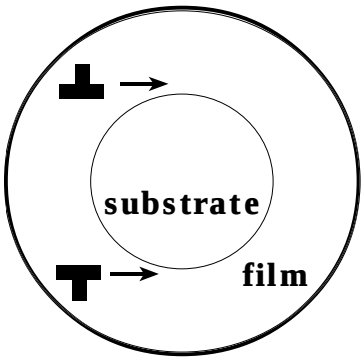

Fig. 19. Nucleation of a dislocation dipole at a free surface and its consequent motion to the interphase boundary.

creases, and the interval $[H_{c1}, H_{c2}]$ decreases when R_1 decreases. As a corollary, wire composites tend to be free from MDs when the substrate radius R_1 decreases. In contrast, f_0 decreases, H_{c1} decreases, and H_{c2} increases with growth of R_1 (see Fig. 17). In the limiting case with $R_1 \to \infty$, we find that $f_0 \to 0$ and $H_{c2} \to \propto$.

Finally, let us briefly discuss possible mechanisms for generation of MDs in wire composites. One of the most effective mechanisms in questions, as with the situation with conventional plate-like composites, is nucleation of edge dislocations at a free surface of a wire composite and their consequent motion (gliding plus climbing) to the interphase boundary (Fig. 18). In this situation, orientation of Burgers vectors of MDs at the interphase boundary relative to cylindrical surface of the boundary is rather arbitrary, because glide planes of the film intersect the interphase boundary surface at widely varied angles. (This is in contrast to MDs in conventional platelike composites where glide planes of the film intersect a plane interphase boundary at fixed angles). Other possible mechanisms for generation of MDs in a wire composite, that are analogies of such mechanisms in conventional platelike composites, are as follows: gliding of dislocations from internal dislocation sources to the interphase boundary; nucleation of dislocation semi-loops at a free surface and their consequent expansion and motion to the interphase boundary; and formation of partial MDs and their consequent merging into perfect MDs. Action of the mechanisms for generation of MDs is sensitive to geometry of a wire composite and, in general, is different from that in conventional platelike composites. More than that, there are mechanisms which are realized in only wire composites. For instance, nucleation of a dislocation dipole at a free surface and its consequent motion to the interphase boundary (Fig. 19) is effective in only wire composites. In doing so, stress fields of the dislocations composing the dipole (Fig. 19) screen each other. As a corollary, the energetic barrier for nucleation of the dipole and its motion near the free surface is lower than that in the situation with an isolated dislocation (Fig. 18).

To summarize, the results [79] of theoretical examinations of MDs at interfaces in wire composite solids, in short, are as follows:

(i) As with the commonly studied situation with platelike film/substrate composites, generation of MDs is energetically favourable in wire composites when their geometric parameters are in certain ranges.

(ii) The set of geometric parameters crucially affecting the generation of MDs in wire composites contains the wire composite radius R_2, the film thickness H, and the misfit parameter f.

(iii) The cylindrical geometry of film/substrate wire composites and finiteness of their substrate radii cause the generation of MDs (as an energetically favourable process) to be limited in such composites as compared with platelike film/substrate composites having semi-infinite substrates. More precisely, in wire composites, at sufficiently small values of their misfit parameter f and internal radius R_1, MDs are not generated at any film thickness, whereas in composites with platelike semi-infinite substrates, there always exists a critical thickness above which MDs may be formed.

These results are important for technological applications of wire composites. In particular, point (iii) is worth noting in context of a technologically interesting possibility of exploiting wire composites

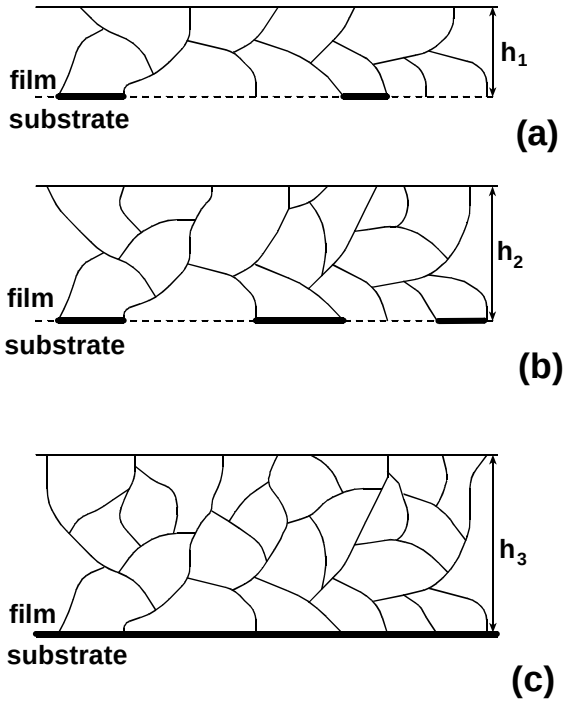

Fig. 20. Coherent to incoherent transformation of interphase boundary fragments with increase of film thickness *h*. (a) $h = h_1$, (b) $h = h_2$, (c) $h = h_3$, where $h_1 < h_2 < h_c$, and $h_3 > \tilde{h}_c$.

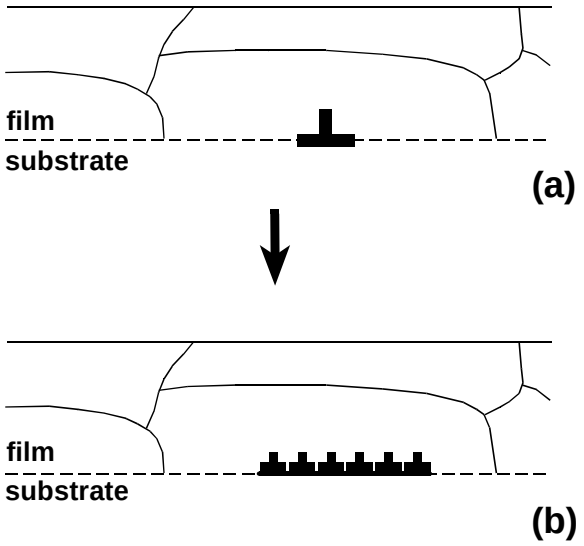

Fig. 21. Splitting of (a) initially perfect misfit dislocation into (b) extended dislocation with delocalized core results in formation of incoherent fragment (delocalized dislocation core) of interphase boundary.

with thin films instead of platelike composites (if it is admissible). Actually, both a large value of the thin film thickness and the coherency of interphase boundaries are often highly desired from an applications viewpoint. In these circumstances, in order to exploit high functional properties of film/substrate composites with comparatively large values of *H* and coherent interphase boundaries, one can use wire composites instead of platelike ones (if it is admissible).

8. PARTLY INCOHERENT INTERFACES

An interphase boundary between a single crystalline substrate and a nanocrystalline (or polycrystalline) film is featured by the existence of many boundary fragments bordered by junctions of the interface boundary and grain boundaries of the nanocrystalline film. In these circumstances, one of the effective micromechanisms for misfit stress relaxation that are specific for nanocrystalline film/substrate systems is the formation of a partly incoherent interface, a partly incoherent interphase boundary (Figs. 3 and 20) [46]. Each such a partly incoherent interface consists of both coherent and incoherent fragments and is characterized, in the first approximation, by a modified misfit parameter, $\tilde{f} = f(1 - \delta)$, depending on the ratio, $\delta = l_i/l_c$, of the sum length, l_i, of the incoherent fragments to the sum length, l_c, of the coherent fragments. In general, when the thickness, *h*, of a film increases resulting in an increase in the elastic energy, this energy effectively relaxes via generation of new incoherent fragments (Fig. 20). In these circumstances, a nanocrystalline or polycrystalline film is characterized by a critical value, $\tilde{h}_c$, of its thickness (that characterizes transition of the interphase boundary from a partly incoherent state to completely incoherent.) That is, the formation of a completely incoherent interface is energetically favourable in films with thickness above $\tilde{h}_c$ (Fig. 20 c).

In paper [80] a theoretical model has been proposed describing partly incoherent interfaces with incoherent fragments treated as delocalized cores of MDs. In these circumstances, each incoherent fragment of an interphase boundary is characterized by Burgers vector "spread" along the fragment and can be resulted from the splitting of an initial perfect MD into extended dislocation with the delocalized core playing the role of the incoherent fragment (Fig.21). The formation of partly incoherent interphase boundaries effectively occurs in systems with low values of energy that characterizes incoherent matching (Fig. 2b) between the adjacent phases.

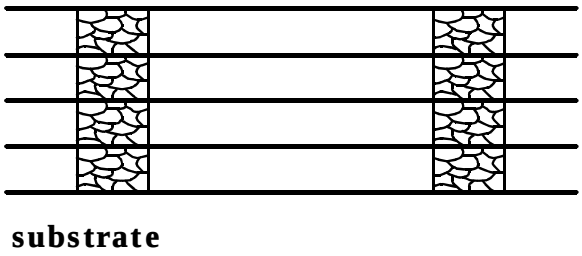

Fig. 22. Coatings with spatially variable structures containing single crystalline and nanocrystalline regions.

9. SOME TECHNOLOGICAL ASPECTS

The theoretical representations on interfacial structures inherent to nanocrystalline and polycrystalline films, discussed in sections 4-8, potentially can be used in both optimization of conventional technologies and design of new technologies for synthesis of films and coatings with desired properties. So, in the light of the representations under consideration, interphase boundaries strongly affect grain boundaries within nanocrystalline and polycrystalline films and vice versa. As a corollary, one can use technologies that control interphase boundary parameters in order to form grain boundary structures with desired properties in nanocrystalline and polycrystalline films. And, on the contrary, one can use technologies that control grain boundaries in order to form interphase boundaries with desired properties in nanocrystalline (or polycrystalline) film/substrate composite coatings.

In particular, effective relaxation of misfit stresses via formation of grain boundary defects in nanocrystalline films potentially allows one to design films and coatings with spatially variable stable structure which consists of single crystalline regions divided by ideal coherent boundaries and nanocrystalline regions causing effective relaxation of misfit stresses. In these circumstances, single crystalline regions with ideal coherent matching exhibit desired functional properties, while nanocrystalline regions play the role of structural elements that provide misfit stress relaxation (see, for instance, Fig. 22).

The coatings with spatially variable structures potentially can be synthesized, for instance, in a two-step manner. At the first step, a coating with the completely nanocrystalline structure is synthesized by conventional methods. At the second step, local heating can be used to induce local recrystallization processes that result in a desired spatially variable structure. This method can serve as a kind of nanolithography.

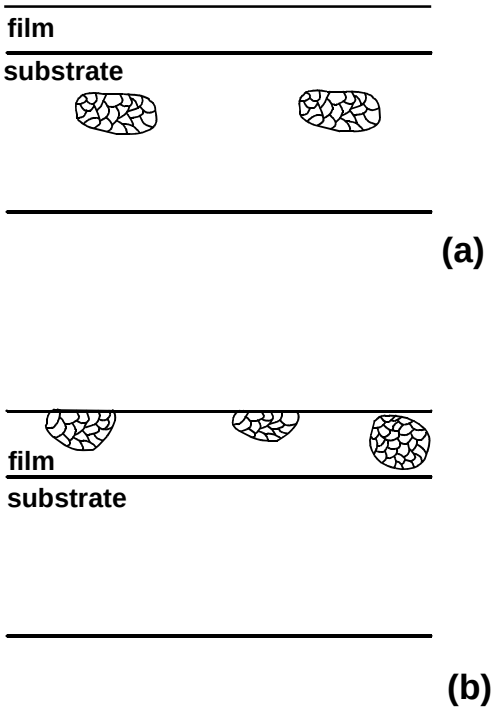

Fig. 23. Local nanocrystalline regions in film/substrate systems. Nanocrystalline regions are located in either (a) substrate or (b) film.

Also, local regions with the nanocrystalline structure in either film or substrate of a composite are capable of effectively contributing to misfit stress relaxation in the system, even if such nanocrystalline regions are located far from the interphase boundary (Fig. 23). This effect can be potentially used in technologies, too.

10. PARTIAL MISFIT DISLOCATIONS IN NANO-LAYERS

Now let us turn to a discussion of the specific structural and behavioral features of interphase boundaries in nano-layer/substrate composites (Fig. 1c). One of such features is the experimentally observed [81-85] enhanced formation of partial MDs (associated with stacking faults) in nano-layers. In this section we, following [49, 86], consider models describing generation and evolution of configurations of partial MDs associated with V-shaped stacking faults in nano-layer/substrate composites.

In general, MDs formed at film/substrate interfaces are either perfect (Fig. 2c) or partial (Figs. 21 and 24). Perfect MDs are characterized by Burgers vectors being crystal lattice vectors and

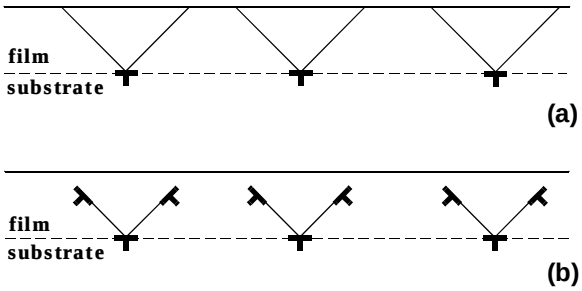

Fig. 24. Configurations of partial misfit dislocations in nano-layer/substrate composites: (a) single partial misfit dislocations associated with V-shaped stacking faults; and (b) complicately arranged configurations of partial misfit dislocations.

just locally, at dislocation line cores, violate the ideal crystalline structure, e.g., [21-40] (Fig. 2c). Partial MDs are characterized by Burgers vectors that commonly are lower than crystal lattice vectors and have line cores which bound plane stacking faults, in which case the ideal crystalline structure is violated at both line cores and plane stacking faults, e.g. [81-87] (Figs. 21 and 24). In most situations the formation of perfect MDs is more energetically favourable compared to partial MDs. Therefore, namely the perfect MDs are the traditional subject of theoretical and experimental studies. However, there are also film/substrate systems in which the formation of partial MDs is more favourable [81-87]. In particular, following theoretical analysis [49], the formation of partial MDs associated with V-shaped stacking faults is energetically favourable in film/substrate systems characterized by low values of film thickness and large misfit between crystal lattice parameters of film and substrate. This statement (supported by experimental data [85]) is highly interesting due to rapidly growing industrial needs in technologies exploiting nano-layer/substrate systems characterized by large misfit parameters.

Let us consider both generation and evolution of complicatedly arranged configurations of partial MDs, namely the experimentally observed [85] configurations each consisting of three partial MDs located at respectively top line and two edge lines that bound a V-shaped stacking fault in a film (Fig. 24b). In the limiting case where the partial MDs located at the edge line of the stacking fault reach the film free surface, a complicately arranged configuration (Fig. 24b) transforms into a simple configuration consisting of one partial MD at top of the V-shaped stacking fault, that connects film free surface and the film/substrate boundary (Fig. 24a). Such simple configurations of partial MDs have been observed in experiments [76].

Let us consider characteristics of complicately arranged configurations of partial MDs (Fig. 24b) in heteroepitaxial (nano-layer/substrate) systems (for details, see [78]). In doing so, for definiteness, we will focus our consideration on partial MDs in heteroepitaxial systems GaAs/Si (001) that are interesting for applications. One of important characteristics of a thin solid film is its critical thickness defined as the thickness at which the formation of MDs in film/substrate system becomes energetically favourable; see, e.g., [12-16]. In the situation discussed (Fig. 24b) the critical thickness h_c of a film is defined as the thickness at which the formation of one complicately arranged configuration of partial MDs is energetically favourable in the film.

Let us consider a model heteroepitaxial system consisting of an elastically isotropic semi-infinite crystalline substrate and an elastically isotropic thin film with thickness h. The shear modulus G and the Poisson ratio ν are assumed to be identical for the substrate and the film. For definiteness, hereinafter we confine our examination to the situation with one-dimensional misfit $f = (a_2 - a_1) / a_1 > 0$, where a_1 and a_2 are the crystal lattice parameters of the substrate and the film, respectively. In the initial state with a coherent interphase boundary, owing to the geometric mismatch between the crystalline lattices of the film and the substrate, the film is elastically uniformly distorted. It is characterized by the elastic strain $\varepsilon = - f < 0$.

Now let us turn to a consideration of the model heteroepitaxial system with a complicately arranged configuration of partial MDs (Fig. 25). Let the "top" partial MD be located at line (h,0) which bounds the top of V-shaped stacking fault, and the partial MDs of the 90 ° type be located at lines (d, $\pm s$) that bound edges of V-shaped stacking fault. Let the top MD be characterized by Burgers vector $\boldsymbol{b}$, and the "lateral" MDs be characterized by Burgers vectors $\boldsymbol{b}_{p1} = - \boldsymbol{b}_x - \boldsymbol{b}_y$ and $\boldsymbol{b}_{p2} = \boldsymbol{b}_x - \boldsymbol{b}_y$, respectively. For our further consideration, the lateral MD at line (d,s) (line (d,-s), respectively) can be effectively represented as the superposition of two edge dislocations with Burgers vectors $\boldsymbol{b}_y$ and $\boldsymbol{b}_x$ ($-\boldsymbol{b}_x$, respectively); see Fig. 25. The V-shaped stacking fault bounded by the top and lateral MDs (Fig. 25) is characterized by top angle 2α.

The elastic energy density (per unit of MD length) W^t of the system under consideration (Fig. 25) has the five basic constituents:

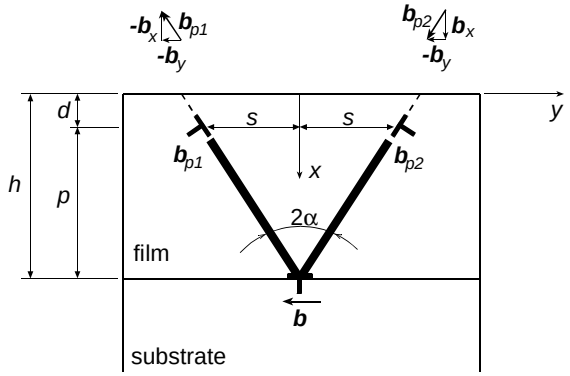

Fig. 25. Model of complicately arranged configuration of partial misfit dislocations.

$$^{t} = W^{f} + W^{n} + W^{fd} + W^{\gamma} + W^{d}, \quad (24)$$

Here W^{f} denotes the elastic energy density associated with the initial misfit; W^{n} the sum energy of MD cores; $b_p^2 = b_{p1}^2 = b_{p2}^2$; W^{fd} the sum energy density of interaction between the MDs and the elastic field of the initial misfit; W^{γ} the energy of stacking fault and W^{d} the elastic energy density of the complicately arranged configuration of MDs, which takes into account interaction between MDs and that between MDs and the film free surface. The critical film thickness h_c at which the formation of a complicately arranged configuration of MDs (Fig. 25) in a film becomes energetically favourable can be found from condition:

$$\Delta W = W^{t} - W^{f} = 0. \quad (25)$$

This condition, according to calculations [86], gives the following transcendental equation for h_c:

$$\begin{aligned}
&2b_p^2 - 8\pi f(1+\nu)(bh + 2b_y d) + \frac{8\pi\gamma(1-\nu)(h-d)}{G\cos\alpha} \\
&+b^2\left(1 - \ln\frac{b}{2h-b} - \frac{2h(h-b)}{(2h-b)^2}\right) - \\
&2bb_y\left(\ln\frac{(h-d)^2+s^2}{(h+d)^2+s^2} - \frac{2s^2}{(h-d)^2+s^2}\right. \\
&\left.+\frac{2(s^2+2dh)}{(h+d)^2+s^2} - \frac{8dhs^2}{[(h+d)^2]^2}\right) + \\
&2bb_x s\left(\ln\frac{2(h-d)}{(h-d)^2+s^2} - \frac{2(h-d)}{(h+d)^2+s^2}\right. \\
&\left.-\frac{8dh(h+d)}{[(h+d)^2+s^2]^2}\right) - \frac{4b_x b_y s d^3}{(d^2+s^2)^2} - \\
&-b_y^2\left(\ln\frac{b_y^2 s^2}{(d^2+s^2)(2d-b_y)^2} + \right. \\
&\left.\frac{4d(d-b_y)}{(2d-b_y)^2} - \frac{d^2(d^2+3s^2)}{(d^2+s^2)^2}\right) - \\
&-b_x^2\left(\ln\frac{b_x^2(d^2+s^2)}{s^2(2d-b_y)^2} + \frac{4d(d-b_y)}{(2d-b_y)^2}\right. \\
&\left.-\frac{d^2(3d^2+s^2)}{(d^2+s^2)^2}\right) = 0.
\end{aligned} \quad (26)$$

where γ is the stacking fault energy density (per unit area). Formula (26) allows one to analyze relationships between characteristics (critical thickness, misfit parameter) of nano-layer/substrate composites with perfect MDs (Fig. 2c), single partial MDs associated with V-shaped stacking faults (Fig. 24a) and complicately arranged configuration of partial MDs (Fig. 24b).

In particular, theoretical analysis [86] based on formula (26) shows the following. The formation of perfect MDs is energetically favourable in composites with comparatively small values of misfit parameter ($f < 0.01$). At the same time, during growth of the films (nano-layers) with comparatively large values of misfit parameter (tentatively $f > 0.01$), the formation of single partial MDs is energetically favourable, if the film thickness h is in the range: $h_c < h < h'_c$. In the situation discussed, when the film thickness h exceeds the critical value h'_c (which commonly is in the range of a few nm and decreases with increase of misfit parameter f), single partial MDs associated with V-shaped stacking faults (Fig. 24a) transform into complicately arranged configurations of partial MDs (Fig. 24b). Further growth of the film thickness leads to the merging of the three partial MDs (that compose a complicately arranged configuration) into a perfect MD at the interphase (film/substrate) boundary, in which case the stacking fault disappears.

The statement that partial MDs transform into perfect MDs during growth of films, resulted from theoretical analysis [86], is in agreement with experimental data [85]. These data are indicative of the fact that density of perfect MDs increases and density of partial MDs decreases with increase of film thickness.

It should be noted that, in general, configurations of partial MDs are capable of being generated in films, having top MDs in the film interior (Fig. 26). This phenomenon is important for tech-

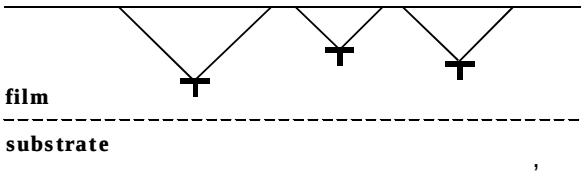

Fig. 26. Partial misfit dislocations associated with V-shaped stacking faults in film interior.

nological applications of heteroepitaxial systems with the functional properties of interphase boundaries, because the configurations in question (Fig. 26) do not violate the coherency of interphase boundaries and, as a corollary, do not cause degradation of their functional properties exploited in applications. Stability of such configurations relative to their transfer to interphase boundary depends on balance between the basic driving force (related to elastic energy release due to the transfer) and the basic hampering force (related to increase of the stacking fault area due to the transfer).

11. MISFIT STRAINS IN NANO-LAYERED COMPOSITE FILMS

Nano-layers often are used as elements of layered composite solids widely exploited in contemporary high technologies. Application of layered composite solids in micro- and nanoelectronics as well as in other areas of high technology commonly imposes strict demands on stability of their structure and properties. However, interphase boundaries as local structural imperfections (plane defects) and sources of misfit strains are capable of causing instability and degradation of the desired – from an applications viewpoint – properties of layered composites; see, e.g., [12-16, 88]. On the other hand, there are technologies which are based on the effects of microstructural and phase transformations at interphase boundaries in layered composites [88-94]. For instance, the effect of solid state amorphizing transformations occurring in multilayer coatings serves as the basis for synthesis of amorphous metallic alloys (in particular, amorphous alloys with specific chemical compositions that can not be obtained with the help of other technological methods of amorphous alloy synthesis); see, e.g., [88-92]. The significant role of interphase boundaries in processes occurring in layered composite solids is of great interest in experimental and theoretical studies of interphase boundaries and their contribution to the macroscopic properties of such solids. In such studies the most attention in

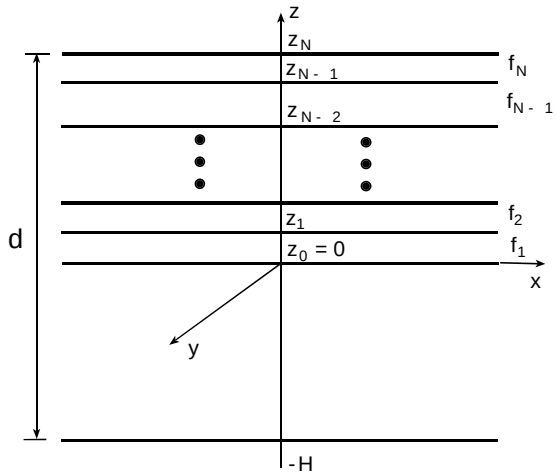

Fig. 27. A multilayer composite consisting of a substrate and *N* layers characterized by eigenstrains f_i.

theoretical studies has been paid to the analysis of interphase boundaries in two-layer systems (mostly film/substrate systems), these being the simplest representatives of layer composites [12-16].

The role of misfit strains (induced by interphase boundaries) in structural and phase transformations in layered composites depends, in general, on many macroscopic factors (e.g., geometric dimensions of composites, temperature) as well as microscopic parameters which describe structural and chemical peculiarities of composites and often cannot be directly identified by current experimental methods. As a corollary, at present, key micromechanisms and specific features of the structural and phase transformations in layered composites have not been unambiguously recognized in many cases. In this section we, following [95], will consider general formulae for misfit strains and the strain energy density in multilayered composites with coherent interphase boundaries. Sections 12 and 13 deal with models describing the effects of misfit strains on phase transformations in layered composites.

Let us consider a multilayered film deposited on a relatively thick substrate. Let *N* be the number of layers in the film (Fig. 27), *H* and h_i (i =1,…., *N*) be the substrate and *i*-th layer thicknesses, respectively, which have arbitrary magnitudes. In this situation, the total thickness of such a layered structure *d* is equal to $H + \sum_{i=1}^{N} h_i$, being assumed to be much smaller than other linear dimensions of the system. Let the misfit strain f_i be a characteristic eigenstrain (with respect to the substrate where the

eigenstrain is assumed to be equal to a zero value) for the *i*-th layer. For definiteness, we consider hereinafter only the case with f_i being a two-dimensional misfit strain which is uniform within the *i*-th layer. Also, let us assume that the outer surfaces of the multilayer composite (Fig. 27) are free of any external loading. The elastic properties of the substrate and layers are supposed to be identical. In these circumstances, according to calculations [95], the elastic strain distribution in a layered composite can be written in the form:

$$\varepsilon(z) = \sum_{i=1}^{N} f_i \left\{ \Theta(z - z_i) - \Theta(z - z_{i-1}) + \frac{h}{d^3}\left[d^2 + 3(H - z_N + 2z)\Psi_i \right] \right\}. \quad (27)$$

Here $\Psi_i = H - z_N + z_i + z_{i-1}$ and $\Theta(z)$ is the Heavyside function equal to 1, for $z > 0$, and 0, for $z < 0$; $z_i = \sum_{k=1}^{i} h_k$; $z_0 \equiv 0$.

To illustrate the result in question, let us consider two simple limiting cases.

First, let us discuss the case with $f_i \equiv f$ and $h_i \equiv h$ – that is, the case of a thin single-layer film specified by both the thickness $h' = Nh$ and the misfit eigenstrain *f*, and deposited on a thick substrate with the thickness *H*. In this case, the general formula (27) is reduced to the following expression:

$$\varepsilon(z) = f\left\{ -\Theta(z) + \frac{h'}{d} + \frac{3h'H(H-h')}{d^3} + \frac{6h'H}{d^3} z \right\}, \quad (28)$$

which is well known in the theory of heteroepitaxial systems [12-16].

Second, let us consider the case with $h_i \equiv h$ and $f_i \equiv f$, if i =1,3,….,*N*-1, and $f_i \equiv 0$, if i = 2,4,……,*N*, where *N* is an even number. This case corresponds to a superlattice deposited on a thick substrate. In the case discussed, the general expression (27) is transformed into the formula

$$\varepsilon(z) = f\left\{ \sum_{n=1}^{2(N-1)} (-1)^n \Theta[z - (n-1)h] + (N-1)\frac{h}{d}\left[1 + \frac{3}{d^3}[H + h(N-3)](H - Nh + 2z) \right] \right\}. \quad (29)$$

In the general situation ($\varepsilon(z)$ is given by (27)), the strain energy of the system (per a unit surface square) can be written as

$$= 2G\frac{1+\nu}{1-\nu}\int_{-H}^{z_N} \varepsilon^2(z)dz = 2G\frac{1+\nu}{1-\nu}\left\{ \sum_{i=1}^{N} f_i^2 h_i - \frac{1}{d^3}\sum_{i,j=1}^{N} f_i f_j h_i h_j (d^2 + 3\Psi_i\Psi_j) \right\}, \quad (30)$$

where *G* is the shear modulus.

In the first limiting case with $f_i \equiv f$, $h_i \equiv h$ and N = 1 (for simplicity), formula (30) gives

$$= 2G\frac{1+\nu}{1-\nu} f^2 h\left(1 - h\frac{d^2 + 3H^2}{d^3} \right), \quad (31)$$

From (31), for $h >> H \approx d$, we have the well known expression [12-16] for the misfit energy in the simplest case of a thin film on a semi-infinite substrate:

$$(h << H \approx d) \approx 2G\frac{1+\nu}{1-\nu} f^2 h. \quad (32)$$

The general expression (30) can be effectively used for analysis of various models of misfitting multilayer composites. The above approach can also be directly generalized to the situation with different elastic moduli of the layer and substrate materials.

12. EFFECT OF MISFIT STRAINS ON PHASE TRANSFORMATIONS AT INTERPHASE BOUNDARIES IN (NANO)LAYERED COMPOSITE FILMS

Let us consider with the help of general approach [95] discussed in the previous section a phase transformation occurring at the interphase boundary in a two-layer composite consisting of layers α and β. The phase transformation causes the pre-existing two-layer system to be transformed into the three-layer system with an intermediate layer (new phase) α–β (Fig. 28). Such phase transformations commonly result from diffusional mixing of atoms of the phases α and β; see e.g. [88-94]. In the context of this section, we will examine the new three-layer composite as a misfitting system (characterized by two misfit parameters) with special attention being paid to the role of misfit strains in initiating the intermediate layer formation – that is, the phase transformation at the interphase boundary in the pre-existing two-layer composite.

Let the thickness of the new three-layer system be $d = H + h$, in which case the new phase α – β forms the intermediate layer with the thickness *a* –

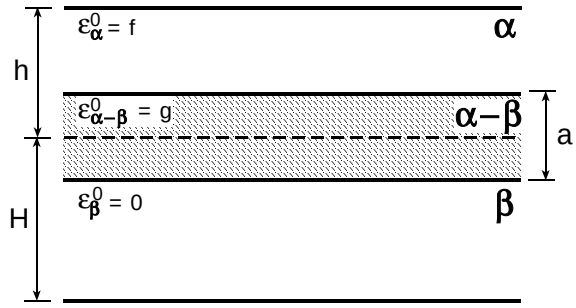

Fig. 28. A three-layer composite consisting of "edge" layers α and β and intermediate layer (new phase) α–β. The pre-existing interphase boundary α/β is shown as a dashed line.

that is, the layer between the initial film α and the substrate β characterized by respectively values $h - a/2$ and $H - a/2$, respectively, of the thickness (Fig. 28). Also, let us suppose that the eigenstrains of dilatation misfit are f and g respectively in the layers α and α – β relative to the layer β characterized by the eigenstrain $\varepsilon^0 \equiv 0$.

The strain energy density of the three-layer composite (Fig. 28) is given by formula (30) which can be re-written in the situation discussed as follows:

$$W_2^c = W_1^c + 2G\frac{1+\nu}{1-\nu}f^2 a\left\{\phi_0 + \phi_1\frac{a}{d} + \phi_2\left(\frac{a}{d}\right)^2 + \phi_3\left(\frac{a}{d}\right)^3\right\}, \quad (33)$$

where

$$\phi_0 = -\frac{1}{2} + \left(1 - 2\frac{g}{f}\right)\frac{h}{d}\left(1 + 3\frac{H(H-h)}{d^2}\right) + \frac{g^2}{f^2},$$

$$\phi_1 = -\frac{1}{4}\left(1 + 3\frac{H^2 + h^2 - 4Hh}{d^2}\right) + \frac{g^2}{f^2}\left(1 - \frac{g^2}{f^2}\right)\left(1 + 3\frac{(H-h)^2}{d^2}\right),$$

$$\phi_2 = -\frac{3}{4}\left(1 - 2\frac{g^2}{f^2}\right)\frac{H-h}{d},$$

$$\phi_3 = -\frac{3}{16},$$

and W_1^c is the strain energy density of the pre-existing composite consisting of layers α and β only (see formula (31)).

Formula (33) is indicative of the fact that the strain energy density W_2^c depends, generally speaking, in a non-linear way on the thickness a of the layer α – β as well as on the other parameters h, H, f and g of the three-layer composite. At the same time, in the limiting situation with infinitely thick substrate (H, $d \to \infty$), the dependence of $\Delta W^c = W_2^c - W_1^c$ on a is linear:

$$\Delta W^c \approx 2G\frac{1+\nu}{1-\nu}f^2 a\left(\frac{g^2}{f^2} - \frac{1}{2}\right).$$

In this situation, ΔW^c does not depend on the film thickness h and, as a corollary, the intermediate-layer formation is energetically favourable ($\Delta W^c < 0$) or unfavourable ($\Delta W^c > 0$) depending on the ratio g^2/f^2. More precisely, the formation in question is energetically favourable ($\Delta W^c < 0$) at $g^2/f^2 < 1/2$ – that is, at $|g| < |f|/\sqrt{2}$.

Now let us turn to the analysis of the situation with layers α and β having the same thickness – that is, $H = h$ and $d = 2h$. In this situation, $\phi_0 = -g/f + g^2/f^2$, $\phi_1 = 1/8 + g/f - g^2/f^2$, $\phi_2 = 0$, $\phi_3 = -3/16$, and, as a corollary,

$$W_2^c = W_1^c + 2G\frac{1+\nu}{1-\nu}f^2 a\left\{-\frac{g}{f} + \frac{g^2}{f^2} + \left(\frac{1}{8} + \frac{g}{f} - \frac{g^2}{f^2}\right)\frac{a}{d} - \frac{3}{16}\left(\frac{a}{d}\right)^3\right\}. \quad (34)$$

Here $W_1^c = \frac{G}{4}\frac{1+\nu}{1-\nu}f^2 h$.

Let us examine with the help of (34) the initial stage of the intermediate-layer formation. In doing so, we focus our attention on the situations with $f > g > 0$ or $-f < -g < 0$, because the formation of the intermediate layer in other situations leads to the increase of the misfitting of a layered composite and, therefore, is definitely unfavourable from an energetic viewpoint. The intermediate layer at the initial stage of its formation is characterized by the thickness $a << d$. This allows us to neglect the term proportional to $(a/d)^3$ on the r.h.s. of formula (34). In doing so, from the reduced version of formula (34) (with the aforesaid term omitted) it is entailed that the intermediate-layer formation is energetically favourable ($\Delta W^c < 0$), if $h > h_c$, the critical thickness

$$h_c \approx \frac{a}{2}\left(1 + \frac{f^2}{8g(f-g)}\right). \quad (35)$$

Formula (35), in particular, is indicative of the fact that there is a minimal critical thickness

$$h_{c,min} \approx \frac{3}{4}a, \qquad (36)$$

which corresponds to the situation with $g = f/2$. The critical thickness at $g \to 0$ is

$$h_c \approx \frac{a}{2}\left(1+\frac{f}{8g}\right),$$

and it decreases with increasing g and increases with increasing f. When $g \to f$,

$$h_c \approx \frac{a}{2}\left(1+\frac{f}{8(1-g/f)}\right),$$

and it increases with increasing g and decreases with increasing f.

Let us estimate numerically the value of h_c in the situation with nucleation of an intermediate layer – that is, the situation with the layer (as the layer of a new phase) characterized by the minimal thickness a_{min}. (The new phase should consist of, at least, several atomic layers, in which case a_{min} is commonly of the order of 1 nm.) Let the misfit parameter in the pre-existing two-layer system be $f = 0.01$. In these circumstances, for values of g = 0.008, 0.009 and 0.0099, from (36) we find the critical thickness $h_c \approx a_{min}$, $1.2a_{min}$, $500a_{min}$, respectively.

In our consideration, we have focused on the effect of misfit strains on phase transformations in layered composites. At the same time, in general, other factors also influence such transformations. First of all, the difference $W^{a\text{-}c}$ between free energy (or another thermodynamic potential) densities of the pre-existing phases (α and β) and a new phase (α – β) usually plays the important role in phase transformations in layered composites. In these circumstances, any comparison of the quantitative estimates (e.g., values of h_c and $h_{c,min}$, the dependence of ΔW^c and h_c on f and g) obtained in this subsection using experimental data as well as other theoretical estimates seems to be unreasonable, because many other factors should be taken into account. A detailed labour-consuming analysis of the contribution of $W^{a\text{-}c}$ to energetic characteristics of intermediate-layer formation (Fig. 28), as well as other factors (different from misfit strains) affecting phase transformations of all types in layered composite solids, are beyond the scope of our consideration. In the next section, we discuss the only type of such transformations – namely the solid state amorphizing transformations in layered composites, taking into account the misfit strain energy density and other energetic characteristics of the new phase – that are capable of influencing the amorphization processes.

13. EFFECT OF MISFIT STRAINS ON SOLID STATE AMORPHIZATION IN NANO-LAYERED COMPOSITES

Solid state amorphizing transformations occur in multilayer composite solids consisting of alternate layers, say, α and β, of elemental metals, e.g. [89-92]. In these circumstances, layers of the new amorphous alloyed phase α – β nucleate at α/β interfaces due to diffusional mixing of atoms α and β. Recently, it has been experimentally revealed that solid-state amorphization does not occur in Ni/Ti multilayer composites having the crystalline layer thickness in a composite below some critical thickness h_c^{am} (which is several nanometers) [92]. We think that this experimental fact gives evidence of a strict relationship between misfit strains (whose contribution to the energy of a composite is dependent on the layer thickness; see sections 11 and 12) and the amorphization processes. More precisely, in the context of our previous consideration of the intermediate-layer formation in a film α/substrate β system, the amorphization occurs as a process with relaxation of misfit strains contributing to its driving force. In this section, we will theoretically examine with the help of results obtained in 11 and 12 sections the effect of misfit strains on the solid-state amorphization in layered composites. In doing so, we also take into account both the energy density of crystal/glass interfaces resulting from the amorphization and the difference $W^{a\text{-}c}$ between the free energy densities of the (new) amorphous and (pre-existent) crystalline phases.

Let us consider the formation of an intermediate amorphous layer α – β in an initially two-layer system consisting of crystalline layers α and β (Fig. 28). The amorphous-layer formation is accompanied, in particular, by the occurrence of two crystal/glass interfaces. Following model [61] of crystal/glass interfaces, the total energy density E_i^{tot} of a crystal/glass interface can be represented as the sum of the two basic terms, E_i^{dil} and E_i^{dis}, which are related to the dilatation misfit (originating from the difference between the mean interatomic distance in the amorphous phase and crystal lattice parameters of the adjacent crystalline phases) and disorder-induced distortions (originated from distortions of the adjacent amorphous phase), respectively. In the context of our paper, in the theoretical exami-

nation of the amorphous-layer formation in a pre-existing two-layer crystalline composite, we will operate with dilatation misfit strains induced by crystal/glass interfaces and their energy density E_i^{dil} by means of methods developed in previous sections, in which case it is identified as the energy density W_2^c. At the same time, the energy density E_i^{dis} will be taken into account as a parameter contributing to the energetic criterion for the amorphous-layer formation (see below).

Let us consider the amorphous layer at the initial stage of its nucleation in a two-layer composite. It is characterized by the minimal thickness a_{min}, the dilatation misfit energy density W_2^c, and the energy density $E_{am}(a_{min})$ (per unit area) which is the sum of its proper free-energy density $W^{a\text{-}c}a_{min}$ and the energy density $2E_i^{dis}$ of two (new) crystal/glass interfaces ($E_{am}(a_{min}) = W^{a\text{-}c}a_{min} + 2E_i^{dis}$). The energy density $E_{am}(a_{min})$ is included in the energetic criterion for the amorphous layer formation, which is as follows:

$$\Delta W^c + E_{am}(a_{min}) < 0. \qquad (37)$$

With criterion (37) taken into account, we find after some analysis the following formula for the critical thickness h_c^{am}:

$$h_c^{am} \approx \frac{a}{2(1-E)}\left(1+\frac{f^2}{8g(f-g)}\right) = \frac{h_c^{cr}}{1-E}, \qquad (38)$$

where

$$E = \frac{E_{am}(1-\nu)}{2G(1+\nu)ag(f-g)} < 1 \qquad (39)$$

and h_c is given by formula (35). In general, h_c^{am} can take widely varying values, depending on E_{am}. In particular, the amorphization does not occur in composites with high values of E_{am} (and, therefore, high values of h_c^{am}).

Let us discuss the effect of the terms $W^{a\text{-}c}a_{min}$ and E_i^{dil} (which are treated here as parameters) on the amorphization. The traditional viewpoint on the solid-state amorphization in layered composites, which does not take into account misfit strains, is that the driving force for the amorphization is associated with a negative $W^{a\text{-}c}$ [89]. Within the framework of these representations, the amorphization occurs if $W^{a\text{-}c} < 0$, and does not occur if $W^{a\text{-}c} > 0$. However, recently, the amorphization has been experimentally observed in immiscible Y/Mo multilayer composites characterized by $W^{a\text{-}c} > 0$ [90]. This is indicative of the crucial effect of interfaces on the amorphization. In the paper [90], this effect was analyzed by the methods of thermodynamics, operating with the fraction of interfacial atoms as the key factor. However, the approach of [90] does not allow one to explain the experimentally revealed [92] existence of the minimal critical thickness h_c^{am} for the amorphization in Ni/Ti multilayer composites. As a corollary, in the context of the theoretical results [95] discussed here, we think that misfit strains play a very important role in the amorphization processes and should definitely be taken into account in any description of the processes in question.

14. MISFIT DISLOCATION WALLS IN (NANO)LAYERED COMPOSITE FILMS

MDs in one-layer films form various structures, depending on the film thickness, misfit parameter, characteristics of materials and crystallography of films and substrates as well conditions of the film deposition onto substrates (e.g., see reviews [13-16] and sections 4-7 of this review). Say, misfit stresses in high-T_c superconducting film/substrate systems characterized by low values of misfit parameter relax mostly via formation of planar rows of MDs [96]. As misfit parameter and/or the film thickness grow, one frequently observes low-angle boundaries in high-T_c superconducting films [96]. Following the model [41] describing misfit stress relaxation via formation of MD walls, that is, low angle boundaries (see also section 4 of this review), it is natural to relate the experimentally observed [96] formation of low-angle boundaries in cuprate one-layer films to the effective contribution of such boundaries – dislocation walls – to relaxation of misfit stresses. In this context, the special peculiarities of MD walls in multilayered films (with the composite structure being more complex than that of one-layer films) are of high interest.

In this section, we will consider a theoretical model [97] that describes the generation of the walls of complete edge MDs at the interfaces of the film composed of alternate layers (Fig. 29). Since the MD walls are terminated at the film/substrate interface, their end points serve as misfit disclinations, rotational defects. The rotational mechanisms of misfit strain accommodation realized through the formation of disclinations or dislocation walls in the case of one-layer film have already been observed experimentally [62-66] and analyzed theoretically [41,57-61] (see also sections 4 and 6 of this review). It has been demonstrated that misfit disclinations or MD walls can be generated at twin

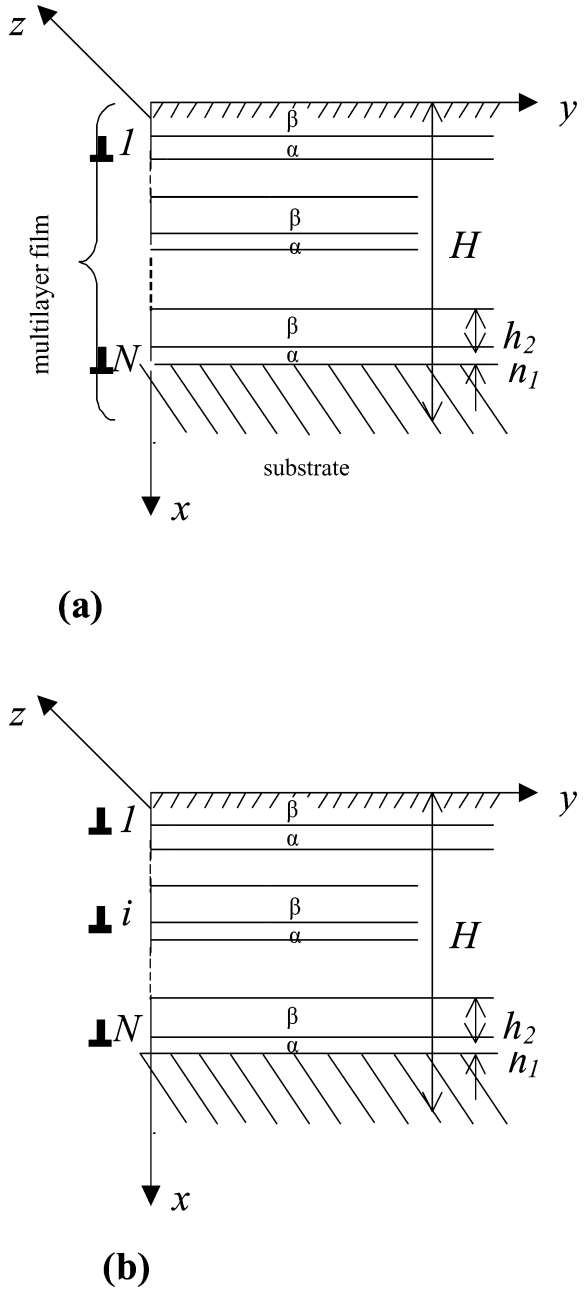

Fig. 29. Misfit dislocation walls in a multilayered film.

or grain boundaries, in single crystalline films on amorphous substrates and in nano- or polycrystalline films [41,57-66]. In multilayered films, dislocation walls can be formed by slip of dislocations from their sources. Let us consider, following [97], the conditions for the formation of a first (individual) MD wall in multilayered film. In doing so, for simplicity, we will suppose that dislocations composed the wall, are regularly spaced and separated from each other by a pair of alternate film layers.

Thus, let us consider a system that consists of a semi-infinite substrate and a multilayered film of thickness H comprised of N pairs of alternate layers α and β of thickness h_1 and h_2, respectively [$H = N(h_1 + h_2)$] (Fig. 29). The film and the substrate are supposed to be elastically isotropic solids and have the same values of the shear modulus G and the same values of the Poisson ratio ν. The misfit of the substrate, layers α and layers β crystal lattices is assumed to be dilatational and characterized by the misfit parameters $f_1 = (a_s - a_\beta)/a_s$ and $f_2 = (a_s - a_\beta)/a_s$ equal in the absence of MDs to the elastic strain within layers α and β, respectively. In the latter relation, a_s, a_α and a_β denote the crystal lattice parameters of the substrate, layers α and layers β. Let the misfit parameters f_1 and f_2 be positive, and the lines and Burgers vectors of the generated MDs be parallel to the film/substrate interface (Fig. 29).

To determine the necessary conditions for the formation of an MD wall, we will use the standard technique comparing the energies of the system with and without the wall. The energy W of the system with an MD wall extending from the film/substrate interface to the free surface (Fig. 29a) per unit length of dislocations can be presented as the sum of three terms:

$$= W^f + W^w + W^{f-w}, \qquad (40)$$

where W^f is the misfit strain energy, W^w the self-energy of the MD wall and $W^{f\text{-}w}$ the interaction energy of the misfit strain and the MD wall. When the MD wall is absent, the energy of the system is related to the misfit strain only and equal to W^f. The necessary condition for the MD wall generation is that the system energy W with the MD wall be smaller than the system energy W^f prior to the MD wall introduction, $\Delta W = W - W^f < 0$, which yields

$$^f + W^{f-\omega} < 0. \qquad (41)$$

In accordance with calculations [97], the necessary condition (41) for the generation of the MD wall (Fig. 29a) can be rewritten as

$$\frac{b}{(N+1)H}\left\{\sum_{i=1}^{N}\left[\ln\frac{2d_i}{b} + 2\sum_{j=1}^{i-1}\left(\ln\frac{d_i+d_j}{d_i-d_j} - \frac{2d_id_j}{(d_i+d_j)^2}\right)\right] + \frac{N}{2}\right\} < 4\pi(1+\nu)f_e. \qquad (42)$$

where the effective misfit $f_e = (f_1h_1 + f_2h_2)/(h_1 + h_2)$, and $d_i = iH/N$.

The energy change $\Delta\tilde{W} = \tilde{} - W^f$ due to the generation of the MD wall shown in Fig. 29b, which is defined as the difference between the system energy $\tilde{}$ with such an MD wall and the system energy W^f without MD walls, is derived similarly to the expression for the ΔW. The final result for $\Delta\tilde{W}$ is given as [97]:

$$\Delta\tilde{W} = \frac{Db^2}{2}\left\{\sum_{i=1}^{N}\left[\ln\frac{2\tilde{d}_i}{b} + 2\sum_{j=1}^{i-1}\left(\ln\frac{\tilde{d}_i+\tilde{d}_j}{\tilde{d}_i-\tilde{d}_j} - \frac{2\tilde{d}_i\tilde{d}_j}{(\tilde{d}_i+\tilde{d}_j)^2}\right)\right] + \frac{N}{2} - 4\pi(1+\nu)\frac{H}{b}\left[(N+1)f_e - \frac{2f_1h_1}{h_1+h_2}\right]\right\}, \quad (43)$$

where $d_i = iH/N - h_1$. From (43) and the condition $\Delta\tilde{W} < 0$ it follows that

$$\frac{b}{(N+1)H}\left\{\sum_{i=1}^{N}\left[\ln\frac{2\tilde{d}_i}{b} + 2\sum_{j=1}^{i-1}\left(\ln\frac{\tilde{d}_i+\tilde{d}_j}{\tilde{d}_i-\tilde{d}_j} - \frac{2\tilde{d}_i\tilde{d}_j}{(\tilde{d}_i+\tilde{d}_j)^2}\right)\right] + \frac{N}{2}\right\} < 4\pi(1+\nu)\left(1 - \frac{2f_1h_2}{(N+1)(f_1h_1+f_2h_2)}\right)f_e. \quad (44)$$

Analysis [97] of formulae (43) and (44) indicates the following. The MD walls can nucleate in films with the thickness exceeding some critical thicknesses H_c and $\tilde{H}_c$ corresponding to zero values of ΔW and $\Delta\tilde{W}$, respectively. If f_1 and f_2 as well as h_1 and h_2 are of the same order, ΔW is lower than $\Delta\tilde{W}$, and $H_c < \tilde{H}_c$; it could easily be predicted. If the multilayered film thickness $H > \tilde{H}_c$, MD walls of both first and second type (shown in Fig. 29a and b, respectively) are favoured. In doing so, both H_c and $\tilde{H}_c$ increase with H.To summarize, the specific behavioral peculiarities of MD walls in multilayer films are as follows [97]:

(i) MD walls in a film with alternate layers can form in some range of parameters including film thickness H, misfits f_1 and f_2, the number N of film layers and the ratio h_2/h_1 of adjoining layer thicknesses.

(ii) The formation of MD walls is energetically favourable in multilayered films with the film thickness exceeding some critical thickness (that depends on f_1, f_2, N and h_2/h_1).

(iii)The critical film thicknesses increase with the number N of film layers.

15. NANO-ISLANDS ON SUBSTRATES WITH MISFIT DISLOCATIONS

The formation of spatially ordered ensembles of nano-islands on crystalline substrates is the subject of intensive theoretical and experimental studies due to their great technological potential for device applications; see, e. g., [97-120]. Of special interest are applications of self-assembled semiconductor nano-islands (quantum dots) exhibiting unique properties for optoelectronic devices with reduced size and weight. In doing so, highly desired, from an applications viewpoint, functional characteristics of nano-islands crucially depend on their spatial arrangement and distributions in size and form. At present, in order to design and fabricate ordered ensembles of nano-islands, several technological parameters and methods of growth of nano-islands are used which influence their spatial positions, size and form. For instance, such parameters are deposited material quantity, deposition rate, substrate temperature, chemical composition, and growth interruption time. This has been considered in detail in reviews [98-100]. Recently (in 1999), a very promising technological method for fabrication of spatially ordered ensembles of quantum dots has been suggested and theoretically examined in papers [10, 110], which is the formation of nano-islands (quantum dots) on free surfaces of substrates with internal interfaces, that is, interphase or low-angle grain boundaries. This method exploits the idea to control spatial organization of arrays of nano-islands by means of the elastic interaction between nano-islands and ordered networks of dislocations at the internal boundaries. The method under consideration is based on continuum models describing ensembles of dislocations in the substrate and ensembles of nano-islands on the substrate free surface. In this section we, following [10, 111], will discuss these models.

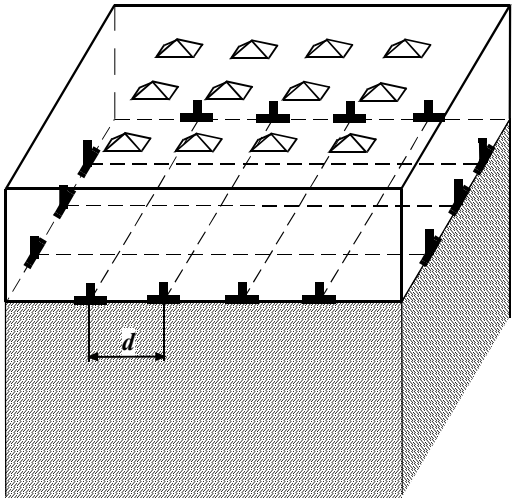

Fig. 30. Pyramid-like nano-islands on composite (consisting of substrates 1 and 2) with misfit dislocations at internal interphase boundary.

In doing so, we will focus our consideration on substrates with semi-coherent interphase boundaries containing networks of MDs. MDs generated at the internal interphase boundary in a composite substrate consisting of substrate 1 and substrate 2 (Fig. 30) create spatially inhomogeneous strain fields on the free surface of the composite substrate (or, in other terms, on the free surface of substrate 2). As a corollary, the lattice parameters of the composite substrate on its free surface depend on spatial coordinates, in which case favourable growth of nano-islands occurs on those substrate surface fragments that are characterized by a minimum misfit between the crystal lattice parameters of a nano-island and the strained substrate. In these circumstances, the spatial positions of nano-islands are strongly influenced by the parameters of MDs which, in their turn, are affected by the human-controlled parameters (materials of substrate 1 and 2, thickness of substrate 2, etc.) of the composite substrate. As a result, the discussed technological scheme (based on the idea of elastic interaction between nano-islands and MDs; see Fig. 30) can be effectively used for design and fabrication of arrays of nano-islands (quantum dots) with controlled spatial organization.

Both size and shape of nano-islands are also crucially affected by a misfit between crystal lattice parameters of nano-islands and substrate [98-100]. As a corollary, owing to the technologically controlled effect of MDs on spatial distribution of the misfit on the dislocated substrate surface (Fig. 30), the discussed technological scheme is promising in design and fabrication of nano-islands (quantum dots) with desired distributions in size and shape.

Let us consider a model composite system consisting of a semi-infinite substrate (phase 1), substrate 2 (phase 2) of finite thickness H, and nano-islands (phase 3) that grow on substrate 2 (Fig. 30). Substrates 1 and 2 as well as nano-islands are assumed to be isotropic and characterized by the same shear modulus G and the same Poisson ratio ν. For definiteness, nano-islands are assumed to be regular pyramids with square bases having edges of length $2a$.

Substrate 2 and nano-islands are elastically strained due to a misfit between crystalline lattices of phases 1, 2 and 3. The misfit is assumed to be two-dimensional, in which case it is characterized by the parameters $f_i = (a_1 - a_i)/[2(a_1 + a_i)]$, where a_i is the crystal lattice parameter for the i-th phase. If the thickness H of substrate 2 is lower than some critical value H_c, the misfit between crystalline lattices of substrate 1 and 2 is accommodated completely by the elastic straining of substrate 2. For $H > H_c$, the formation of MDs is energetically favourable, which effectively contribute to accommodation of the misfit (relaxation of the misfit stresses). For simplicity, in this section we will focus on consideration of edge MDs located at the substrate 1/substrate 2 boundary and characterized by identical Burgers vectors $\boldsymbol{b}$ that are parallel with the boundary plane (Fig. 30).

The elastic interaction between nano-islands and MDs causes nano-islands to have favorable spatial positions on the free surface of the composite substrate. Let us consider, following [10, 111], interaction of a nano-island and a MD network consisting of two orthogonal rows of periodically spaced (with a period d) MDs (Fig. 30). The nano-island in its equilibrium position is equally distant from two nearest MDs that belong to the orthogonal dislocation rows. The energy W^{ar} of elastic interaction between the nano-island and the MD network is as follows:

$$^{ar} = \left[(f_3 - \varepsilon^{ar}(x_0))^2 - f_3^2\right]. \qquad (45)$$

Here

$$\varepsilon^{ar}(x_0) = \sum_{n=-\infty}^{\infty} \varepsilon^{d}(x_0 - nd), \qquad (46)$$

in which case $\varepsilon^d(x_0\text{-}nd)$ denotes the strain in the substrate region under the nano-island, created by two dislocations with the lines ($x = nd$, $z = H$) and

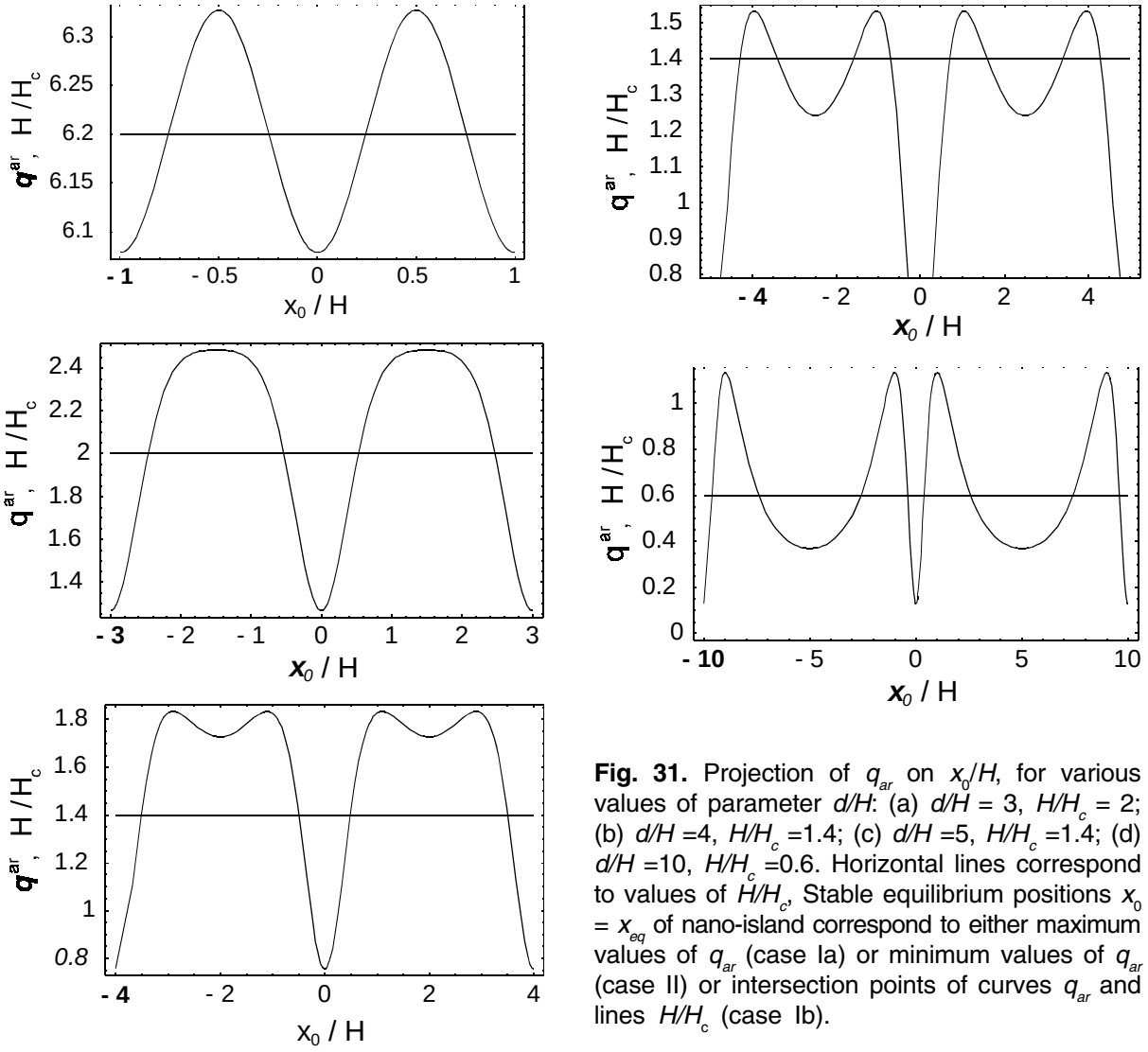

Fig. 31. Projection of q_{ar} on x_0/H, for various values of parameter d/H: (a) d/H = 3, H/H_c = 2; (b) d/H =4, H/H_c =1.4; (c) d/H =5, H/H_c =1.4; (d) d/H =10, H/H_c =0.6. Horizontal lines correspond to values of H/H_c, Stable equilibrium positions $x_0 = x_{eq}$ of nano-island correspond to either maximum values of q_{ar} (case Ia) or minimum values of q_{ar} (case II) or intersection points of curves q_{ar} and lines H/H_c (case Ib).

($y = nd$, $z = H$). From (45) and (46) it follows that there are following (sub)cases, depending on the parameters f_2, f_3 and H:

(Ia) $f_2 f_3 > 0$ and $\varepsilon^{ar}_{max} < |f_3|$, where ε^{ar}_{max} is the maximum absolute value of the strain created by the MD network on the surface of substrate 2. In this case stable equilibrium positions $x_0 = x_{eq}$ correspond to the points where the function $|\varepsilon^{ar}|$ has its minimum (Fig. 31). Such points depend on parameter d/H. So, for $d/H < 3.15$, that is, for a high density of MDs, the function $|\varepsilon^{ar}|$ has its maximum values above the centers of MD network cells, squares formed by MD lines (Fig. 31a). For $d/H > 3.15$, where d and H are of the same order, stable equilibrium positions of the nano-island are located in vicinities of the points above vertices of the MD network (Fig. 31b and c). For $d/H << 1$, interaction of the nano-island and the MD network is reduced to that between the nano-island and two nearest orthogonal dislocations, causing stable equilibrium positions of the nano-island to be distant by H from the dislocation lines (Fig. 31d).

For $f_2 f_3 > 0$, case (Ia) is realized, if the thickness H of substrate 2 is larger than some critical value H_c^{ar} ($< H$) that depends on the parameters f_3 and d. As shown in Fig. 31, $H_c^{ar} > H_c$, and H_c^{ar} decreases with growth of d, period of the MD network. For $d \to \infty$, $H_c^{ar} = H_c$.

(Ib) $f_2 f_3 > 0$ and $\varepsilon^{ar}_{max} > |f_3|$. In this case stable equilibrium positions correspond to the points where the curve $q^{ar}(x_0/H)$ and the line H/H_c intersect (Fig. 31). Either one or two stable equilibrium positions exist in the points located above the segments that connect nodes of MD network cells (squares with edges of length d) and their centers (The segments in question correspond to the interval, $0 < x_0 < d/2$, presented in Fig.

31.) More precisely, there is one stable equilibrium position, for $d/H < 3.15$ (see Fig. 31a); and either one or two stable equilibrium positions of the nano-island exist, for $d/H > 3.15$, depending on value of $|f_3|$. For $d/H > 3.15$, stable equilibrium positions are approaching nodes of the MD network cells with increase of the ratio d/H.

(II) $f_2 f_3 \leq 0$. In this case f_3 and ε^{ar} have the same sign. Stable equilibrium positions of the nano-island correspond to a minimum of $|\varepsilon^{ar}|$. In these circumstances, for $d/H < 3.15$ (Fig. 31a), stable equilibrium positions $x_0 = x_{eq} = nd$ are located at the points above nodes of the MD network. For $d/H > 3.15$ (Fig. 31b and c), there are stable equilibrium positions ($x_{eq} = nd$) of the nano-island at the points above nodes of the MD network as well as quasiequilibrium positions ($x'_{eq} = n(d+1/2)$) at the points above centers of MD network cells.

Thus the growth of nano-islands on a composite (two-layer) substrate with MDs at an internal interphase boundary (Fig. 29) is an effective method for fabrication of spatially ordered ensembles of nano-islands (e.g., quantum dots). Due to elastic interaction between nano-islands and MDs, spatial positions (and generally speaking, size and shape) of nano-islands are highly sensitive to the characteristics of the dislocated composite substrate. This potentially allows one to design arrangements of nano-islands with desired functional characteristics on a composite substrate, using technologically controlled parameters (materials of layers composing the two-layer substrate, thickness of the "upper" layer, etc.) of the substrate.

16. INTERFACES IN HIGH-T_c SUPERCONDUCTING FILMS

16.1. Introductionary notes

Grain boundaries in high-transition-temperature (T_c) superconducting thin films and bulk materials dramatically suppress the transport critical-current density (J_c). Values of J_c in polycrystalline high-T_c superconductors are essentially lower (often by orders) than those of their single crystalline counterparts, e.g. [121-126]. The weak-link behavior of grain boundaries in high-T_c superconducting films forms the foundation of integrated-circuit technologies based on Josephson effect. At the same time, the dramatic depression of J_c across grain boundaries prevents applications of polycrystalline superconducting cuprates in high-electric-current technologies; see, e.g. [125,126]. Besides technologically motivated attention to grain boundaries, an adequate description of their specific behavior in thin-film and bulk high-T_c superconductors is very important for the fundamental understanding of nature of high-T_c superconductivity. At present, though there are many experimentally documented facts concerning the effect of grain boundaries on the transport critical-current density in high-T_c superconductors (see reviews [125-127]), its physical mechanism(s) is (are) under discussion [125-144].

In general, grain boundaries in high-T_c superconducting films exhibit some specific structural and behavioral features differing such boundaries from grain boundaries in high-T_c bulk superconductors. However, both the structure and behavior of grain boundaries in high-T_c superconducting films, in many respects, are similar to those in bulk cuprate superconductors. With this taken into account, in this section, first, we will discuss the general aspects of the effect of grain boundaries on high-T_c superconductivity in bulk and thin-film cuprates. Then the attention will be paid to the specific structural and behavioral peculiarities of grain boundaries in high-T_c superconducting films.

16.2. Key experimental data and theoretical representations on the grain boundary effect on high-T_c superconductivity

The key experimentally documented facts related to the effect of grain boundaries on high-T_c superconductivity in bulk and thin-film cuprates, in short, are as follows:

(i) There is a dramatic discrepancy between the transport properties of low- and high-angle boundaries; see, e.g., [121-127]. Thus, J_c across low-angle boundaries shows a sharp exponential drop with rising boundary misorientation α, while the critical current density across high-angle boundaries is weakly dependent on α and is lower by two or three orders than the critical current density in the bulk phase [121-127].

(ii) Existence of hole depletion zones in vicinities of grain boundaries [127, 145, 146].

(iii) Existence of deviations from bulk stoichiometry near grain boundaries in samples fabricated at highly non-equilibrium conditions [125, 138, 147].

(iv) Existence of variations of the superconducting properties along grain boundary planes [125, 148-152].

(v) Doping-induced enhancement of J_c in Ca-doped YBaCuO superconductors [136].

(vi) High-quality twist boundaries have been fabricated in BiSrCaCuO superconductors, that are characterized by boundary cores of zero thickness and exhibit the enhanced transport properties [153-155]. Such boundaries carry critical current as high as their consistuent single crystals [152-155].

(vii) Spatial variations of the critical current have been detected in BiSrCaCuO tapes; the most supercurrent flows through the thin layer of superconductor next to the silver sheet (see [156] and references therein).

(viii) Grain boundary structures undergo transformations that are capable of strongly influencing their transport properties [157-160]. For instance, the splitting and amorphization of dislocation cores composing low-angle boundaries in high-T_c cuprates have been experimentally observed [157, 158]. Amorphization and chemical composition inhomogeneities at high-angle boundary cores have been detected in experiments; see, e.g., [159, 160].

Theoretical models which describe the effect of grain boundaries on high-T_c superconductivity should take into account these experimental facts. Let us briefly discuss the key points of current models [127-144] of grain boundaries in high-T_c superconductors and analyze correspondence of predictions of these models to data of experiments with polycrystalline high-T_c cuprates.

In papers [138, 139] compositional variations at grain boundaries are treated as those responsible for reduction of the critical current density J_c across boundaries. However, fabrication of (thin-film) samples where non-stoichiometry is not exhibited (or, at least, is non-detectable in experiments), but grain boundaries show the same transport bahavior, makes the idea [138, 139] on the critical role of compositional variations to be discussive.

The model [128] treats the crystallographic disorder within grain boundary cores and strains induced by grain boundary dislocations to be responsible for the superconducting-to-insulating phase transition in strained regions within and near grain boundary cores. In doing so, the value of strain $\varepsilon_c \approx 0.01$ along the *a* or *b* axis is assumed to be critical, that is, the transition occurs in regions characterized by strain (along the *a* or *b* axis) $\varepsilon > \varepsilon_c$ [128]. This approach and its versions [130-132] do not take into account stoichiometric and electric-charge inhomogeneities at grain boundaries. In particular, the model [118] does not explain the experimentally detected [127, 145, 146] existence of hole-depletion regions in vicinities of grain boundaries. Also, it meets the question related the fact that strain fields of periodic dislocation walls (which serve as models of low-angle symmetric tilt boundaries; Fig. 1a) drop as exp(-*x*/*d*), where *x* denotes the distance from the grain boundary plane, and *d* the period that characterizes arrangement of dislocations composing the dislocation wall. The period *d* is in following relationship with tilt boundary misorientation α: $b/d = 2\sin(\alpha/2)$ [161], where *b* is the magnitude of the dislocation Burgers vector. With this relationship taken into consideration, the strain fields discussed should give rise to shrinkage of strained regions in vicinities of low-angle tilt boundaries and, therefore, to increase of the critical current density $J_c(\alpha)$ across tilt boundaries with increase of misorientation angle a from 0° to tentatively 10°. This is in a contradiction with experimental data [121-126].

In papers [140, 141] the approach [128] has been modified to the situation with chaotically arranged dislocations at tilt boundaries in high-T_c superconductors. Disordered arrays of dislocations create stress fields whose dispersion increases with rising a in the low-angle range [140-142]. This, in the framework of the approach [128], should result in a decrease of the critical current density $J_c(\alpha)$ across disordered tilt boundaries with rising α for $\alpha \leq 10°$. However, grain boundaries that contain chaotically arranged dislocations [140-142] are partial cases of grain boundary structures in cuprates. Such disordered grain boundaries are expected to exist only in high-T_c superconductors fabricated at highly non-equilibrium conditions. Therefore, the discussed modifications [140-142] of the approach [128] can not reply to all questions to its validity in the general situation.

The idea on stress-induced suppression of high-T_c superconductivity has been exploited also in paper [129]. Authors of this paper have theoretically described (in terms of the Ginzburg-Landau formalism) the angular dependence of the critical current density J_c across low-angle tilt boundaries in cuprates, taking into consideration the effect of crystal lattice anisotropy on stress fields of grain boundary dislocations as well as the effect of electric-charge inhomogeneities caused by stress fields of the dislocations on the superconducting order parameter. In doing so, however, the model [129] focused on the range of α from 5° to tentatively

25° leaving the dependence $J_c(\alpha)$ unclear, for $\alpha <$ 5° and $\alpha >$25°. In addition, the electric-charge inhomogeneities have been described as those associated with stress-induced inhomogeneities of the averaged (over an elementary cell) ion density, in which case the polyatomic structure of cuprates has been ignored. In the framework of this model description, the role of stoichiometric inhomogeneities driven by stress fields has been not taken into account.

In papers [133-136] the excess electric charge within high-angle boundary cores has been treated as that responsible for the formation of hole-depletion zones in vicinities of grain boundaries. In doing so, origin of the excess charge in question has been attributed to crystallographic disorder existing within high-angle boundary cores as well as to the *d*-wave type symmetry of the superconducting order parameter. However, in the framework of the model description [133-136], the excess electric charge can be either positive or negative, in which case hole-enhancement zones in vicinities of grain boundaries could be expected to form as likely as hole-depletion zones do [136]. At the same time, only hole-depletion layers have been detected in electron energy loss spectroscopy experiments [127, 145, 146]. This causes questions to the choice of origin of the excess electric charge, given by the model [133-136]. A modified version of the approach [133-136] is the so-called bond-valence model [127] which attributes the excess electric charge of grain boundary cores to variations of valency of copper atoms in atomic chains (existing between Cu-O planes) in YBaCuO superconductors. This model is based on results of computer simulations of the atomic structure of grain boundaries in YbaCuO materials, in which case the atomic potentials are empirical and can, therefore, lead to errors. Also, an uncertainty of the origin of hole-depletion layers is inherent to model [137] which uses the existence of such layers and their experimentally measured characteristics as an experimentally documented input of the Ginzburg-Landau-formalism-based description of the transport properties of tilt boundaries in YBaCuO superconductors.

Authors of paper [143] have focused on the role of the crystallographic disorder within grain boundary cores in the suppression of the critical current density J_c. More precisely, the model [143] treats the mechanism of the grain boundary effect on J_c to originate from breaking and rearrangement of interatomic bonds at the boundary core that induce modification of the local electronic states. Following the electronic structure calculations for grain boundaries in YBaCuO superconductors, it has been concluded that the Cu2-O2 interatomic bonds broken at the grain boundary are a very important factor controlling the local electron state perturbation and, therefore, the superconducting order parameter behavior in boundary area [143]. At the same time, removals of O1, Ba or Y atoms from the lattice are theoretically shown to weakly influence the local electron states in YBaCuO superconductors. The model [143] is based on results of computer simulations of the atomic and electronic structures of five grain boundaries in YBaCuO superconductors. In doing so, just qualitative conclusions about the crucial effect of breaking the Cu2-O2 interatomic bonds on J_c have been made; values of J_c have been not estimated. Nevertheless, results of the model [143] are very interesting for understanding the nature of the grain boundary effect on the critical current density J_c and can be used in further quantitative analysis of J_c across grain boundaries in high-T_c superconductors.

The model [144] explains the grain boundary effect on high-T_c superconductivity as that caused by electric-charge inhomogeneities within and near grain boundary cores, which are associated with stoichiometric inhomogeneities induced by dilatation stresses and mediated by enhanced grain boundary diffusion. This model, in fact, treats the combined effects of dilatation stress fields, stoichiometric and electric-charge inhomogeneities on the critical current density across grain boundaries as those responsible for the experimentally detected features, (i)-(vi) (see above), of high-T_c polycrystalline cuprates. Also, the model allows one to make predictions of those doping elements that are capable of enhancing the critical current density across grain boundaries in doped high-T_c cuprates and to give a qualitative explanation of the specific transport properties of high-quality *c*-axis twist boundaries in BiSrCaCu superconductors. In next subsection we will discuss the basic representations of the model [144] in more detail.

16.3. Dilatation stresses and the grain boundary effect on high-T_c superconductivity

The generic feature of all cuprate superconductors is their polyatomic structure [125,162]. The generic feature of all grain boundaries in cuprates (as well in other solids) is their role as sources of

dilatation stress fields [161]. Since atoms of different types exhibit different behaviors in response to dilatation stresses [163], dilatation stresses associated with grain boundary cores induce local violations of ideal (optimal for high-T_c superconductivity) stoichiometry within grain boundary cores in polyatomic cuprates. This is generic feature of all polycrystalline high- T_c cuprates.

Let us discuss the effects of grain-boundary-induced dilatation stresses on stoichiometry in the examplary cases of YBaCuO and BiSrCaCuO superconductors that are of high importance in applications. High-T_c superconducting cuprates are polyatomic solids whose lattices consist of negatively charged ions (anions) of oxygen O^{2-} and positively charged ions (cations) of other chemical elements (Y, Ba, Cu in the case of YBaCuO superconductors, and Bi, Sr, Ca, Cu in the case of BiSrCaCuO superconductors) composing the cuprates. Oxygen ions are small compared to the cations composing crystalline lattices of cuprates, in which case small oxygen ions tend to move to regions where compressive stresses exist, while comparatively large cations tend to move to regions where tensile stresses exist.

More precisely, according to the general theory of diffusion in stressed solids [163], the elastic interaction between dilatation stresses ($\sigma_{xx}(x,y,z)$, $\sigma_{yy}(x,y,z)$, $\sigma_{zz}(x,y,z)$) and diffusing species (small and large ions in our case) in a stressed solid is specified by the interaction energy given as:

$$E_{int} = (\sigma_{xx} + \sigma_{yy} + \sigma_{zz})\frac{\Delta V}{3}. \qquad (47)$$

Here ΔV is the atomic volume difference that characterizes the diffusing species. In the discussed situation with stress-driven diffusion in polyatomic cuprates, diffusional exchange of small oxygen anions and large cations occurs. In this case values of ΔV that figures on the r.h.s. of formula (47) are as follows:

$$\Delta V_k = V_k - \frac{V_k + V_O}{2} > 0, \qquad (48)$$

$$\Delta V_O = V_O - \frac{V_k + V_O}{2} < 0, \qquad (49)$$

where V_k denotes the atomic volume of cation of the k-th type, V_O the atomic volume of oxygen ($V_k > V_O$). The elastic interaction in question forces large cations (small anions O^{2-}, respectively) to move to regions where tensile (compressive, respectively) stresses exist.

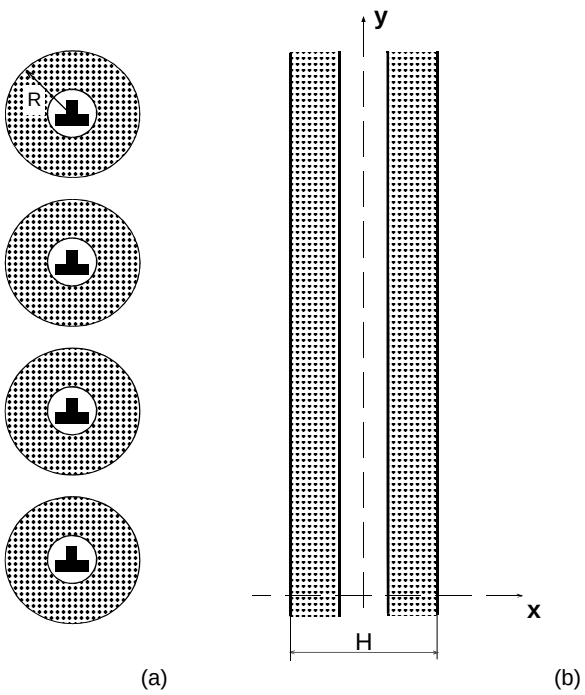

Fig. 32. Stoichiometric and electric-charge inhomogeneties within and near tilt boundaries. (a) Cores of lattice dislocations (composing low-angle boundaries) and (b) cores of high-angle boundaries are characterized by deviations from bulk stoichiometry and an excess positive charge density Q_{gb}. Their vicinities (dotted regions) are hole depletion zones.

Grain boundary core regions – plate-like cores (with thickness being of the order of 1 nm) of high-angle boundaries and cylinder-like cores (with diameter being of order of 1 nm) of lattice dislocations composing low-angle boundaries (Fig. 32) – are characterized by a low atomic density compared to the bulk or, in other terms, by a positive dilatation [163-165]. The component of the rigid body translation normal to a high-angle boundary, that characterizes the excess free volume of the boundary, is in the order of 1/10 to 1/100 of the lattice parameter [163,164]. In accordance with calculations [165], the excess free volume of dislocation cores (that compose low-angle boundaries) can be estimated as that in the order of 1/10 of magnitude of one or two atomic volumes. In doing so, the excess free volume of edge dislocations is larger than that of screw dislocations [165]. In addition, due to a low atomic density of grain boundary cores, they exhibit the enhanced diffusional properties: coeffi-

cients of self-diffusion, that characterize high-angle boundary cores and dislocation cores (composing low-angle boundaries), are higher by several orders than the bulk diffusion coefficient [163].

Thus, in context of our previous discussion, boundary core regions are regions where tensile stresses exist, in which case the elastic interaction (47) gives rise to enhanced-diffusion-mediated deviations from bulk stoichiometry within these regions. According to formulae (47)-(49), large cations substitute small anions O^{2-} within grain boundary cores (Fig. 32), resulting in creation of an excess positive charge density Q_{gb} (>0) of such cores. The concentration of cations within grain boundary cores, resulted from the substitution processes in question, weakly deviates from the bulk concentration. Actually, if the substitution does not occur, the concentration of cations within grain boundary cores is lower than that in the bulk phase due to a low atomic density inherent to the grain boundary phase. The substitution of small oxygen anions by relatively large cations of other elements of a cuprate results in an increase of the initially low concentration of cations up to value close to the bulk concentration of cations. This is why experiments often do not reveal deviations from the bulk concentration of cations within grain boundary cores. At the same time, in accordance with our model, grain boundary cores should be deficient in oxygen, giving rise to the excess positive charge density Q_{gb}. The oxygen concentration is experimentally measured with large errors [125] (due to low atomic weight of oxygen), in which case deviations from bulk concentration of oxygen within grain boundary cores may be not detectable in experiments.

In order to screen the excess positive charge density Q_{gb}, hole depletion zones characterized by an excess negative charge density Q_z (< 0) are formed in vicinities of grain boundary cores (Fig. 32). Such hole depletion zones have been detected in electron energy loss spectroscopy experiments [127,145,146]. Due to high sensitivity of high-T_c superconductivity to stoichiometry and hole concentration [162], it is natural to treat the grain boundary cores and hole depletion zones in their vicinities as non-superconducting regions responsible for suppression of critical current density J_c across grain boundaries in cuprates.

Let us discuss the effect of stoichiometric and electric-charge inhomogeneities within and near grain boundary cores (Fig. 32) on the critical current density J_c across tilt boundaries in cuprates. The superconducting properties of cuprates are experimentally revealed to be suppressed by even weak deviations from the ideal (optimum) stoichiometry corresponding to maximum critical transition temperature T_c [162, 166, 167]. Also, electric-charge inhomogeneities strongly suppress the superconducting critical current; see discussion in papers [129, 133-136]. Therefore, it is natural to treat the regions with "non-ideal" stoichiometry and electric-charge inhomogeneities within and near grain boundary cores (Fig. 32) as non-superconducting ones.

According to the theory of electron pairs tunneling in superconductors (see, e.g. [168,169]), reduction of the critical-current-density across a non-superconducting layer is approximately described by factor $\exp\{-h/\xi\}$. Here h denotes the layer thickness and ξ the characteristic decay length which can be the tunneling length for insulating grain boundaries or the proximity length for metallic grain boundaries (which is close to the coherence length).

Parallel with stoichiometric and electric-charge inhomogeneities, additional geometric factors are capable of affecting the critical current density across tilt boundaries. Thus, recently, the symmetry of the order parameter in many high-T_c superconductors has been experimentally recognized as being $d_{x^2-y^2}$ [170-175] or $d_{x^2-y^2}$ mixed with an s-wave component [176]. The $d_{x^2-y^2}$ symmetry causes a dependence of the critical-current density $J_c(\alpha)$ across a grain boundary on boundary misorientation α and orientation of boundary plane relative to adjacent grains [133, 177, 178]. With this taken into consideration, the faceted microstructure of tilt boundaries, that is often detected experimentally (see, for instance, [158,179-182]), also influences the transport properties of tilt boundaries in high-T_c superconductors.

With description [178] of the influence of d-symmetry and grain boundary faceting on J_c taken into account, one finds that the combined effects of dilatation-induced stoichiometric and electric-charge inhomogeneities, $d_{x^2-y^2}$ symmetry and faceting cause the following angular dependence of J_c in the case of [001] tilt boundaries [144]:

$$\frac{J_c(\alpha)}{J_c(0^\circ)} \approx \frac{1}{S} < \prod_{m=1,2} [(\sin\alpha_m)^2 - (\cos\alpha_m)^2 >_F \int_S \exp\left\{-\frac{h(y,z)}{\xi}\right\} dydz, \qquad (50)$$

Here α_m (m =1,2) is the smallest angle between the grain boundary plane and a principal crystallographic axis ($\vec{a}$ or $\vec{b}$) of adjacent grain m ($\alpha_1 + \alpha_2 = \alpha$, and $< ... >_F$ denotes the averaging that takes into account the faceted boundary microstructure (for details, see paper [178]). $h(y)$ denotes the thickness of the regions with stoichiometric and electric-charge inhomogeneities (Fig. 32), y denotes the coordinate along grain boundary plane.

The angular dependence of J_c – curve 1 in Fig. 33 – attributed to the combined effects in question has been calculated with the help of formula (50); see [144].In doing so, for high-angle ($\alpha \geq 20°$) boundaries, h has been taken as $H \approx 3$ nm. For low-angle ($\alpha \leq 19°$) boundaries, the scale h has been choosen, according to Fig. 32a, as y-dependent thickness of boundaries composed of lattice dislocation cores and their vicinities with "non-ideal" stoichiometry and charge density, that are characterized by diameters $2R \approx 3$ nm. (In this case interspacing between periodically arranged lattice dislocations composing low-angle boundaries (Fig. 32a) depends on α as [161]: $2d = b\sin(\alpha/2)$, where b is the magnitude of the dislocation Burgers vector.) In the intermediate range of α from 19° to 20°, h has been taken as interpolation of corresponding values of h for low- and high-angle boundaries. Results of the averaging $<...>_F$ have been taken from paper [178] where the averaging procedure is discussed in detail. ξ has been taken as 1.5 nm. This corresponds to the coherence length in [001] planes that carry the current [162]. (In general, various values of ξ are discussed in scientific literature. In paper [132] the length ξ has been taken as that close to the coherency length (≈ 1.5 nm). In papers [127,169] ξ has been taken as ≈ 0.13 nm. The model [144] uses value of $\xi \approx 1.5$ nm as that giving the most effective correspondence to experimental data with the angular dependence of the critical current density across grain boundaries.)

The theoretical dependence $J_c(\alpha)$ (curve 1 in Fig. 33) [144] is in a satisfactory agreement with experimental data [121-124] (curve 2 in Fig. 33) for YBaCuO superconductors. This allows one to think that the idea on the combined effects of dilatation-induced stoichiometric and electric-charge inhomogeneities, $d_{x^2-y^2}$ symmetry of the superconducting order parameter and the faceted microstructure of grain boundaries is effective in description of the dramatic distinction between the transport properties of low- and high-angle boundaries.

Now let us discuss the doping of polycrystalline high-T_c cuprates, which is capable of strongly influencing the critical current densities J_c across grain boundaries. The remarkable experimental fact in this area is a record enhancement of J_c (by about a factor of 8) in Ca-doped YBaCuO superconductors [136].

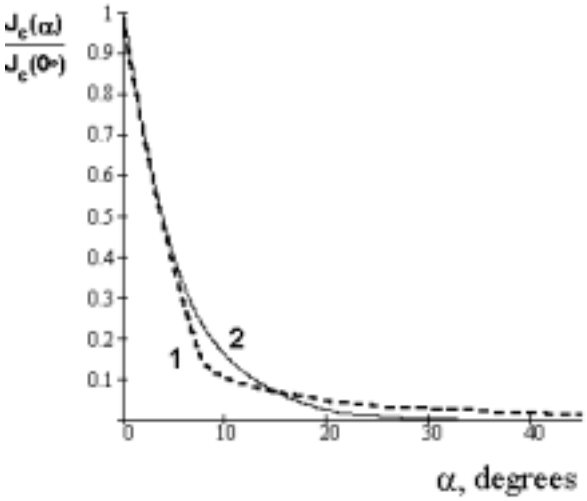

Fig. 33. Angular dependences of the critical current density J_c across [001] tilt boundaries. Dashed curve 1, according to formula (50), is attributed to the combined effects of stoichiometric and electric-charge inhomogeneities, $d_{x^2-y^2}$ symmetry and the faceted microstructure of tilt boundaries. The experimentally detected [121-124] angular dependence of J_c is shown, according to [178], as solid curve 2.

In the framework of the model [144], doping can decrease value of Q_{gb} and, therefore, enhance values of J_c across grain boundaries in the following cases: (A) valency $\tilde{v}$ of dopant cations is lower than that (v_k) of host cations; (B) radius $\tilde{r}$ of dopant cations is larger than that (r) of host cations. In the case (A) the excess charge Q_{gb} decreases directly due to the doping-induced decrease of the sum charge of cations within grain boundary core. In the case (B) the doping decreases the effect of dilatation stresses. That is, substitution of relatively small host cations by relatively large subsitute cations results in an increase of the atomic density within grain boundary cores. As a corollary, dilatation stresses associated with grain boundary cores are decreased, in which case so is the driving force for diffusional exchange of cations and oxygen anions within boundary cores, thus decreasing Q_{gb}. In context of the former mechanism (A) of the influence of doping on the critical current density J_c across grain boundaries, the Ca-doping of

$YBa_2Cu_3O_{7-\delta}$ bi-crystals results in the experimentally detected [136] J_c enhancement due to the following. Commonly Ca^{2+} cations substitute Y^{3+} cations in YBaCuO cuprates [183]. This gives rise to a decrease of the excess positive charge density Q_{gb}, associated with $Ca^{2+} \rightarrow Y^{3+}$ substitution in grain boundary cores, and, as a corollary, to the J_c enhancement.

In context of point (A), it is potentially interesting to experimentally test the effect of Na-doping on J_c in bi-crystalline YBaCuO. Actually, Na^{1+} cations substitute Y^{3+} cations in $YBa_2Cu_3O_{7-\delta}$ cuprates [184]. This non-isovalent doping can substantially decrease Q_{gb} and, therefore increase J_c in bi-crystalline $Y_{1-x}Na_xBa_2Cu_3O_{7-\delta}$ superconducting cuprates.

Recently, high-quality *c*-axis twist boundaries have been fabricated in BiSrCaCuO superconductors, that exhibit the enhanced transport properties [153-155]. These twist boundaries carried critical current as high as their constituent single crystals (adjacent grains), regardless of the misorientation angle [153-155]. The specific structural feature of high-quality twist boundaries is the zero thickness of boundary core. That is, the twist boundaries are atomically intact and clean, with no detectable *c*-axis spacing increase or chemical changes between the BiO double layers [153, 154]. A direct consequence of the zero thickness of high-quality twist boundary cores is the fact that there are no dilatation stresses associated with such cores. In context of the model [144], it means that high-quality twist boundaries should not affect the critical current density. The aforesaid is in correspondence with experimental data [153-155].

Now let us briefly discuss the effect of grain boundary dislocations on stoichiometric inhomogeneties in vicinities of grain boundaries along boundary planes. According to the model [144], such inhomogeneities in the bulk phase adjacent to grain boundary cores are resulted from the bulk diffusion driven by stress fields of grain boundary dislocations. To do so, the bulk diffusion should be intensive, at least, during the synthesis of a cuprate. The situation in question comes into play, in particular, if a cuprate is synthesized at highly non-equilibrium conditions (say, by fast sintering technique). In this circumstances, the most mobile ions in the bulk of high-T_c superconducting YBaCuO and BiSrCaCuO cuprates are ions, Cu and O, because they are small compared to other ions and, therefore, are characterized by a low activation energy for their motion in a crystalline lattice. The ion volume of copper V_{Cu} is larger than that of oxygen V_O, in which case comparatively large ions Cu (small ions O, respectively) move to regions where tensile (compressive, respectively) stresses exist that are created by grain boundary dislocations.

As with low-angle boundaries consisting of lattice dislocations (Fig. 32a), high-angle boundaries (Fig. 32b) commonly contain grain boundary dislocations, e.g. [161]. Both low- and high-angle boundary dislocations create spatially inhomogeneous dilatation stress fields outside grain boundary cores. Spatial arrangements of grain boundary dislocations in solids, after relaxation of their grain boundary structures, are close to periodic: they are periodic, quasiperiodic [161,185,186] or weakly disordered [187,188]. Dislocations arranged in a tentatively periodic way along grain boundary force tentatively periodic modulations of dilatation stress fields and, therefore, tentatively periodic modulations of "non-ideal" stoichiometry in the case of intensive bulk diffusion. Such tentavively periodic modulations of "non-ideal" stoichiometry have been observed experimentally in vicinities of grain boundaries in YBaCuO superconductors fabricated by sintering technique [147]. Their theoretical description in the framework of the idea on the crucial role of grain-boundary-induced dilatation stresses on stoichiometric inhomogeneities has been done in paper [144].

Thus, the combined effects of dilatation-induced stoichiometric and electric-charge inhomogeneities at grain boundaries, $d_{x^2-y^2}$ symmetry and grain boundary faceting account for the experimentally observed reduction of the critical current density J_c with increasing grain boundary misorientation angle and existence of hole-depletion zones in vicinities of grain boundaries in high-T_c superconductors as well as existence of deviations from bulk stoichiometry near grain boundaries and variations of the superconducting properties along grain boundary planes in cuprate samples fabricated at highly non-equilibrium conditions. Also, the representations on these effects can be used in understanding the nature of the enhancement of J_c across high-quality twist and doped grain boundaries in cuprates.

16.4. Effects of misfit stresses on the structure and transport properties of low-angle tilt boundaries in polycrystalline superconducting films.

Following [41, 46, 51] (see also sections 4 and 5 of this review), grain boundary dislocations in polycrystalline films can play the role as misfit defects

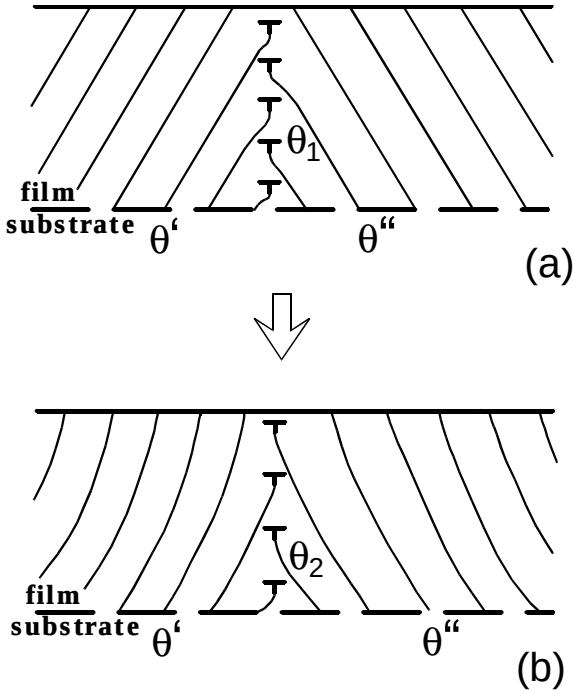

Fig. 34. Transformation of the low-angle boundary structure from initial state (a) with misorientation θ_1 to final state (b) with misorientation θ_2 ($<\theta_1$).

compensating for, in part, misfit stresses generated at interphase boundaries. In doing so, misfit stresses influence the grain boundary structures which, therefore, are different from those in bulk materials. Let us consider this effect of misfit stresses in the examplary case of a low-angle tilt boundary composed of lattice dislocations of the edge type in a polycrystalline thin-film cuprate. Let the grain boundary dislocations be parallel with the interphase boundary plane and be periodically arranged in some initial state of the as-synthesized polycrystalline film (Fig. 34a); and the dislocations provide misorientation of the adjacent grains of the film and do not contribute to relaxation of misfit stresses. In particular, it means that misorientation θ_1 of the grain boundary in its initial state is consistent with misorientations, θ’ and θ”, of interphase boundary fragments adjacent to the grain boundary (Fig. 34a). That is, $\theta_1 = -\theta'-\theta''$.

Let us consider, following paper [189], a transformation of the low-angle boundary from its initial state with misorientation θ_1 (Fig. 34a) into a state with misorientation θ_2 ($<\theta_1$) (Fig. 34b). The transformation occurs via climbing of m ($m \geq 1$) grain boundary dislocations towards the film free surface, where these dislocations disappear. Due to the transformation, the low-angle boundary acquires an “uncompensated” dislocation density associated with difference $\Delta\theta = \theta_2 - \theta_1$ between its misorientations in final and initial states. The low-angle boundary with the uncompensated dislocation density creates stress fields which compensate for, in part, misfit stresses [41,46,51]. As a corollary, the transformation of the boundary structure (Fig. 34) is driven by a release of misfit stresses in the film.

Let us examine the energetic characteristics of the transformation (Fig. 34) with the assumptions that (i) the film contains identical low-angle boundaries periodically spaced along the interphase boundary; and (ii) dislocations that compose the low-angle boundaries in their final state (after the transformation) are arranged periodically. In the framework of the suggested approximation, the transformation of the low-angle boundary dislocation structures (Fig. 34) is equivalent to the formation of the periodic row of misfit disclinations (rotational defects each is characterized by strength $\omega = \theta_2-\theta_1 < 0$) at the interphase boundary, whose stress fields compensate for, in part, misfit stresses; for more details, see [41, 58] and section 6 of this review. In the following, for definiteness and the sake of simplicity, we restrict our consideration to the case with one-dimensional misfit parameter $f = (a_s - a_f)/a_s > 0$, where a_s and a_f are the crystal lattice parameters of the substrate and the film, respectively. Also, the thin film and the (model) semi-infinite substrate are assumed to be isotropic and characterized by the same values of the shear strength G and the same values of Poisson ratio ν. In these circumstances, following calculations [58] (see also section 6 of this review), the energy density change ΔE^{ω} related to the formation of the misfit disclination row is given by formulae (15) and (16). It depends on the film thickness h, the distance l between neighbouring misfit disclinations, and ratio $\tilde{h} = h/l$ (see formulae (15)and (16)).

The energy density $\Delta E^b \approx mGb^2/4\pi(1-\nu)l$ characterizes the core energy density of m dislocations with Burgers vectors $\boldsymbol{b}$, disappeared during the transformations of grain boundary structures (Fig. 34). From geometry of a transformed low-angle boundary, we have the following relationship between its parameters: $mb \approx h\,|\omega|$ at $|\omega| << 1$. With this relationship, ΔE^{ω} (given by formulae (15) and (16)) and ΔE^b taken into account, we find the energy density change ΔE related to the transformation (Fig. 34) to be as follows:

$$\Delta E = E_2 - E_1 = \frac{Gb}{4\pi(1-\nu)}\left[\frac{m^2}{h^2}\Phi\left(\frac{h}{l}\right) - \right.$$

$$\left. - \frac{4\pi\tilde{f}mh}{l} - \frac{mb}{l}\right], \qquad (51)$$

where E_1 (E_2) is the energy density of the film with the low-angle boundary in its initial (final, respectively) state. In the wide ranges of parameters characterizing the film, $\Delta E < 0$ (for details, see paper [189]), that is, the misfit-stress-induced transformation (Fig. 34) is energetically favourable.

According to experimental data [123,190], the critical current density across [001] tilt boundaries in $YBa_2Cu_3O_{7-\delta}$ superconductors at temperature T = 4.2K depends on boundary misorientation θ tentatively as follows:

$$J_c(\theta) = J_{bulk} \exp\left[-\frac{\theta}{\theta_0}\right], \qquad (52)$$

where $\theta_0 \approx 6.3°$, the typical bulk current density $J_{bulk} \approx 2 \cdot 10^7$ A/cm^2, and θ ranges from 0° to 45°. Owing to the highly non-linear character of dependence $J_c(\theta)$ given by formula (52), we find that the misfit-stress-induced transformation of the low-angle boundary structures (Fig. 34) enhances the critical current density across low-angle tilt boundaries in superconducting films. Ratio of the critical current density ($J_c(\theta_2)$) across the low-angle boundary in its final state to that ($J_c(\theta_1)$) in its initial state is given as: $J_c(\theta_2)/J_c(\theta_1) = \exp[(\theta_1-\theta_2)/\theta_0]>1$, for $\theta_2 < \theta_1$.

The misfit-stress-driven transformations of tilt bouindary structures (Fig. 34) require grain boundary dislocations to climb towards the film free surface, in which case the dislocations should overcome some energetic barriers related to emission or absorption of point defects at the dislocations cores [42]. Pressure and thermal treatment are capable of enhancing the climbing of dislocations and, therefore, according to our model, increasing J_c. In this context, recent experimental data [191] on a significant enhancement of J_c by hot pressing in Bi-2223/Ag multifilamentary tapes can indicate in favour of the model suggested in this paper.

In the framework of the model [189], tilt boundary structures have been assumed to be transformed into those with misorientation parameters being constant along boundary planes. In general, however, the influence of misfit stresses on spatial positions of grain boundary dislocations in a film varies along the boundary; the effect is strong in vicinity of the film/substrate boundary and becomes weaker as the distance from the film/substrate boundary increases. This is related to the fact that a contribution of a (misfit) dislocation to relaxation of misfit stresses decreases, when the distance between the dislocation and the film free surface decreases. In paper [192] a theoretical model has been suggested describing spatially inhomogeneous distributions of dislocations at grain boundaries in films, resulted from the effect of misfit stresses. The model [192] predicts a high (moderate, respectively) enhancement of J_c near the film/substrate boundary (the film free surface, respectively). This is in agreement with experimental data [156] indicating that the most supercurrent in BiSrCaCuO tapes deposited onto silver sheets flows through the thin layer next to the interphase boundary.

Thus, according to results of theoretical analysis given in papers [189,192], misfit stresses are capable causing structural transformations of tilt boundaries, that enhance the critical current density across such boundaries in high-T_c superconducting thin-film cuprates. This potentially allows one to use technologically controlled parameters (misfit parameters, crystallography of interphase boundary, film thickness) of film/substrate systems in synthesis and design of high-T_c superconducting films with enhanced transport properties.

16.5. Stress fields and structural transformations of grain boundaries in high-T_c superconductors

In general, grain boundaries in high-T_c thin-film and bulk superconductors can undergo structural transformations induced by their intrinsic stress fields (see experimental data [96, 125, 127, 157-160, 179-182, 193-199] and theoretical models [200, 201]). Such transformations dramatically change grain boundary core structures and cause re-distribution of stress fields in vicinities of grain boundaries, in which case, they are capable of strongly influencing the critical current density across grain boundaries. Thus, as it has been revealed in the experiments [157], the structure of low-angle [100] tilt boundaries in $YBa_2Cu_3O_{7-\delta}$ superconductors drastically changes with boundary misorientation α. So, in contrast to conventional situation with low-angle tilt boundaries consisting of periodically spaced perfect (lattice) dislocations, for $\alpha \approx 5°$ [100], tilt boundaries represent walls of split dislocation configurations each consisting of three partial dislocations of the edge type (Fig. 35a). The sum Burgers vector of a split dislocation configuration is the crystal lattice vector $\boldsymbol{B}$ = (0,0,B) in conventional (a,b,c)-crystallography of high-T_c superconducting cuprates, where $B \approx 1.17$ nm. Each partial disloca-

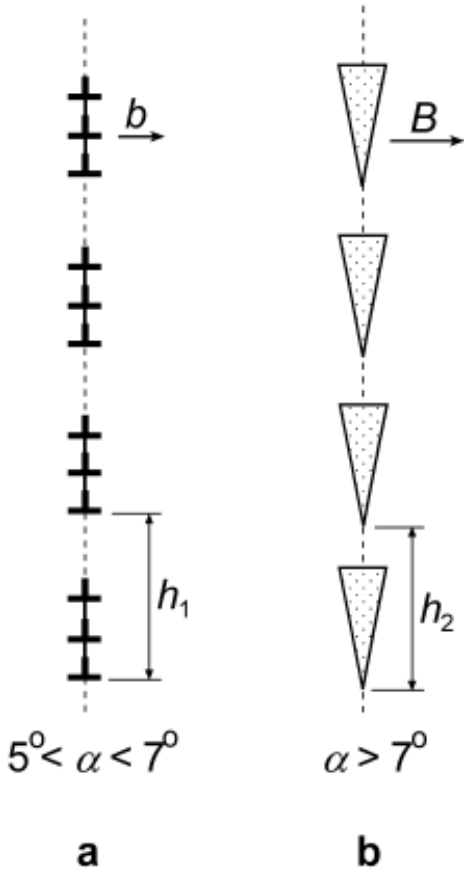

Fig. 35. Dislocation structures at low-angle tilt boundaries in high-T_c superconductors: (a) split and (b) amorphous dislocation structures.

tion composing a split dislocation configuration (Fig. 35a) is characterized by Burgers vector ***b*** =(0,0,*b*) with *b* being equal to *B*/3. The neighbouring partial dislocations in the boundary with $\theta \approx 5°$ are distant by tentatively 12*b*.

Low-angle [100] tilt boundaries with $\theta \approx 7°$represent walls of dislocation configurations with amorphous cores having triangle-like sections [157] (Fig. 35b). Such "amorphous" dislocation configurations as elements of low-angle boundaries provide misorientation of adjacent crystalline grains in $YBa_2Cu_3O_{7-\delta}$ superconductors and are characterized by Burgers vectors of the (0,0,*B*) type [157].

In paper [201] a theoretical model has been elaborated describing the structural transformations of low-angle tilt boundaries in high-T_c superconductors (Fig. 35). In the framework of the model [201], the trnasformations (Fig. 35) are driven by a release of intrinsic stresses of dislocations composing such boundaries.

Grain boundaries in high-T_c superconducting films and bulk materials often posses the faceted microstructure; see, e.g., [96, 125, 158, 179-182]. In many cases, grain boundaries in thin-film and bulk materials exhibit respectively "wavy" (non-equilibrium) and saw-tooth-shaped (equilibrium) faceted microstructures. Dislocations along individual facets of grain boundaries frequently are inhomogeneously distributed; certain types of dislocations repeatedly are grouped near the facet centers and ends [158]. These structural peculiarities of grain boundaries in high-T_c superconductors are naturally viewed to be related to intrinsic stresses induced by boundary dislocations. However, for the unambigious identification of the reasons causing these structural peculiarities of grain boundaries in high-T_c cuprates, their further detailed theoretical and experimental studies are desired.

The critical current density J_c across low-angle tilt boundaries in high-T_c superconductors drastically decreases with boundary misorientation angle α in the range from 0° to tentatively 15° [121-127]. Current models of the grain boundary effect on high-T_c superconductivity are based on the representation of low-angle tilt boundaries as walls of perfect dislocations (Fig. 32a). However, in the light of both experiments [96, 125, 127, 157-160, 179-182, 193-199] and theoretical models [200,201], the transformations of low-angle tilt boundaries should be definitely taken into consideration of the effects of grain boundary stress fields and core structures on high-T_c superconductivity.

17. CONCLUDING REMARKS

Thus interfaces in nanostructured and polycrystalline films are characterized by the specific structural and behavioral features associated with generation and evolution of misfit defects in such films. So, in general, interphase boundary between a nanocrystalline (or polycrystalline) film and a single crystalline substrate is partly coherent, semi-coherent and incoherent; it consists of coherent, semi-coherent and incoherent fragments (Fig. 3). Also, the elastic interaction between grain boundary defects and interphase boundaries in nanocrystalline (or polycrystalline) film/substrate composites causes grain boundary defects – dislocations and disclinations - to serve as misfit defects compensating for misfit stresses. The formation of grain boundary defects as misfit defects does not induce any extra violations of the interphase boundary coherency. It is desired, from an applications viewpoint, in situation with interphase boundaries used

as functional elements. The action of the mechanisms discussed is most effective in nanocrystalline films where the volume fraction of the grain boundary phase is extremely high and grain boundary defects (capable of playing the role as misfit defects) are intensively generated. The effective contribution of grain boundary defects to relaxation of misfit stresses in nanocrystalline films explains the experimentally documented (see discussion in paper [50]) fact that residual stresses are low in nanocrystalline coatings synthesized by thermal spray methods.

One of the specific structural and behavioral features of interphase boundaries in nano-layer/substrate composites (Fig. 1c) is the experimentally observed [81-85] enhanced formation of partial MDs associated with stacking faults. Partial MDs (Fig. 24) transform into perfect MDs with increase of film thickness. This statement resulted from theoretical analysis [86] (see also section 10) is in agreement with experimental data [85] indicative of the fact that density of perfect MDs increases and density of partial MDs decreases with increase of film thickness.

Interphase-boundary-induced misfit strains are theoretically revealed to play the important role in phase transformations in nano-layered composites (see sections 11-13). In particular, the effect of misfit strains causes the experimentally revealed [92] existence of the minimal critical thickness h_c^{am} for the amorphization in Ni/Ti multilayer composites.

The growth of nano-islands on a composite (two-layer) substrate with MDs at an internal interphase boundary (Fig. 30) is an effective method for fabrication of spatially ordered ensembles of nano-islands (e.g., quantum dots). Due to elastic interaction between nano-islands and MDs, spatial positions (and generally speaking, size and shape) of nano-islands are highly sensitive to the characteristics of the dislocated composite substrate. This potentially allows one to design arrangements of nano-islands with desired functional characteristics on a composite substrate, using technologically controlled parameters (materials of layers composing the two-layer substrate, thickness of the "upper" layer, etc.) of the substrate.

Grain boundaries in high-T_c superconducting films and bulk materials dramatically suppress the critical current density J_c. The physical mechanism(s) of this phenomenon is(are) the subject of controversy. In particular, the behavior of grain boundaries in high-T_c superconductors can be associated with the combined effects of dilatation-induced stoichiometric and electric-charge inhomogeneities at grain boundaries, $d_{x^2-y^2}$ symmetry and grain boundary faceting. These effects account for the experimentally observed reduction of the critical current density J_c with increasing grain boundary misorientation angle and existence of hole-depletion zones in vicinities of grain boundaries in high-T_c superconductors as well as existence of deviations from bulk stoichiometry near grain boundaries and variations of the superconducting properties along grain boundary planes in cuprate samples fabricated at highly non-equilibrium conditions. Also, the representations on the effects discussed can be used in understanding the nature of the enhancement of J_c across high-quality twist and doped grain boundaries in cuprates. Misfit stresses in high-T_c superconducting polycrystalline films are capable of strongly influencing the structure and transport properties of grain boundaries in such films.

The specific structural and the behavioral features of interfaces and misfit defects in nanostructured and polycrystalline films cause the specific effects of such interfaces on the macroscopic properties of such films. These effects should definitely be taken into account in experimental research and theoretical description of the structure and behavior of nanostructured and polycrystalline films.

ACKNOWLEDGEMENTS

This work was supported, in part, by the Russian Foundation of Basic Researches (grant 98-02-16075), the Office of US Naval Research(grants N00014-99-1-0569 and N00014-99-1-0896), INTAS (grant 99-01216), and Volkswagen Foundation (Research Project Nr. 05019225). Author would like to thank M.Yu. Gutkin, A.L. Kolesnikova, K.N. Mikaelyan, A.B. Reizis, A.E. Romanov and A.G. Sheinerman for permanent collaboration, valuable contributions, fruitful discussions and encouragements.

REFERENCES

[1] *Polycrystalline Thin Films: Structure, Texture, Properties and Applications II*, ed. by H.J. Frost, M.A. Parker, C.A. Ross and E.A. Holm (MRS, Pittsburgh, 1996).

[2] *Nanostructured Films and Coatings*, *NATO Science Ser.*, ed. by G.-M. Chow, I.A. Ovid'ko and T. Tsakalakos (Kluwer, Dordrecht, 2000).

[3] *Nanotechnology Research Directions*, ed. by M.C. Roco, R.S. Williams and P. Alivisatos (Kluwer, Dordrecht, 2000).
[4] *Nanomaterials: Synthesis, Properties and Applications*, ed. by A.S. Edelstain and R.C. Camarata (Institute of Physics Publ., Bristol and Philadelphia, 1996).
[5] *Materials Science of Carbides, Nitrides and Borides*, *NATO Science Series*, ed. by Yu.G. Gogotsi and R.A. Andrievskii (Kluwer, Dordrecht, 1999).
[6] *R\&D Status and Trends in Nanoparticles, Nanostructured Materials, and Nanodevices in the United States*, ed. by R.W. Siegel, E. Hwu and M.C. Roco (International Technology Research Institute, Baltimore, 1997).
[7] H. Gleiter // *Progr. Mater. Sci.* **33** (1989) 223.
[8] *Nanostructured Materials: Science and Technology*, *NATO ASI Series*, ed. by G.-M. Chow and N.I. Noskova (Kluwer, Dordrecht, 1998).
[9] *Russian Research and Developement Activities on Nanoparticles and Nanostructuted Materials*, ed. by I.A. Ovid'ko and M.C. Roco (International Technology Research Institute, Baltimore, 1999).
[10] A. Bourett // *Surf. Sci.* **432** (1999) 37.
[11] G.Mobus, E.Schummann, G. Dehm and M. Ruhle // *Phys. Stat. Sol. (a)* **150** (1995) 77.
[12] Yu.A. Tkhorik and L.S. Khazan, *Plastic Deformation and Misfit Dislocations in Heteroepitaxial Systems* (Naukova Dumka, Kiev, 1983) (in Russian).
[13] E.A. Fitzgerald // *Mater. Sci. Rep.* **7** (1991) 87.
[14] J.H. van der Merve // *Crit. Rev. Sol. State and Mater. Sci.* **17** (1991) 187.
[15] S.C. Jain, J.R. Willis and R. Bullough // *Adv. Phys.* **39** (1990) 127.
[16] S.C.Jain, A.H.Harker and R.A.Cowley // *Philos. Mag. A* **75** (1997) 1461.
[17] J.H. van der Merve // *Proc. Phys. Soc. London A* **63** (1950) 616.
[18] W. Wunderlich, G. Frommeyer and P. V. Carnowski // *Mater. Sci. Eng.A* **A164** (1993) 421.
[19] A.F. Shwartzman and R. Sinclair // *J. Electron. Maters.* **20** (1991) 805.
[20] N. Burle, B. Pichaud, N. Guelton and R.G. Saint-Jacques // *Phys. Stat. Sol. (a)* **149** (1995) 123.
[21] C.J. Gibbings, C.G. Tuppen and M. Hockly // *Appl. Phys. Lett*. **54** (1989) 148.
[22] K. Jagannadham and J. Narayan // *J. Electron. Maters.* **20** (1991) 767.
[23] V.M. Ievlev, A.S. Ognev and S.B. Kushchev // *Fiz. Met. Metallov.* **65** (1988) 1021 (translated in *Phys. Met. Metall.*).
[24] Y. Fukuda, Y. Kohama, M. Seki and Y. Ohmachi // *Jpn. J. Appl. Phys.* **28** (1989) L19.
[25] H.-H. Park and J.Y. Lee // *Jpn. Appl. Phys.* **33** (1995) 255.
[26] C.G. Tuppen and C.J. Gibbings // *Thin Solid Films* **183** (1989) 133.
[27] W.A. Jesser and J. Kui // *Mater. Sci. Eng. A* **164** (1993) 101.
[28] A. Rocket and C.J.Kiely // *Phys. Rev. B* **44** (1991) 1154.
[29] A. Atkinson and S.C. Jain // *Thin Solid Films* **222** (1992) 161.
[30] A. Atkinson and S.C. Jain // *J. Appl. Phys.* **72** (1992) 2242.
[31] T.J. Gosling, S.C. Jain, J.R. Willis, A. Atkison and R. Bullough // *Phil. Mag. A* **66** (1992) 119.
[32] M.Yu. Gutkin and A.E. Romanov // *Phys. Stat. Sol. (a)* **129** (1992) 117.
[33] S.C. Jain, T.J. Gosling, J.R. Willis, D.H.J. Totterdell and R. Bullough // *Phil. Mag. A* **65** (1992) 1151.
[34] T.J. Gosling, R. Bullough, S.C. Jain and J.R. Willis // *J. Appl. Phys.* **73** (1993) 8267.
[35] M.Yu. Gutkin, A.L. Kolesnikova and A.E. Romanov // *Mater. Sci. Eng. A* **164** (1993) 433.
[36] U. Jain, S.C. Jain, J. Nijs, J.R. Willis, R. Bullough, R.P. Mertens and R. van Oversraeten // *Solid State Electron.* **36** (1993) 331.
[37] T.J. Gosling and J.R. Willis // *Phil. Mag. A* **69** (1994) 65.
[38] M.Yu. Gutkin and A.E. Romanov // *Phys. Stat. Sol. (a)* **144** (1994) 39.
[39] J.R. Willis, S.C. Jain and R. Bullough // *Phil. Mag. A* **62** (1990) 115.
[40] J. Petruzzello, D.J. Olego, X. Chu and J.P. Faurie // *J. Appl. Phys.* **63** (1988) 1783.
[41] I.A. Ovid'ko // *J. Phys.: Cond. Matter.* **11** (1999) 6521.
[42] J.P. Hirth and J. Lothe, *Theory of Dislocations* (Mc Graw-Hill,New-York, 1968).
[43] A.E. Romanov and V.I. Vladimirov, In: *Dislocations in Solids*, *vol.9,* ed. by F.R.N. Nabarro (North-Holland Publ., Amsterdam, 1992) p.191.

[44] J.W. Matthews // *J.Vacuum Sci. Tech.* **12** (1975) 126.
[45] V.M. Ivlev, L.I. Trusov and V.A. Khomyanskii, *Structural Transformations in Thin Films* (Metallurgiya, Moscow, 1988) (in Russian).
[46] I.A. Ovid'ko, In: *Nanostructered Films and Coatings, (NATO Science Series)*, ed. by G.-M. Chow, I.A. Ovid'ko and T. Tsakalakos (Kluwer, Dordrecht, 2000) p. 231.
[47] A.A.Nazarov, A.E.Romanov and R.Z.Valiev // *Solid State Phenom.* **35-36** (1994) 381.
[48] A.A.Nazarov, A.E.Romanov and R.Z.Valiev // *Acta Metall.Mater.* **41** (1993) 1033.
[49] M.Yu.Gutkin, K.N. Mikaelyan and I.A.Ovid'ko // *Phys.Sol.State* **40** (1998) 1864.
[50] L.Kabacoff, In: *Nanostructured Films and Coatings, NATO Science Ser.,*ed. by G.-M.Chow, I.A.Ovid'ko and T.Tsakalakos (Kluwer, Dordrecht, 2000) p.373.
[51] I.A. Ovid'ko and A.G. Sheinerman // *J.Nanosci.Nanotechnol.* (2001), in press.
[52] Y.Q. Wang, Z.L. Wang, T. Brown, A. Brown and G. May // *Appl. Phys. Lett.* **77** (2000) 223.
[53] U. Jain, S.C. Jain, J. Nijs, J.R. Willis, R. Bullough, R.P. Mertens and R. van Oversraeten // *Solid State Electron.* **36** (1993) 331.
[54] V.G. Gryaznov and L.I. Trusov // *Progr. Mater. Sci.* **37** (1993) 289.
[55] M.Seefeldt // *Materials Physics and Mechanics* **1** (2000) 54.
[56] M.Seefeldt and P.van Houtte // *Materials Physics and Mechanics* **1** (2000) 133.
[57] I.A. Ovid'ko // *Phys.Sol.State* **41** (1999) 1500.
[58] A.L. Kolesnikova, I.A. Ovid'ko and A.E. Romanov // *Solid State Phenom.*, in press.
[59] J.S.Speck, A.C.Daykin, A.Seifert, A.E.Romanov and W.Pompe // *J. Appl. Phys.* **78** (1995) 1696.
[60] A.E.Romanov, M.J.Lefevre, J.S.Speck, W.Pompe, S.K.Streiffer and C.M.Foster // *J. Appl. Phys.* **83** (1998) 2754.
[61] I.A. Ovid'ko // *Phil.Mag.Lett.* **79** (1999) 709.
[62] F.K. LeGoues, M.Copel and R.Tromp // *Phys. Rev. Lett.* **63** (1989) 1826.
[63] F.K. LeGoues, M.Copel and R.Tromp // *Phys. Rev.* **42** (1990) 11690.
[64] C.S. Ozkan, W.D. Nix and H. Gao // *Appl. Phys .Lett.* **70** (1997) 2247.
[65] P. Müllner, H. Gao and C.S. Ozkan // *Phil. Mag. A* **75** (1997) 925.
[66] H.Gao, W.D.Nix, J.A. Zimmerman and L.B. Freund // *Phil. Mag. A* **79** (1999) 349.
[67] N.Rivier // *Adv. Phys.* **36** (1987) 95.
[68] I.A. Ovid'ko, *Defects in Condensed Media: Glasses, Crystals, Quasicrystals, Liquid Crystals, Magnetics, Superfluids* (Znanie, St.Petersburg, 1991) (in Russian).
[69] V.Yu. Gertsman, A.A. Nazarov, A.E. Romanov, R.Z. Valiev and V.I. Vladimirov // *Phil. Mag. A* **59** (1989) 1113.
[70] A.A. Nazarov, A.E. Romanov, and R.Z. Valiev // *Acta Metall.Mater.* **41** (1993) 1033.
[71] K.K. Shih and J.C.M. Li // *Surface Sci*. **50** (1975) 109.
[72] W. Bollmann // *Mater.Sci.Eng. A* **113** (1989) 129.
[73] M.Yu.Gutkin and I.A. Ovid'ko // *Phil. Mag. A* **70** (1994) 561.
[74] A.V. Osipov and I.A. Ovid'ko // *Appl. Phys. A* **54** (1992) 517.
[75] M.Yu. Gutkin // *Rev. Adv. Mater. Sci.* **1** (2000) 27.
[76] M. Seefeldt and P. Kilimanek // *Modelling Simul. Mater. Sci. Eng.* **6** (1998) 349.
[77] V.V. Rybin // *Large Plastic Deformation and Fracture of Metals* (Metallurgiya, Moscow, 1986) (in Russian).
[78] V. Klemm, P. Klimanek and M. Seefeldt // *Phys. Stat. Sol. (a)* **175** (1999) 569.
[79] M.Yu. Gutkin, I.A. Ovid'ko and A.G. Sheinerman // *J. Phys.: Cond. Matter* **12** (2000) 5391.
[80] A.E. Romanov, T. Wagner and M. Ruhle // *Scr. Mater.* **38** (1998) 869.
[81] B.C. De Cooman and C.B. Carter // *Acta Metall.* **37** (1989) 2765.
[82] B.C. De Cooman, C.B. Carter, Kam Toi Chan and J.R. Shealy // *Acta Metall.* **37** (1989) 2779.
[83] J. Zou and D.J.H. Cockayne // *Appl. Phys. Lett.* **69** (1996) 1083.
[84] M. Loubradou, R. Bonnet, A. Vila and P. Ruterana // *Mater. Sci. Forum.* **207-209** (1996) 285.
[85] M. Tamura // *Appl. Phys. A* **63** (1996) 359.
[86] M.Yu. Gutkin, K.N. Mikaelyan and I.A. Ovid'ko // *Phys.Sol.State* **43** (2001) 42.
[87] A.K. Gutakovskii, O.P. Pchelyakov and I.O. Stenin // *Kristallographia* **25** (1980) 806 (in Russian).
[88] A.F. Jankowski // *NanoStruct. Maters.* **6** (1995) 179.
[89] K. Samwer // *Phys. Rep.* **161** (1988) 1.

[90] Y.G. Chen and B.X. Liu // *J. Phys. D* **30** (1997) 510.
[91] L.J. Chen, J.H. Lin, T.L. Lee, W.Y. Hsieh, J.M. Liang and M.H. Wang, In: *Micromechanics of Advanced Materials*, ed. by S.N.G. Chu, P.K. Liaw, R.J. Arsenault, K. Sadananda, K.S. Chan, W.W. Gerberich, C.C. Chau and T.M. Kung (The Minerals, Metals & Materials Society, Cleveland, 1995) p. 519.
[92] A.F. Jankowski, P. Sandoval and J.P. Hayes // *NanoStruct. Maters.* **5** (1995) 497.
[93] I.V. Grekhov, T.S. Argunova, M.Yu. Gutkin, L.S. Kostina and T.V. Kudryavtzeva // *Mater. Sci. Forum* **196—201** (1995) 1853.
[94] T.S. Argunova, I.V. Grekhov, M.Yu. Gutkin, L.S. Kostina, E.N. Belyakova, T.V. Kudryavtseva, E.D. Kim and D.N. Park // *Phys. Solid State* **38** (1995) 1832.
[95] M.Yu. Gutkin and I.A. Ovid'ko // *J.Phys.: Cond. Matter* **11** (1999) 8607.
[96] A.F. Marshall and R. Ramesh, In: *Interfaces in High-T_c Superconducting Systems*, ed. by S.L. Shinde and D.A. Rudman (Springer, New York etc., 1994) p.71.
[97] D.Yu.Baskov, M.Yu.Gutkin, I.A.Ovid'ko and A.G.Sheinerman // *Materials Physics and Mechanics* **2** (2000) 10.
[98] N. N. Ledentsov, V. M. Ustinov, V. A Shchukin, P. S. Kop'ev, Zh. I. Alferov and D. Bimberg // *Semiconductors* **32** (1998) 343.
[99] V. A. Shchukin and D. Bimberg // *Rev. Mod. Phys.* **71** (1999) 1125.
[100] V.M. Ustinov, In: *Nanostructured Films and Coatings*, *NATO Science Series*, ed. by G.M. Chow, I.A. Ovid'ko and T. Tsakalakos (Kluwer, Dordrecht, 2000) p. 41.
[101] D.J. Eaglesham and M. Cerullo // *Phys. Rev. Lett.* **64** (1990) 1943.
[102] Y.-W. Mo, D.E. Savage, B.S. Shwartzentruber and M.G. Lagally // *Phys. Rev. Lett.* **65** (1990) 1020.
[103] M. Krishnamurthy, J. S. Drucker and J.A. Venables // *J. Appl. Phys.* **69** (1991) 6461.
[104] P. Shittenhelm, M. Gail, J. Brunner, J. F. Nutzel and G. Abstreiter // *Appl. Phys. Lett.* **67** (1995) 1292.
[105] T.I. Kamins, E.C. Carr, R.S. Williams and S.I. Rosner // *J. Appl. Phys.* **81** (1997) 211.
[106] S.A. Chaparro, J. Drucker, Y. Zhang, D. Chandrasekhar, M.R. Mc Cartney and D.J. Smith // *Phys. Rev. Lett.* **83** (1999) 1199.
[107] S.A. Chaparro, Y. Zhang, J. Drucker and D.J. Smith // *J. Appl. Phys.* **87** (2000) 2245.
[108] J. Tersoff, C. Teichert and M.G. Lagally // *Phys. Rev. Lett.* **76** (1996) 1675.
[109] T.T. Ngo, P.M. Petroff, H. Sakaki and J.L. Merz // *Phys. Rev. B* **53** (1996) 9618.
[110] A.E. Romanov, P.M. Petroff and J.S. Speck // *Appl. Phys. Lett.* **74** (1999) 2280.
[111] I.A. Ovid'ko and A.G. Sheinerman// *Appl. Phys*. A (2001), in press.
[112] M. Strassburg, V. Kutzer, U.W. Pohl, A. Hoffmann, I. Broser, N.N. Ledentsov, D. Bimberg, A. Rosenauer, U. Fisher, D. Gerthsen, I.L. Krestnikov, M.V. Maximov, P.S. Kop'ev and Zh.I. Alferov // *Appl.Phys.Lett.* **72** (1998) 942.
[113] J.A. Floro, M.B. Sinclair, E. Chason, L.B. Freund, R.D. Twesten, R.Q. Hwang and G.A. Lucadamo // *Phys. Rev. Lett.* **84** (2000) 701.
[114] P. Sutter and M.G. Lagally // *Phys. Rev. Lett.* **84** (2000) 4637.
[115] N. Liu, J. Tersoff, O. Baklenov, A.L. Holmes and C.K. Shin // *Phys. Rev. Lett.* **84** (2000) 334.
[116] C.-P. Liu, J.M. Gibson, T.I. Kamins, D.P. Basile and R.S. Williams // *Phys. Rev. Lett.* **84** (2000) 1958.
[117] D.E. Jesson, M. Kästner and B. Voigtländer // *Phys. Rev. Lett.* **84** (2000) 330.
[118] G.E. Cirlin, N.K. Polyakov, V.N. Petrov, V.A. Egorov, D.V. Denisov, B.V. Volovik, V.M. Ustinov, Zh.I. Alferov, N.N. Ledentsov, R. Heitz, D. Bimberg, N.D. Zhakharov, P. Werner and U. Gösele // *Mater. Phys. Mech.* **1** (2000) 15.
[119] T.I. Kamins, E.C. Carr, R.S. Williams and S.I. Rosner // *J. Appl. Phys.* **81** (1997) 211.
[120] E. Pehlke, N. Moll, A. Kley and M. Shaefer // *Appl.Phys. A* **65** (1997) 525.
[121] D.Dimos, P.Chaudhari, J.Mannhart, and F.K.LeGoues // *Phys.Rev.Lett.* **61** (1988) 219.
[122] D.Dimos, P.Chaudhari and J.Mannhart // *Phys.Rev.B* **41** (1990) 4038.
[123] Z.G.Ivanov, P.-Å.Nilsson, D.Winkler, J.A.Alarco, T.Claeson, E.A.Stepantsov and A.Ya.Tzalenchuk // *Appl.Phys.Lett.* **59** (1991) 3030.
[124] S.E.Russek, D.K.Lathrop, B.H.Moeckly, R.A.Buhrmann and D.H.Shin // *Appl.Phys.Lett.* **57** (1990) 1155.

[125] S.E.Babcock and J.L.Vargas // *Annu. Rev. Mater. Sci*. **25** (1995) 193.
[126] M.Prester // *Super. Sci. Technol.* **11** (1998) 333.
[127] N.D. Browning, E.M. James, K. Kyosuke, I. Arslan, J.P. Buban, J.A. Zaborac, S.J. Pennycook, Y. Xin and G. Duscher // *Rev. Adv. Mater. Sci*. **1** (2000) 1.
[128] M.F.Chisholm and S.J.Pennycook // *Nature* **351** (1991) 47.
[129] A.Gurevich and E.A.Pashitskii // *Phys.Rev.B* **57** (1998) 13878.
[130] D.Agassi, C.S.Pande and R.A.Masumura // *Phys. Rev. B* **52** (1995) 16237.
[131] J.A. Alarco and E. Olsson // *Phys. Rev. B* **52** (1995) 13625.
[132] K. Jagannadham and J. Narayan // *Philos. Mag. B* **61** (1990) 129.
[133] H.Hilgenkamp and J.Mannhart // *Appl. Phys. A* **64** (1997) 553.
[134] H.Hilgenkamp and J.Mannhart // *Appl. Phys. Lett.* **73** (1998) 265.
[135] J.Mannhart and H.Hilgenkamp // *Supercond. Sci. Technol.* **10** (1997) 880.
[136] A. Schmehl, B. Goetz, R.R. Schulz, C.W. Schneider, H. Bielefeldt, H. Hilgencamp and J. Mannhart // *Europhys. Lett.* **47** (1999) 110.
[137] H. Betouras and R. Joynt // *Physica C* **250** (1995) 256.
[138] D.M.Kroeger, A.Choudhury, J.Brynestad, R.K.Williams, R.A.Padgett and W.A.Coghlan // *J.Appl.Phys.* **64** (1988) 331.
[139] A.M. Campbell // *Supercond. Sci. Technol.* **2** (1989) 287.
[140] E.Z. Meilikhov // *Physica C* **271** (1996) 277.
[141] S.A. Kukushkin, A.V. Osipov and I.A. Ovid'ko // *Mater. Phys. Mech.* **1** (2000) 49.
[142] S.A. Kukushkin, I.A. Ovid'ko and A.V. Osipov // *Techn.Phys.Lett*. **26** (2000) 609.
[143] S.V. Stolbov, M.K. Mironova and K. Salama // *Supercond. Sci. Technol.* **12** (1999) 1071.
[144] I.A. Ovid'ko // *Mater. Sci.Eng.A* (2001), in press.
[145] N.D. Browning, M.F. Chisholm, S.J. Pennycook, D.P. Norton and D.H. Lowndes // *Physica C* **212** 185 (1993).
[146] S.E. Babcock, X.Y. Cai, D.C. Larbalestier, D.H. Shin, and N. Zhang // *Physica C* **227** 183 (1994).
[147] S.E.Babcock and D.C.Larbalestier // *Appl.Phys.Lett.* **55** (1989) 393.
[148] B.H. Moeckly, D.K. Lathrop and R.A. Buhrman // *Phys. Rev. B* **47** (1993) 400.
[149] E.A. Early , R.L. Steiner, A.F. Clark and K. Char // *Phys. Rev. B* **50** (1994) 9409.
[150] E.A. Early, A.F. Clark and K. Char // *Appl. Phys. Lett.* **62** (1993) 3357.
[151] M. Carmody, B.H. Moeckly, K.L. Merkle and L.D. Marks // *J.Appl. Phys.* **87** (2000) 2454.
[152] B.Vuchic, K.L.Merkle, K.Char, D.B.Buchholz, R.P.H.Chang and L.D.Marks // *J.Mater.Res.* **11** (1996) 2429.
[153] Y. Zhu, Q. Li, Y.N. Tsay, M. Suenaga, G.D. Gu and N. Koshizuka // *Phys. Rev. B* **57** (1998) 8601.
[154] Q. Li, Y.N. Tsay, M. Suenaga, G.D. Gu and N. Koshizuka // *Supercond. Sci. Technol.* **12** (1999) 1046.
[155] Q. Li, Y.N. Tsay, M. Suenaga, R.A. Klemm, G.D. Gu and N. Koshizuka // *Phys.Rev.Lett.* **83** (1999) 4160.
[156] S.Li, M.Bredehöft, W. Gao, T. Chandra and S.X. Dou // *Supercond. Sci.Technol*. **11** (1998) 1011.
[157] M.F. Chisholm and D.A. Smith // *Philos. Mag. A* **59** (1989) 181.
[158] I.-F. Tsu, J.-L. Wang, D.L. Kaiser and S.E. Babcock // *Physica C* **306** 163.
[159] B. Vuchik, K.L. Merkle, K. Char, D.B. Buchholz, R.P.H. Chang and L.D. Marks // *J. Mater. Res.* **11** (1996) 2429.
[160] T.S. Orlova, J.Y. Laval and B.I. Smirnov // *Mater. Phys. Mech.* **1** (2000) 39.
[161] A.P.Sutton and R.W.Baluffi, *Interfaces in Crystalline Materials* (Claredon Press, Oxford, 1995).
[162] N.M. Plakida, *High-Temperature Superconductors* (Springer-Verlag, Berlin, 1995).
[163] L.A.Girifalco and D.O.Welch, *Point Defects and Diffusion in Strained Metals* (Gordon and Breach, 1967).
[164] M.I.Buckett and K.L.Merkle // *Ultramicroscopy* **56** (1994) 71.
[165] A.Seeger and P.Haasen // *Philos.Mag*. **3** (1958) 470.
[166] R.J.Cava, A.V.Hewat, E.A.Hewat, B.Batlogg, M.Marezio, K.M.Rabe, J.J.Kraewski, W.F.Peck and L.W.Rupp Jr.// *Physica C* **165** (1990) 419.
[167] L.H. Greene, B.G. Bagley, In: *Physical Properties of High-T_c Superconductors*, ed. by M. Ginsberg (World Scientific, Singapore, 1990) p. 509.

[168] A.Barone and G.Paterno, *Physics and Applications of the Josephson Effect* (Wiley, N.Y., 1982).
[169] J. Halbritter // *Phys. Rev. B.* **46** (1991) 14861.
[170] C.C.Tsuei, J.R.Kirtley, C.C.Chi, Lock See Yu-Jahnes, A.Gupta, T.Shaw, J.Z.Sun and M.B.Ketchen // *Phys.Rev.Lett.* **73** (1994) 593.
[171] J.H.Miller, Q.Y.Ying, Z.G.Zou, N.Q.Fan, J.H.Xu, M.F.Davis and J.C.Wolfe // *Phys.Rev.Lett.* **74** (1995) 2347.
[172] D.A.Wollman, D.J.Van Harlingen, D.J.Lee, W.C.Lee, D.M.Ginsberg and A.J.Legget // *Phys.Rev.Lett.* **71** (1993) 2134.
[173] D.A. Brawner and H.R. Ott // *Phys. Rev. B* **50** (1994) 6530.
[174] D.J.Van Harlingen // *Rev.Mod.Phys.* **67** (1995) 515.
[175] Y.Ishimaru, J.Wen, K.Hayashi, Y.Enomoto and N.Koshizuka // *Jpn.J.Appl.Phys.* **34** (1995) L1532.
[176] K.A.Müller // Nature **377** (1995) 133.
[177] M.Sigrist and T.M.Rice // *Rev.Mod.Phys.* **64** (1995) 503.
[178] H.Hilgenkamp, J.Mannhart and B.Mayer // *Phys.Rev.B* **53** (1996) 14586.
[179] S.J.Rosner, K.Char and G.Zaharchuk // *Appl.Phys.Lett.* **60** (1992) 1010.
[180] C.Traeholt, J.G.Wen, H.W.Zandbergen, Y.Shen and J.W.M.Hilgenkamp // *Physica C* **230** (1994) 425.
[181] D.J.Miller, T.A.Roberts, J.H.Kang, J.Talvaccio, D.B.Buchholtz and R.P.H.Chang // *Appl.Phys.Lett.* **66** (1995) 2561.
[182] B.Kabius, J.W.Seo, T.Amrein, U.Dähne, A.Sholen and K.Urban // *Physica C* **231** (1994) 123.
[183] J.T. Kucera and J.C. Bravman // *Phys. Rev. B* **51** (1995) 8582.
[184] Y. Dalichaouch, M.S. Torikachvili, E.A. Early, B.W. Lee, C.L. Seaman, K.N. Yang, H. Zhou and M.B. Maple // *Sol. State Commun.* **65** (1988) 1001.
[185] I.A. Ovid'ko // *Mater. Sci. Eng. A* **280** (2000) 354.
[186] K.N. Mikaelyan, I.A. Ovid'ko and A.E. Romanov // *Mater. Sci. Eng. A* **259** (1999) 132.
[187] G.Saada and D.Sornette // *Acta Metall.Mater.* **43** (1995) 313.
[188] E.Bouchard and J.-P.Bouchard // *Philos.Mag. A* **65** (1992) 339.
[189] I.A. Ovid'ko // *J.Phys.: Cond.Matter* **13** (2001) L97.
[190] N.F. Heinig, R.D. Redwing, I.F. Tsui, A. Gurevich, J.E. Nordman, S.E. Babcock and D.C. Larbalestier // *Appl.Phys.Lett.* **69** (1996) 577.
[191] R. Zeng, B. Ye, J. Horvat, Y.C. Guo, B. Zeimetz, X.F. Yang, T.P. Beales, H.K. Liu and S.X. Dou // *Supercond. Sci.Technol* **11** (1998) 1101.
[192] S.V. Bobylev, I.A. Ovid'ko and A.G. Sheinerman // *IPME Preprint No 152* (2000).
[193] Y. Gao, G. Bai, D.J. Lam and K.L. Merkle // *Physica C* **173** (1991) 487.
[194] Y. Gao, K.L. Merkle , G. Bai, H.L.M. Chang and D.J. Lam // *Physica C* **174** (1991) 1.
[195] J.A. Alarco, E. Olsson, Z.G. Ivanov, P.A. Nilsson, D. Winkler, E.A. Stepantsov, O.I. Lebedev, A.L. Vasiliev, A.Ya. Tzalenchuk and N.A. Kiselev // *Physica C* **247** (1995) 263.
[196] J.A. Alarco, E.Olsson, Z.G. Ivanov, P.A. Nillson, D. Winkler, E.A. Stepantsov and A.Ya. Tzalenchuk // *Ultramicroscopy* **51** (1993) 239.
[197] A.H. Carim and T.E. Mitchell // *Ultramicroscopy* **51** (1993) 228.
[198] M. Mironova, G. Du, S. Sathyamurthy and K. Salama // *Phil.Mag. A* **79** (1999) 1079.
[199] J.-Y. Wang, A.H. King Y. Zhu, Y.-L. Wang and M. Suenaga // *Phil.Mag. A* **78** (1998) 1039.
[200] M.Yu. Gutkin and I.A. Ovid'ko, *Defects and Plasticity Mechanims in Nanostructured and Non-Crystalline Materials* (St.Petersburg, Yanus, 2001) (in Russian).
[201] M.Yu. Gutkin and I.A. Ovid'ko // *Phys.Rev. B* **63** (2001) 064515.